Oncolytic Viral and Immunotherapy Models Combined with Strategies to Ameliorate Cancer Burden

by

Ilyssa Aimee Summer

A Dissertation Presented in Partial Fulfillment
of the Requirements for the Degree
Doctor of Philosophy

Approved April 2016 by the
Graduate Supervisory Committee:

Carlos Castillo-Chavez, Co-Chair
John Nagy, Co-Chair
Anuj Mubayi
Yun Kang

ARIZONA STATE UNIVERSITY

May 2016

ABSTRACT

Combination therapy has shown to improve success for cancer treatment. Oncolytic virotherapy is cancer treatment that uses engineered viruses to specifically infect and kill cancer cells, without harming healthy cells. Immunotherapy boosts the body's natural defenses towards cancer. The combination of oncolytic virotherapy and immunotherapy is explored through deterministic systems of nonlinear differential equations, constructed to match experimental data for murine melanoma. Mathematical analysis was done in order to gain insight on the relationship between cancer, viruses and immune response. One extension of the model focuses on clinical needs, with the underlying goal to seek optimal treatment regimens; for both frequency and dose quantity. The models in this work were first used to estimate parameters from preclinical experimental data, to identify biologically realistic parameter values. Insight gained from the mathematical analysis in the first model, allowed for numerical analysis to explore optimal treatment regimens of combination oncolytic virotherapy and dendritic vaccinations. Permutations accounting for treatment scheduled were done to find regimens that reduce tumor size. Observations from the produced data lead to in silico exploration of immune-viral interactions. Results suggest under optimal settings, combination treatment works better than monotherapy of either type. The most optimal result suggests treatment over a longer period of time, with fractioned doses, while reducing the total dendritic vaccination quantity, and maintaining the maximum virotherapy used in the experimental work.

DEDICATION

I would like to dedicate this work to my father, for his struggle with brain cancer. I knew nothing about cancer upon his diagnosis, know a little bit now, and hope to learn enough to help maintain healthy longevity for those who may face such life threatening obstacles.

ACKNOWLEDGMENTS

Firstly, I would like to thank my committee chairs Dr. Carlos Castillo-Chavez and Dr. John Nagy for all the advice and direction. I have learned much from conversing with Dr.Castillo-Chavez over the years and greatly appreciate his support. I am grateful for all efforts made by Dr.John Nagy to assist me with oncological concepts and assistance. I would also like to thank my committee members Dr.Anuj Mubayi and Dr. Yun Kang for their guidance, discussions and support. Thanks to them all, I have grown.

I would like to thank my family, for letting me stay in school longer than expected. They have learned to support me with this great accomplishment, where post college was never a discussion, until it became reality. Thank you for the love.

My dearest colleague, Dr.Angela Peace, has supported me and provided me with academic stationary via mental motivation whenever I would run out, even when there were no back to school sales. I am forever grateful to have had the privilege to have worked with her and to grow alongside such an intelligent, creative and optimistic scientist.

I would like to thank the mice that were sacrificed in the pre-clinical experimental trials that I used data from. Without their sacrifices, I would have no data fits, that assisted in the model developments of this work, with the hopes of improving the longevity of cancer patients.

Lastly, I would like to thank scientists that were themselves, sacrificed in history under positions of disbeliefs from others. Science will only progress with innovative actions, moreover, people should not keep unconventional views to themselves.

TABLE OF CONTENTS

CHAPTER Page

LIST OF TABLES

Table Page

Table Page

LIST OF FIGURES

Figure Page

Figure Page

GLOSSARY

Acronym	Definition
CTL	Cytotoxic T-Lymphocyte
D	Dendritic cell vaccination used in regimens
DC	Dendrtic cells
MTD	Maximum Tolerated Dose
ODE	Ordinary Differential Equations
OV	Oncolytic Virus
OVIT	Oncolytic Viral-Immunotherapy
OVT	Oncolytic Virotherapy
V	Oncolytic Virus count used in regimens

Chapter 1

INTRODUCTION

1.1 Conventional Cancer Treatments

The basic principle which underlies cancer treatment is to specifically attack cancer cells and spare normal cells. Since cancer cells are derived from normal cells, it is a difficult challenge to select cancer cells, as it is unclear how to separate the differences therapeutically, aside from many characters specific to cancer cells. Cancer is a complex collection of diseases involving abnormal growth of cells, which tend to proliferate in an uncontrolled way and in many cases, metastasize. The six main hallmarks of cancer proposed by Hanahan and Weinberg, include sustained proliferation, evading growth suppressors, resistance to cell death, enabling replicative immorality, inducing angiogenesis, and activating invasion and metastasis (Hanahan and Weinberg (2011)). Treatments have been developed towards disrupting these traits.

Conventional cancer treatments are often accompanied by side effects associated with unsatisfactory quality of life near time of diagnosis that persists through treatment and recovery. Many specific cancers are inoperable, and the three modalities: surgery, chemo- and radiotherapy are given in a variety of combinations, depending on the situation. In a more general setting, if operable most patients with solid tumors primarily undergo surgery. Radiation therapy, which uses high energy wave particles to kill cancer cells and shrink tumors by ionizing the target tissue, is generally recommended after surgery. Side effects can occur because radiation can also damage healthy cells and tissues near the treatment area. The effects depend on the form

of cancer, location doses, and general health of the patient. Effects commonly include patient fatigue, a decrease in blood count, and skin problems amongst others. Chemotherapy follows which uses drugs to destroy both cancer and healthy cells, often resulting in harmful side effects to the patient. Some negative outcomes of radiation and chemotherapy include toxicity to normal cells and resistance by cancer cells (Mullen and Tanabe (2002)). Immunotherapy, also referred to as biotherapy, is a cancer treatment that stimulates certain parts of the immune system to work harder to attack cancer cells. This process, however, can be quite slow to target cancer effectively. Targeted therapy is a type of medication that blocks the growth of cancer cells by interfering with specific targeted molecules needed for carcinogenesis. With this in mind, every case is unique and includes diverse orders and combinations of treatments. Therefore, there is still a need to explore more creative anticancer treatments, including those involving oncolytic virotherapy.

1.2 Oncolytic Virotherapy

Virotherapy is a treatment that uses biotechnology to convert viruses into therapeutic agents by reprogramming viruses to treat diseases. Oncolytic virotherapy (OVT) can be separated in terms of oncos, "cancer," lytic, "lysing, bursting or killing," and virotherapy; i.e. a virus as a means of therapy that kills cancer. Oncolytic viruses (OV) have attracted the attention of clinicians, oncologists, experimentalists: (Bell and McFadden (2014),Russell *et al.* (2012),Huang *et al.* (2010), Breitbach *et al.* (2011),Chen *et al.* (2001),Power *et al.* (2007),Varghese and Rabkin (2002)])and mathematical modelers: (Komarova and Wodarz (2014),Tian (2011), Dingli *et al.* (2009),Bajzer *et al.* (2008),Wang *et al.* (2007),Wodarz (2001)).

Viral life cycle

Living organisms are considered having the ability to reproduce, either asexually or sexually. Viruses are not quite considered living organisms, as they are only able to replicate themselves by hijacking the genome of their host. The life cycle of viruses occurs with viral entry, replication, and shedding; respectively. In order to enter the host cell, proteins found of the surface of the virus interact with proteins of the host cell. A hole forms in the host cell membrane, which allows the viral particle or its genetic content to be released into the host cell. This commences viral reproduction. Assuming the virus has the ability to replicate, it will take control of the host cell's replication mechanisms, which allows the virus to make copies of itself. It is possible the virus can lie dormant within a cell, which can be this lysogenic part of the viral cycle. Once the virus is reactivated, it will use up the host cells resources and must find a new host. The process by which viral copies are released to find new hosts is viral shedding. Viral shedding allows the progeny of viruses to leave the cell by 3 common ways: budding, exocytosis or apoptosis. For enveloped viruses, budding enables viruses to it the host cell, which must acquire a host-derived membrane enriched in viral proteins. Exocytosis is the orioles by which viruses leave the cell, but do not destroy the host cell. Viral apoptosis is the self-destruction of the host cell while under viral attack. This is considered the lysis effect from the OV.

Oncolytic virotherapy (OVT) is a targeted therapy that uses engineered viruses to selectively infect and kill cancer cells. Oncolytic viruses(OVs) can be DNA or RNA, and wild-type or engineered. Oncolytic viruses have the DNA region that controls replication, deleted and then modified. Since the replication region is deleted, it is not possible for the virus to replicate in normal cells, which is a novel feature of OVs. Genetic or chemical modifications to OVs have been used to selectively target the

tumor cell surface, de-target sensitive tissues, or can create dual target viruses to enhance both vascular targeting and tumor infections (Russell *et al.* (2012)). In the majority of pre-clinical and clinical trials, OVs not only "die," but they are "lysed," broken down by the virus, producing viral cells that are equipped to attack more cancer cells. An illustration of how oncolytic viruses encounter normal and cancer cells is shown in Figure 1.2.

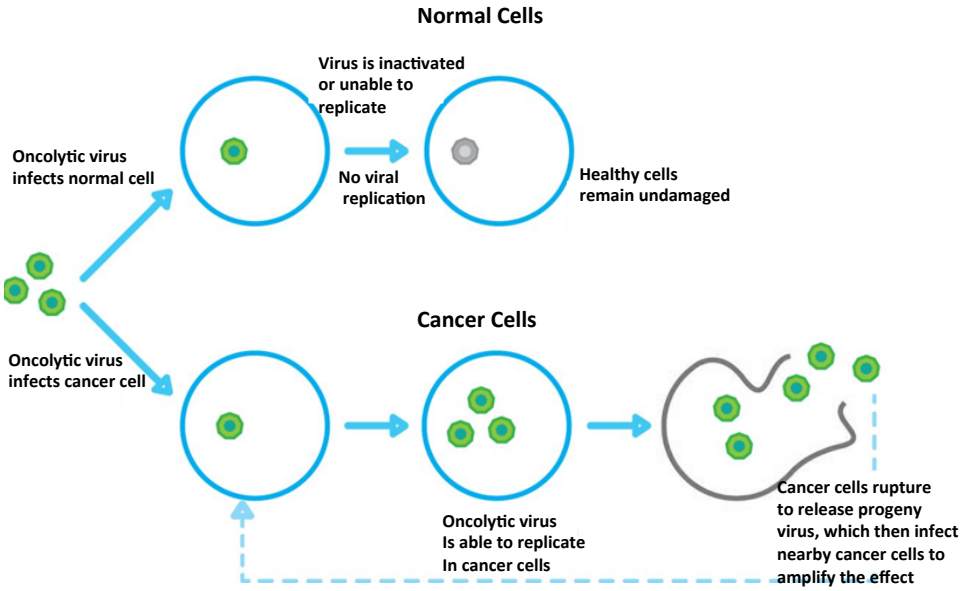

Figure 1.1: Generalized diagram of the cancer specificity of oncolytic viruses (Donnelly *et al.* (2013)).

OV can directly promote lysis or promote cell death via the immune response. The next novel feature of OVs is its immunogenicity; the ability of a substance, an antigen, or an epitope, to stimulate a host immune response. This may be mediated via innate immune effectors, adaptive antiviral immune responses or adaptive anti tumor immune responses. There is preclinical and clinical evidence supporting the importance of immune interactions (Prestwich *et al.* (2008)). Upon an OV infection, a change in the pre-existing immunosuppressive microenvironment occurs. After cancer

cells are infected, they generate "therapeutic" immune responses. These responses, are stimulated from the antigen message, to help cancer commit suicide (induce apoptosis). Therefore, the presence of an OV within or near cancer cells, promotes the immune system to start killing cancer cells. OVs can also be used as vectors to carry immune-inducing proteins to the cancer site. Thus, the immune system will start responding to the antigens nearby and attack the cancer. This process can also assist with eliminating neoplastic cells prior to tumor development, since immune cells are already at the site of infection where cancer is being produced (Shors (2011)). These OVs include an inherent form of immunotherapy.

The immune system, plays both ally and enemy when externally or genetically teamed up with oncolytic viruses. It was originally thought that oncolytic viruses would just be impaired by the immune system, such that as the virus would spread, the immune system would work towards liberating the body from the viral burden. However, the second side to this coin is that the actions from the virus help trigger a response within the tumor that signal the immune system to attack the effected environment (Pol *et al.* (2012)).

Although the idea of oncolytic virotherapy has been around since the mid 1950s, research was delayed due to inadequate technological availability (Russell *et al.* (2012)). Viruses became more understood during the 1950s and 1960s, in parallel with the advent of cell and tissue culture systems, allowing for *ex vivo* virus propagation(Kelly and Russell (2007), Gey *et al.* (1952)). As technology advanced, the practice of using viruses therapeutically has fallen hand in hand. In 1991, herpes simplex virus-1 (HSV-1) with deletion of thymidine kinase UL23 gene, became the first genetically engineered and replication specific oncolytic virus to be experimentally tested. Adenovirus, with

E1B 55K gene deletion, named Oncorine, was approved as the worlds first oncolytic viral therapy, used for head and neck cancer (Toth and Wold (2010)). Now, there are extended genetic oncolytic viruses being developed as a new class of anti-tumoral agents towards several solid tumors. Some of the best studied families of oncolytic viruses are oncolytic herpes simplex virus (oHSV), adenovirus, Newcastle disease virus (NDV), and vaccinia virus. Recent to this dissertation, oncolytic viruses have been reinvigorated, as the first oncolytic virus approved for use in the United States by the US Food and Drug Administration (FDA) occurred on October 27, 2015. This genetically engineered herpes simplex virus type 1, Talimogene Laherparepvec (T-VEC), will be used to treat advanced melanoma. T-VEC is designed to replicate within tumors and produce an immunostimulatory protein called "granulocyte-macrophage colony-stimulating factor" (GM-CSF) (Ledford (2015)). In short, OV's are booming within the evolution of cancer treatments.

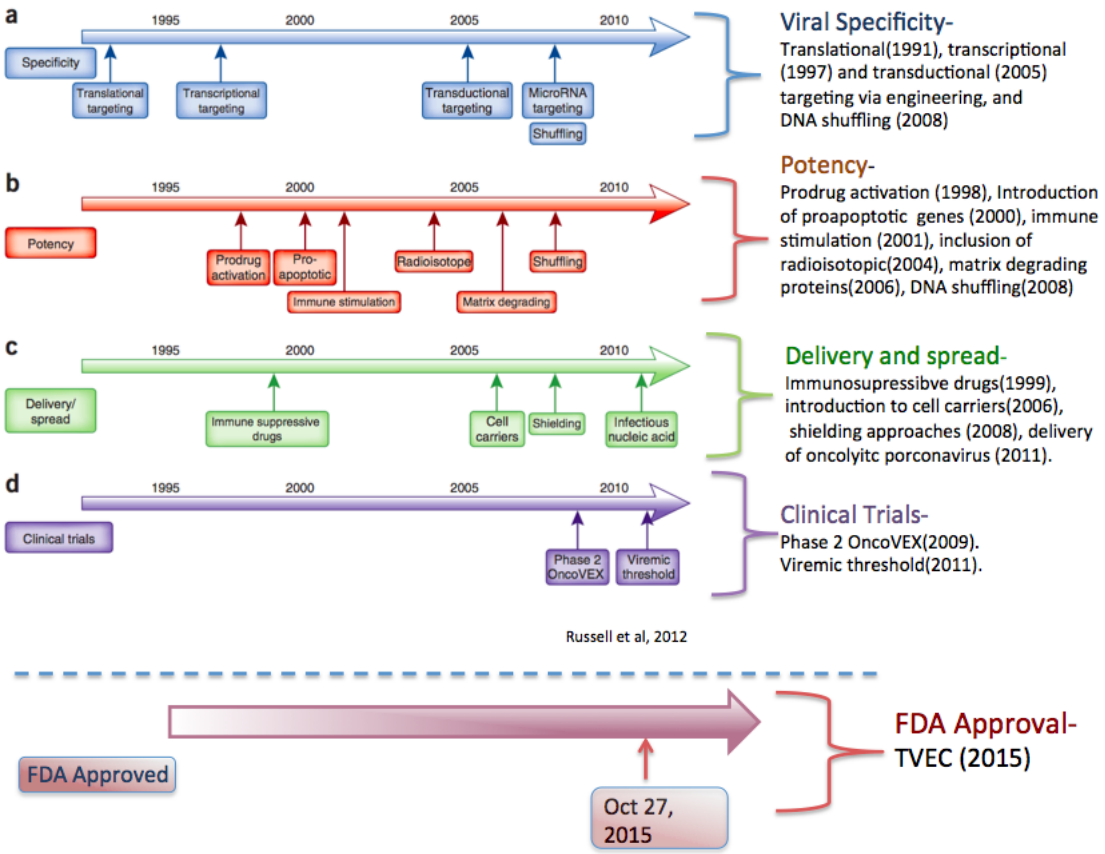

Figure 1.2: Timeline of recent milestones in oncolytic virotherapy. Image modified from (Russell *et al.* (2012))

Combination Therapy

Many cancer treatments use oncolytic virotherapy in combination with other treatments Relph *et al.* (2016). Viral oncolysis combined with immunotherapy consists of enhancing tumor killing through adoptive T cellular therapy (transfusion of lymphocytes). A common approach of adoptive T cellular therapy is to attach cytokines, interleukins, and immune stimulatory proteins to the OV, using it as a vector, that further stimulate the immune system with viral entry. Cytokines, derived from Greek cyto,"cell" and "kines," "movement," are secreted proteins and signal molecules im-

portant in cell signaling. The term interleukin, inter- "as a means of communication" and leukin-"deriving from", is a group of cytokines. Cytokines and interleukins are commonly attached and expressed with oncolytic viruses to enhance the immune system towards the cancer site. Immunostimulatory protein, Granulocyte-Macrophage Colony-Stimulating Factor (GM-CSF) plays diverse roles in cancer therapy. It can be used either as a monotherapy, or adjuvant to chemo-immunotherapy, adjuvant with cancer vaccines, GM-CSF expressing oncolytic immunotherapy, and systematic combination immunotherapy. Cytokines, interleukins, and immunostimulatory factors, such as GM-CSF, are commonly attached to oncolytic viruses to enhance immune efficacy.

Another approach is to combine OV with dendritic cell vaccines. Dendritic cell (DC) based vaccines have potential for cancer immunotherapy, where their use in clinical trials has been performed with patients diagnosed with prostate cancer, melanoma, lymphoma, and renal cancer (Nesrua *et al.* (1998), Tjoa *et al.* (1997), Hsu *et al.* (1996), Wierecky *et al.* (2006)). The main function of DCs are to process antigens and present it to T lymphocytes in the adaptive immune system. DC's are professional antigen-presenting cells (APCs) that have a significant role in the initiation and regulation of immune responses, as they act as messengers between the innate and the adaptive immune response. DCs can induce anti-tumor immunity by activating innate immune cells and tumor-specific lymphocytes that target cancer cells (Zhang *et al.* (2011) Kim *et al.* (2015b)). However, clinical trials have shown an immunosuppressed microenvironment under tumor influence thoroughly suppresses antitumor immunity and inhibits vaccine efficacy. This tumor microenvironment (TME) carries several immunosuppressive mechanisms that impair DC functions and block the development of anti-tumor immunity, which can lead to decreases in efficacies of immunotherapies

Rabinovich *et al.* (2007). There are many efforts towards improving immunotherapy success via dendritic cells, one of the more promising is the use of oncolytic virotherapies. Immunosuppression in the tumor microenvironment allows for an infection-vulnerable environment that can allow viral replication. Subsequently, cancer cells will be lysed by the viruses. DCs contribute to anti-viral innate immune responses via activation of innate immune elements, such as NK cells and inflammatory cytokines.

Gene-Based Cancer therapy

Gene therapy is a technique used for the correcting defective genes responsible for disease development. The two major classes of methods use recombinant viruses and DNA complexes. Viral vectors are common tools used by molecular biologists to deliver genetic material into cells. RNA is commonly used to encode a functional, therapeutic gene to replace a mutated gene. A mutation, is by definition, a permanent change of the nucleotide sequence of the genome of an organism, virus, extrachromosomal DNA, or other genetic elements.

Gene-based Immunotherapy

Gene-based immunotherapy is an effective strategy for patients with cancer. The main cell type that has emerged responsible for initiating and controlling cellular immune responses are dendritic cells. They are the most powerful antigen-presenting cell (APC) and potent stimulators of naïve T cells (Srinivasan *et al.* (2015)).

Adenoviruses are highly effective in gene based cancer therapy for its ability to efficiently transduce (transfer genetic material from on organism to another) cells, both dividing and non-dividing (Walsh *et al.* (2011)). Adenoviral vectors are used in suicide gene therapy, gene-based immunotherapy, gene replacement strategies and in a

variety of approaches that combine gene-based therapy with chemotherapy (Srinivasan *et al.* (2015)). For the purpose of this dissertation, the oncolytic viruses used are adenovirus. Oncolytic adenoviruses commonly have E1A deleted, a gene expressed during adenovirus replication. Adenoviral proteins E1A and E1B inactive proteins, pRB and p53 in normal cells, respectively. The binding site for the cell cycle related transcription factor E2F, is an E1A response element. Since E2F is a protein critical for normal cell cycle regulation and E1A is mutated, the altered adenovirus is unable to replicate in normal cells (Vähä-Koskela and Hinkkanen (2014),Veal *et al.* (1998)).

Safety Considerations

Oncolytic virus do not perform as well as monotherapy. One primary reason is that for as much engineering there is done to make OV cytotoxic, there is to keep the OV safe. The treatment of oncolytic virotherapy is considered safe since they are engineered to cause minimal stress or damage to the body. Adverse genes are removed and genes that assist with oncolysis are kept or inserted (Patel and Kratzke (2013)). Furthermore, it has been suggested that dose delivery could be safer when administered intratumorally. For safety reasons, viral vectors based on vaccinia virus, adenovirus, reovirus, newcastle-disease virus, coxsackievirus, and herpes simplex virus have been administered via intramural injection in early phase clinical trials (Shah *et al.* (2003), Kaufman *et al.* (2005), Chiocca *et al.* (2004), Harrow *et al.* (2004)).

The molecular basis of tumor selectivity is crucial prior to use in clinical human studies. Oncolytic viruses must be assayed in vitro for cytotoxicity(lysis) and/or replication on tumor-permissive and non-permissive cell lines. In many cases, selectivity is only demonstrated during in-vivo non-clinical studies. Tests are done to search for altered replication of selective or oncolytic profiles, in order to demonstrate the

genetic stability of the oncolytic virus.

Toxicity could depend on the route of administration of the oncolytic virus; therefore, the route and dosing schedule should mimic the intended clinical scenario as close as possible. Since oncolytic viruses are still incompletely understood, many questions remain to be addressed in early phase clinical trials. A common strategy used for oncolytic viral administration is to follow a stepwise approach with intratumoral injection, then move on to the regional or local administration, and finishing at the systematic administration.

1.3 Treatment Regimens

Oncolytic virotherapy is currently under investigation for phase I-III clinical trials for approval for new cancer treatments. The dosing quantity, frequency and administration could alter the effectiveness of treatments.

Drug Dosing

Cancer therapeutics are generally quite toxic, where the range between achieving maximum benefit and severe side effects is diminutive. Dose concentrations can be adjusted to the size of an individual by either drug dose per unit body mass or Body Surface Area (BSA). Each dose measures the amount of medicine or treatment taken at one time. Depending on the individual or protocol, doses and frequency vary.

Metronomic Therapy

The goal of most cancer treatments and studies, in vivo or in silico, seem to share the commonality to eliminate all cancer cells. However, this goal has been proven to be unrealistic and unnecessary to patient viability (Hahnfeldt *et al.* (2003)). Aside from

the dose quantity, the administration regimen plays a large role in cancer treatment success.

A metronome, used to indicate the exact tempo of music by producing sounds from a pendulum with an adjustable period of swing, was first examined by Galileo Galilei around 1602, for timekeeping; it was globally used as the most accurate timekeeping technology until the 1930s. Perhaps this pendulum could represent a distance that produces a beat on a homogeneous time distance for inducing cancer treatment.

"Metronomic" dosing allows for regularly spaced dosing. The idea was created to "resensitize" heterogeneous cell populations to treatments, with intentions to minimize total tumor burden, rather than complete eradication (Hahnfeldt *et al.* (2003)). If feasible, this approach is more practical than complete eradication; maintain a lower level of cancer instead of cancer elimination. This idea of metronomic therapy is usually used as metronomic chemotherapy, but in this work, I will introduce the idea of "Metronomic Oncolytic Viral-Immunotherapy (MOVIT)."

1.4 Motivation and Goals

There is much work to be done in understanding protocol treatments for cancer patients. More specifically, as OVT is increasingly being used clinically, there are many questions pertaining to this nature of dosing and scheduling for various OVs for diverse cancer types. This work investigates dose size and administration scheduling for oncolytic virotherapy combined with immunotherapy and dendritic cell vaccination. Since oncolytic virotherapy is still developing, there is much room for mathematical growth to develop models of cancer treatment questions, synergistically using OVs.

The research goals are as follows: 1) Develop a mathematical model that can represent clinical variations for administering oncolytic viral therapy. 2) Parameterize models using empirical data 3) Shed light on the complex dynamics of combined oncolytic viral and immunotherapy and 4) Identify optimal treatment strategies (dose sizes, treatment schedules) for a proposed personalized medicine model.

Chapter 2 presents a literature review of important models representing interactions between cancer, viruses and the immune system. First, viral dynamic models of uninfected, infected and free viral variables are discussed. The immune response is then introduced into the models. The second section introduces models of oncolytic viral therapy.

Chapter 3 opens the first model created for this work, constructed as an oncolytic virotherapy model with immune response. Mathematical analysis was performed in order to gain qualitative insight of the biological dynamics between viruses and cancer in the presence of the immune system.

Chapter 4 presents the Oncolytic Viral-Immunotherapy (OVIT) model, that questions the optimal combination of viral and immunotherapy under varying treatment regimens. This includes altering time of combination use, dose and frequency of treatments.

Chapter 5 summarizes the results of the research goals of this work and describes the overall impact from the results. Following the models used in this work, further models are presented which could have unique mathematical and biological impacts.

Chapter 2

LITERATURE REVIEW

Beyond clinical and experimental research; mathematical, computational and *in silico* models can be quite useful towards the advancements of disease treatments. In combination with data, carefully developed mathematical models could show subsequent stages of an experiment. Furthermore, mathematical models can present the evolution of how systems interact under ideal, hypothetical and blemished conditions. Hinged upon relevant biological assumptions and *a priori* information, mathematical models provide insight, direction and make predictions that clinical, nor experimental work would be able to achieve.

Creative approaches at the interface of interdisciplinary fields between mathematics, biology, computational biology, bioengineering and other relevant disciplines, are essential to improve our understanding of complex biological systems. These approaches are specifically needed to unravel the oncological complexity involved from the initiation, progression and metastatic phases of cancer. Mathematical models can be challenging to develop, since the independent limits of mathematical methods and biological information tend towards infinity. To start, making the biology a finite subset from the mass amount of growing information will bring certain mathematical methods to surface, in a fashion of functions that are not always injective nor surjective. For science to grow, it is healthy to choose mathematical methods contingent upon the biological question. Many biological systems can be represented with differential equations(DEs). For dynamics considering large population sizes, ordinary differential equations (ODEs) are a suitable tool. Delay differential equations (DDEs) can repre-

sent the biological role where time delays are hypothesized to be crucial. For questions pertaining to tumor growth, invasion and angiogenesis, partial differential equations (PDEs) can be used to represent fluid flow. Stochastic Differential Equations (SDEs) are used when the state of a variable is not predictable at a given moment in time. Cellular automata and agent based models are used to represent spatial questions. Clearly, there are many variants of scientific models representing the biological perplexity of cancer. The choice of methods used within these systems can depend on the quantity of parameters needed, parameters known, biological complexity, interaction between variables and/or what the question is.

Basic Cancer Growth Models

Tumor growth models have roots within the works of Ludwig von Bertalanffy and Benjamin Gompertz. Both produced models of growth, independent of cancer, but later applied to cancer. Gompertz published in 1825 his growth model for "Gompertzian growth" and Von Bertalanffy's contribution came in 1957. The von Bertalanffy's growth model:

$$M = kW^{\frac{2}{3}}$$

where M is the metabolic process, W is the organism's mass and k is a constant. Since von Bertalanffly noted that not all processes scale as a $\frac{2}{3}$ power of the mass, this was later replaced with λ and the general relation is:

$$M = kW^{\lambda}$$

where $\frac{2}{3} \leq \lambda \leq 1$

Modeling the von Bertalanffy starts with conservation equation: growth equals "birth"="death". In the context of cancer, this equation parallels to "proliferation"-"apoptosis". Originally, this process was used for anabolism and catabolism. Then the growth in mass (W(t)):

$$\dot{W} = \alpha W^{\lambda} - \beta W^{\mu}$$

Letting α and β be per capita birth and death rates, where $\lambda = \mu = 1$, yield the exponential model:

$$\dot{W} = (\alpha - \beta)W$$

where $\alpha > \beta$ leads to exponential growth and $\alpha < \beta$ leads to exponential decay.

For $\lambda = 1$ and $\mu = 2$, this form evolves into the next simple case of modeling cancer. As a population of cells with potential grow followed by saturation , it is represented by the logistic ordinary differential equation (Verhulst (1838)):

$$\dot{W} = \alpha W - \beta W^2 = \alpha W\Big(1 - \frac{W}{K}\Big), \quad W(0)$$

where $\dot{W}$ is the time derivative, $W = W(t)$ is the number of cancer cells at time t, r is the growth rate and K is the carrying capacity, i.e. the maximal size the population of cells can reach, given the proper nutrients, oxygen, spatial constraints, etc. The solution of the logistic ODE is a "sigmoidal" curve, exponentially growing in early stages and then saturating at its maximum.

Instead of a homogeneous population of cancer cells, suppose a population of heterogeneous cancer cells, i.e., diverse clones, competing with each other and healthy cells for nutrients, oxygen and space. The growth for cancer can be represented as follows:

$$\dot{x_i} = rx_i - \phi x_i, \quad 0 \leq i \leq n, \quad x_i(0) = \hat{x_i}$$

where $\hat{x_i}$ is the number of cells of type i, with corresponding growth rate r_i. With n cell lines, the competition can be shown with term ϕ in a variety of ways, such as:

$$\phi = \frac{\sum_{i=0}^{n} r_i x_i}{N}$$

where, $N = \sum_{i=0}^{n} \hat{x_i}$ in a general case, N representing the total number of cells in the system, assumed to be constant in this model (Wodarz and Komarova (2005)).

This is modeled by

$$\dot{x_i}(t) = e^{(r-\mu)}x_i(0)$$

Kareva *et al.* (2012) showed competition models of over-consumption. Interactions between consumers and shared resources were modeled. This model introduced a population of consumes x_c as clones, competing for common resources $\hat{z}$, which determines the carrying capacity of the popuation.

$$\begin{aligned} \dot{x_c} &= rx_c\Big(c - \frac{b\sum_A x_c}{\hat{kz}}\Big) \\ \dot{\hat{z}} &= \gamma + \frac{e}{\hat{z} + \sum_A x_c}\Big(\sum_A x_c(1-c)\Big) - d\hat{z} \end{aligned}$$

where each clones x_c is characterized by the values of the parameter c, with contest per capita birth rate r. The per capita death rate is proportional to $\frac{b\sum_A x_c}{\hat{kz}}$, where b is the rate of resource consumption, and k is the efficacy of resource consumption by each individual x_c and A is the range of possible values of c.

Cancer cells are similar to Lotka-Volterra equations, also referred as predator-prey systems, in ecology (Lotka (1910),Lotka *et al.* (1925)). Gatenby and Vincent (2003) presented the competition model:

$$\begin{aligned} \dot{x} &= r_x x\Big(1 - \frac{x + a_{xy}y}{K}\Big) \\ \dot{y} &= r_y y\Big(1 - \frac{y + a_{yx}x}{K}\Big) \end{aligned}$$

where x and y represent population of cancer and healthy cells, respectively, r_x, r_y, maximum growth rates, a_{xy}, a_{yx} the competition coefficients and carrying capacity, K, including growth promotion and constraints within the tissue. Competition systems alike have been a basis for variants of cancer models (Okamoto *et al.* (2014), Nagy

(2005), Wodarz (2001), Michelson *et al.* (1987)).

The models listed above are general principles to illustrate basic phenomena, not representative of an entire cancer system. These equations are tools to be modified by incorporating particular properties of a biological system in question, in order to establish conditions and gain insight of certain cancer dynamics.

2.1 Viral and Immune Models

Viral models are of the infectious disease models base. Infectious disease models started in the 1766 by Daniel Bernoulli, a trained physician that created a mathematical model to defend the practice of inoculating against smallpox. Ronald Ross than created a modern structure for theoretical epidemiology. Kermack and McKendrick published a simple deterministic model in 1927 (Kermack and McKendrick (1927)). Some epidemic models were studied through (Hethcote (1976),Miller (1983), Anderson *et al.* (1980),Brauer *et al.* (2001)).

A hearty quantity of mathematical modeling of the immune system were developed in Los Alamos National Laboratory (Perelson *et al.* (1976), Perelson and Oster (1979), Perelson (1989),Farmer *et al.* (1986), Bell (1970). Dibrov *et al.* (1977), De Boer *et al.* (1990)). This work overlapped into the works of May *et al.* (1976) and Oster and PERELSON (1987).

2.2 Viral Dynamic Models

Simple Viral Model

Viral replication in host, was modeled by many, and includes examples from Nowak and Bangham (1996), who represented populations of uninfected cells, x; infected

cells, y; and free virus particles, v. These population sizes can either denote the total abundance in a host, or the abundance in a given volume of blood or tissue.

$$\begin{aligned} \frac{dx}{dt} &= \lambda - dx - \beta xv, \\ \frac{dy}{dt} &= \beta xv - ay, \\ \frac{dv}{dt} &= \kappa y - \delta v \end{aligned} \tag{2.1}$$

The susceptible target cell population is produced at a constant rate λ, dies at rate d and becomes infected by virus at rate β. Infected cells die at rate a and produce free virus at rate k,with the viral decay rate of δ.

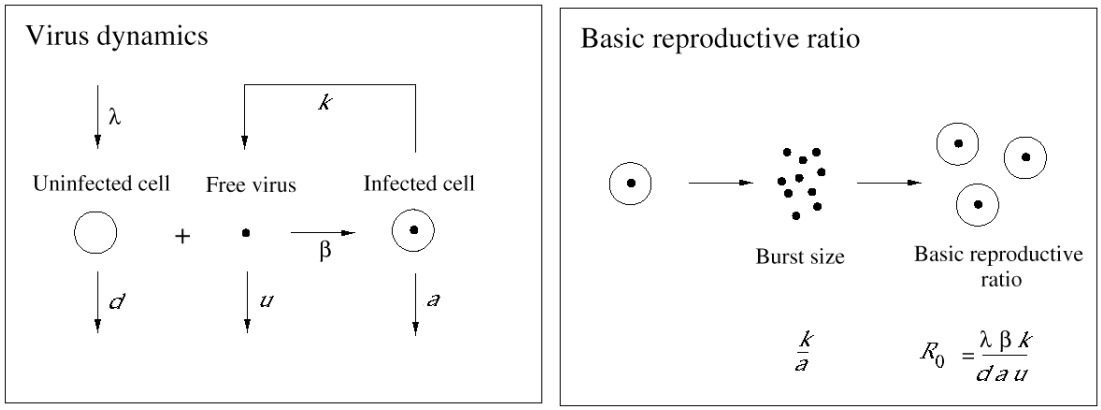

(a) (b)

Figure 2.1: Schematic illustrations of the basic viral dynamics 2.1a. The basic reproductive number is presented in terms of the burst size, $(\frac{k}{a})$ 2.1b. Let $u = \delta$ in the above diagram. Nowak and May (2000)

This model assumes that the cell population is initially uninfected, and a small amount of viral particles are added. The invading virions manage to infect a number

of cells, producing new virions, and subsequently infect cells. Two outcomes can occur when this chain reaction has started: the infesction dies out or it persists. The outcome depends on the basic reproductive number, R_0. Similar to the approach one takes in epidemiology, this dimensionless ratio is fundamental in discussing the demography of populations of living things: humans, plants, insects, animals, etc (Brauer *et al.* (2001)). Viruses,are considered replicators, rather than forms of life, which possess genes, evolve by natural selection and replicate by creating multiple copies of themselves via self-assembly[1] (Forterre (2010)). Viruses are not considered life forms because 1) they are obligate parasites and cannot reproduce on their own, and 2) have no independent metabolism. For a viral infection, R_0, is representative of the average number of infected cells produced from any one infected cell at the start of an infection. Figure 2.1b shows a schematic representation of this ratio. The rate at which one infected cell gives rise to new infected cells is given by $\frac{\beta k x}{\delta}|_{x=\frac{\gamma}{d}}$, when all cells are uninfected. Since the lifetime of an infected cell is $\frac{1}{a}$,

$$R_0 = \frac{\beta\gamma k}{ad\delta}$$

If every infected cell on average produces less than one newly infected cell, $R_0 < 1$, suggesting the infection will be inviable. With time, the virus will disappear. Otherwise, for $R_0 > 1$, the infection could expand throughout the population, but there is no guarantee it will infect the entire population of cells. This model suggests that at the endemic equilibria, (x^*, y^*, v^*), it is not necessary to evoke an immune response to achieve a stable equilibrium level of virus in a persistent infection. This equilibria was found to have limitations: 1) for cytopathic viruses. The Cytopathogenic Effect(CPE) from virus-structural changes in the host cells that are cause by viral invasion. The

[1]Molecular self-assembly is the process by which molecules adopt a defined arrangement without guidance or management from an outside source.

infecting virus causes lysis of the host cell or when the cell dies without lysis due to an inability to reproduce (Albrecht T (1996)). The total abundance of cells will be greatly reduced, and 2)for non-cytopathic viruses, most cells will be infected. The more cytopathic a virus is, i.e.,$a >> 0$, the smaller the steady state abundance of uninfected cells.

For further classification of the differences between the upcoming models, see Notion Table 2.1.

Table 2.1: Notational Reference Table

Variable	Description
x	Uninfected Cells
y	Infected Cells
v	Free Virus particles
z	CTL [2] Cells

Parameter	Description
λ	Constant production rate
r, d	Uninfected cell growth/death rate
β	Replication rate of virus
a	Infected cell death rate from virus
κ	Free virus production rate
δ	Viral decay rate
c, b	CTL production/decay rate
p	death from immunity upon uninfected/infected

The dynamics of immune responses can be studied to understand the interactions between abundance of viral and magnitude of the anti-viral immune response. Apart from functional immune response, which reduce viral load, the correlation between viral load and immune abundance can be positive or negative. The simplest model for the interaction between a virus and an immune response will be considered first. Virions will replicate according to the basic model of viral dynamics (2.1). An immune response is triggered by encountering a foreign antigen, the tapers off to a constant level independent of the concentration of virions or infected cells. Cytotoxic T-Lymphocyte (CTL) cells represent the immune response, for their clear importance of defending against viral infections.

CTL response

Nowak and May (2000) shows a simple of example of the CTL response in the following model:

$$\begin{aligned} \frac{dx}{dt} &= \lambda - dx - \beta xv \\ \frac{dy}{dt} &= \beta xv - ay - pyz \\ \frac{dv}{dt} &= ky - \delta v \\ \frac{dz}{dt} &= c - bz \end{aligned} \tag{2.2}$$

In this model, CTL cells are produced at rate c and die at rate bz. It is assumed $c > 0$ when $y > 0$. Otherwise, $c = 0$. Infected cells are eliminated by the CTL response a rate pyz. where $\frac{dz}{dt} = cyz - bz$ represents the nonlinear case, immune response proportional to the abundance of CTL: and $\frac{dz}{dt} = cy - bz$ is linear:immune response

[2]Cytotoxic T-Lymphocyte

induced at a rate proportional to the abundance of infected cells, but independent of the CTL abundance

The basic reproductive number, R_0 in the presence of CTL cells is:

$$R_0 = \frac{\beta\gamma k}{(a - a^1)d\delta}.$$

The rate at which infected cells are eliminated by the CTL response at its equilibrium level is denoted by, $a^1 = \frac{cp}{b}$. For models with self-regulating immune responses, there is always a negative correlation between virus load and abundance of immune mediators, immune cells, chemokines or antibodies. Patients with weak antiviral responses have high virus load, as opposed to patients with strong anti-viral response that have low viral load (Nowak and May (2000)).

2.3 Oncolytic Viral Models with Immune Response

Model Differences	Description	Citation
$\frac{dx}{dt} = rx\left[1 - \frac{(x+y)^\epsilon}{K^\epsilon}\right] - \beta xv - \rho xy$ $\frac{dy}{dt} = \beta xv - ay$ $\frac{dv}{dt} = \kappa y - \delta v - \beta xv$	$f(x,y) = rx\left[1 - \frac{(x+y)^\epsilon}{K^\epsilon}\right]$; Assumes untreated tumor growth term, from the Bertalanffy-Richards (BR) model. $h(x,y) = \rho xy$, cell-to-cell fusion ; $g(v,x) = \beta xv$	Bajzer *et al.* (2008)
$\frac{dx}{dt} = rx\left(1 - \frac{(x+y)}{K}\right) - \beta xv$ $\frac{dy}{dt} = \beta xv - ay$ $\frac{dv}{dt} = Nay - \delta v - \beta xv$	$f(x,y) = \lambda x\left(1 - \frac{(x+y)}{K}\right)$; Logistic growth; $f(v,y) = Nay$; $g(v,x) = \beta xv$	Tian (2011)

Table 2.2: Table of Model differences

The base oncolytic model with immune response was modeled by Wodarz (2001).

$$\frac{dx}{dt} = rx\left(1 - \frac{x+y}{K}\right) - dx - \beta\, xy$$
$$\frac{dy}{dt} = \beta\, xy + sy\left(1 - \frac{x+y}{K}\right) - ay - p_v y z_v$$
$$\frac{dz}{dt} = c_v y z_v - b z_v$$

where infected cell proliferation rate $sy(1 - \frac{x+y}{K})$;Logistic growth of infected cells

Model 2.3 assumes a CTL response occurred at a constant rate, which is not biologically realistic. The nonlinear CTL response is an immune response proportional to the abundance of CTL and infected cells, cyz, represented in Table 2.3. Similar to the previous model, the nonlinear model of the CTL response also leads to a negative correlation between immune abundance and viral load, if patients differ in their CTL responsiveness, c. The CTL abundance, z, declines for high values of c. When the response rate is high, CTLs destroy viral cells, and thus, there are fewer viral cells to stimulate the immune response, leading to a decrease in z. On the other hand, for low values of c, the correlation is negative, such that patients with small immune response have a low CTL response, leading to high viral loads. This model shows the viral load is, in fact, a better indicator of immune responsiveness, rather the abundance of immune cells. The linear CTL response in an immune response induced at a rate proportional to the abundance of infected cells, but independent of the CTL abundance which gives rise to model 2.3. The main difference in this model is that the equilibrium viral load does not only depend on the immunological parameters, which is more realistic (Nowak and May (2000)).

A model with general immune response was used in (Wang *et al.* (2007)), where CTL proliferation describes the rate of immune response from virus activation and p is the actual rate of immune response. Depending on the assumption, the growth rate of CTL cells, z, from infected cells,y, can have several different representations in model 2.3. This work explored routes to chaos with increase in time delay, when

CTL proliferation is $cy(t-\tau)$. Periodic solutions were found. It is believed the larger time delay of immune response and strength of the lytic term can give rise to viral oscillation in the host (Wang *et al.* (2007)).

Wodarz (2001) represents a base model consisting of 3 variables uninfected tumor cells (x), infected tumor cells (y) and virus-specific CTL cells (z_v).The model assumes a quasi steady state for the viral population, including it in the infected class. The difference here is that logistic growth is assumed for both uninfected and infected tumor cells. The model assumes upon division of infected cells, the virus is passed onto both daughter cells.

As the interest of OVT has grown, mathematical models are gradually increasing. Bajzer *et al.* (2008) introduced a model for a vaccine strain of measles virus to kill tumors, shown in Table (2.2) using the Bertalanffy-Richards (BR) growth model for the untreated tumor growth. The extended death in uninfected cells, ρxy, from $\frac{dx}{dt} = rx\left[1 - \frac{(x+y)^{\epsilon}}{K^{\epsilon}}\right] - \kappa xv - \rho xy$, represents the cell-to-cell fusion with neighboring cells to form syncytia, which ultimately die. The assumptions in this model were that syncytia ultimately cause cell death, such that there is a one to one death of each virus for every uninfected cell. Thus, an elimination term of free virus, βxv, represents the assumed one-to-one cell death from virus to uninfected cancer cell. The growth curve data for untreated tumor were fitted (Dingli *et al.* (2006)) by using Gompertz, logistic (L) and BR models(Bajzer *et al.* (1996) ,Byrne (2003), Marušic *et al.* (1994)). Parameters r, K and ϵ were fit to experimental data for multiple myeloma xenografts grown in SCID mice (Dingli *et al.* (2004)) and parameters were estimated using Monte Carlo simulations. These works suggest weakly cytopathic viruses, i.e. small a cause more tumor cytoreduction than viruses that destroy cells rapidly.

Table (2.2) includes the model Tian (2011), presentes the replicability of an oncolytic virus. This model includes the burst size of virions, N, viral compartment

to compensate for infectious growth rate, and death of virus upon infection, $-\beta xv$. The analysis of this model shows that there are two threshold values of the burst size. Below the first threshold, the tumor will grow to its maximum carrying capacity, K. Above this threshold, there is a locally stable positive equilibrium solution appearing through a transcriptional bifurcation. At or above the second threshold, a family of Hopf bifurcations arise, as there are one or three groups of periodic solutions. The study suggests the tumor load can drop to a near undetectable level during the oscillation or when the burst size is ample Tian (2011).

These base models all suggest the cytotoxic infected cell death rate, a, is of importance to the abundance of uninfected cancer cells (Bajzer *et al.* (2008), Tian (2011), Nowak and Bangham (1996)). Regardless of the changes in the model, they suggest the burst size , $\frac{k}{a}$, or N in (Tian (2011)), will be the contributing factor for the reduction of uninfected tumor cells.

Modeling Dendritic Cells

There is much literature that captures the dynamics between tumor and immune system (Kareva *et al.* (2010), Kareva and Hahnfeldt (2013), Kirschner and Panetta (1998), de Pillis *et al.* (2006), de Pillis *et al.* (2005), Wodarz *et al.* (1998),Worgall *et al.* (1997)).

Dendritic cells are professional antigen presenting cells. Dendritic cell vaccines have been used with some success in clinical studies of immunotherapy for a variety of cancers. Portz and Kuang (2013) modeled the efficiency of dendritic cell vaccines when used in combination with continuous or intermittent androgen deprivation therapy (Kuang *et al.* (2016)) .

Kareva and Hahnfeldt (2013) discussed how tumors escape recognition by the adaptive immune systems. Dendritic cells have shown to switch to glycol's in an

activate state. In the tumor microenvironment, however, the DCs activation is often suppressed, which produces an expansion of immature myeloid cells (MDSCs). The activation of the adaptive immune response comes from the activity of the innate immune response. was modeled for (Kareva *et al.* (2010)). Kareva *et al.* (2010) modeled predator-prey dynamics between immune cells: antigen presenting cells, mature myeloid cells and mature myeloid cells with the prey, as the cancer. Their results suggest in the absence of treatment and having a weak immune system, cancer cells grow unrestrained. If the number of cancer cells in the body is low enough, however, there exists a region where the patient can recover without treatment for a sufficiently stimulated immune system. This dissertation will investigate how the immune response and immune system as a means of therapy effect tumor size.

Chapter 3

MATHEMATICAL ASSESSMENT OF ONCOLYTIC VIROTHERAPY

Oncolytic virotherapy is a targeted therapy that uses engineered viruses to selectively kill and infect cancer cells with the goal to have them eliminated. Deterministic population models have been considered to represent these interactions (Wodarz (2001),Wodarz (2003), Wu *et al.* (2001), Dingli *et al.* (2006) and Bajzer *et al.* (2008)). Replicative adenoviruses have been tested in clinical trials for head and neck cancer (Nemunaitis *et al.* (2001)), as well as metastatic colon carcinoma (Reid *et al.* (2002)). This work represents the viral-tumor interaction with immune presence, with the goal to minimize the uninfected cancer cell population, x.

3.1 Model

We have here an ODE system of four variables: the population sizes of uninfected cancer cells,x; infected cancer cells,y; CTL abundance, z; and free viral particles, v. The uninfected cancer cells grow logistically at intrinsic rate of increase r, representing the rate of maximum uninfected tumor cell growth and dies at rate μ. The carrying capacity of the tumor population, K, including both uninfected and infected tumor cells, competing for space. Free virus particles infect uninfected cells at a rate proportional to the product of their abundances, βxv. The rate constant β includes the effectiveness of this action, which includes the contact rate and probability of successful infection. Since the model is assuming the virus is passed onto both daughter cells, the infected tumor cells grow logistically by term $sy\left(1-\frac{x+y}{K}\right)$, at rate s and are lysed by the virus at rate, α. The free virions production rate is the burst size, N times the infected cell mortality rate, αy, assuming cells die when they shed virus.

The model is shown below:

$$\begin{aligned}
\frac{dx}{dt} &= rx\left(1-\frac{x+y}{K}\right)-\mu x-\beta\, xv \\
\frac{dy}{dt} &= \beta\, xv+sy\left(1-\frac{x+y}{K}\right)-\alpha y-\rho yz \\
\frac{dz}{dt} &= \sigma yz-\phi z \\
\frac{dv}{dt} &= N\alpha y-\xi v
\end{aligned} \tag{3.1}$$

The nonlinear term σyz is the proliferation of CTL cells in response to viral antigens and the term ρyz represents the killing of infected cells by CTL cells. In the absence of antigenic stimulation, CTL cells die at rate ϕ. The oncolytic virus is produced at lysing rate α and dies at rate ξ. A description of variables and parameters used is represented in Table 3.1.

Table 3.1: Model Description of Variables and Parameters

Variable	Description
x	Uninfected cancer cells
y	Infected cancer cells
z	CTL abundance
v	Free Viral Particles
Parameter	Description
r	Maximum uninfected tumor cell growth rate
μ	death rate for uninfected cells
K	Carrying capacity of overall tumor population
β	Viral infectious rate
s	Growth rate of infected cancer cells.
ρ	CTL response rate
ϕ	immune cell decay rate
N	Viral burst size
ξ	viral decay rate

3.2 Analysis

Proposition 3.2.1. (3.1) *is positive invariant.*

Let $\Delta = \{(x, y, z, v) : 0 \leq x + y \leq K, 0 \leq z(t), 0 \leq v(t)\}$.

If $\Big(x_0, y_0, z_0, v_0\Big) \in \Delta \rightarrow \forall t\Big(x(t), y(t), z(t), v(t)\Big) \in \Delta$.

Stability and Existence

The stability of the fixed points can be studies with the eigenvalues in the linearized system around the fixed points :equilibria with negative real parts are stable, positive real parts are unstable (Strogatz (2014)).

The system (3.1) has six steady states:

$E_0 = (0, 0, 0, 0)$, $E_1 = (\frac{K(r-\mu)}{r}, 0, 0, 0)$, $E_2 = (0, \frac{K(s-\alpha)}{s}, 0, \frac{NK\alpha(s-\alpha)}{s\xi})$,

$E_3 = (0, \frac{\phi}{\sigma}, \frac{\sigma K(s-\alpha)-s\phi}{\sigma\rho K}, \frac{\phi N\alpha}{\sigma\xi})$,

$E_4 = (\frac{\xi(\xi(\alpha r-\mu s)-\beta KN\alpha(s-\alpha))}{\beta N\alpha(\beta KN\alpha+\xi(r-s))}, \frac{\xi(\beta KN\alpha(r-\mu)-\xi(\alpha r-\mu s))}{\beta N\alpha(\beta KN\alpha+\xi(r-s))}, 0, \frac{\beta KN\alpha(r-\mu)-\xi(\alpha r-\mu s)}{\beta(\beta KN\alpha+\xi(r-s))})$,

$E_5 = \frac{\xi(r(\sigma K-\phi))-K(\beta N\alpha\phi+\sigma\xi\mu)}{\sigma r\xi}, \frac{\phi}{\sigma}, \frac{\beta KN\alpha[(\xi)(\sigma(\mu-r))-\beta N\alpha\phi(1+\xi(s-r))]-\xi^2[\sigma(\mu s-\alpha r)]}{\sigma r\rho\xi^2}, \frac{\phi N\alpha}{\sigma\xi})$

For the stability and existence, please refer to Table(3.2)

Theorem 1. *In the model* (3.1) *trivial equilibrium,* $E_0 = (0, 0, 0, 0)$. E_0 *is L.A.S whenever*

$$r < \mu, \qquad s < \alpha,$$

otherwise E_0 *is unstable.*

Proof: See Appendix.

Theorem 2. *The model* (3.1) *has boundary equilibrium* E_1 *if and only if* $r > \mu, s < \alpha$. *In case of* $\alpha r - \mu s > 0$, *the Viral Free Equilibria (VFE),* E_1, *is locally-asymptotically stable if and only if* $R_0 < 1$ *and unstable* $R_0 \geq 1$. *In case of* $\alpha r - \mu s < 0$ E_1 *is unstable.*

Proof: See Appendix.

Theorem 3. *Let $s > \alpha, r < \mu$. Model* (3.1) *has complete viral prevalence at E_2 is locally asymptotically stable whenever* $\sigma < \frac{\phi s}{K(s-\alpha)}$

Proof:See Appendix.

Theorem 4. *Let $s > \alpha, r < \mu, \sigma > \frac{\phi s}{K(s-\alpha)}$. Model* (3.1) *has a boundary equilibrium point E_3 and it is locally asymptotically stable whenever $r < \frac{K}{K-\frac{\phi}{\sigma}}(\mu + \frac{\beta N \alpha \phi}{\sigma \xi})$, otherwise it is unstable.*

Proof: See Appendix.

Table 3.2: Existence Table in the Positive cone

Eq. Point	Case I	Case II	Case III	Case IV	Case V	Case VI
	$s < \alpha$, $r < \mu$	$s < \alpha, r > \mu$	$s > \alpha, r < \mu$, $\sigma < \frac{\phi s}{K(s-\alpha)}$	$s > \alpha, r < \mu$, $\sigma > \frac{\phi s}{K(s-\alpha)}$	$s > \alpha, r > \mu$, $\sigma > \frac{\phi s}{K(s-\alpha)}$	$s > \alpha, r > \mu$, $\sigma < \frac{\phi s}{K(s-\alpha)}$
E_0 (0,0,0,0)	Exist, Stable	Exist, Unstable	Exist, Unstable	Exist, Unstable	Exist, Unstable	Exist, Unstable
E_1 (x^*,0,0,0)	Not Exist	Exist, Stable	Not Exist	Not Exist	Exist, Unstable	Exist, Unstable
E_2 (0,y^*,0,v^*)	Not Exist	Not Exist	Exist, Stable	Exist, Unstable	Not Exist	Not Exist
E_3 (0,y^*,z^*,v^*)	Not Exist	Not Exist	Not Exist	Exist, Unstable	Exist, Unstable	Not Exist

Table 3.2 represents the conditions for any one of the 6 equilibria to exists. Case descriptions:

When $s < \alpha$, this represents the growth of the infected cancer cells is less than that of it's cytotoxic cell death, also referred as the lysing rate. Therefore, when $s < \alpha$, E_0 and E_1 could exist, depending on other conditions. Else, for $s > \alpha$ E_2, E_3, E_4 and E_5 could exist.

When $r < \mu$, this represents the growth of the uninfected cancer cells is less than that

of it's death rate. Therefore, when $r < \mu$, E_0, E_2 and E_3 could exist. Else, for $r > \mu$, E_1, E_4 and E_5 could exist

When $\sigma < \frac{\phi s}{K(s-\alpha)}$, the cell response rate is not high enough for the existence of the CTL population at equilibria. Therefore, when $\sigma < \frac{\phi s}{K(s-\alpha)}$, E_0, E_1, $E_2$and E_4 can exist. Else, E_3 and E_5 exist.

The Trivial Equilibrium, E_0, exist for all values of the parameters. Biologically, this condition has little relevance as it is unrealistic all populations will tend to zero. Further, it we are investigating the growth of cancer, which must allow for $r > \mu$. Else, for $r < \mu$, the cancer cells would have been dying faster than they would be growing, which would have prevented the birth of a tumor.

The Virus Free Equilibrium (VFE), E_1 has at least one non-zero entity.

$E_1 = (\frac{K(r-\mu)}{r}, 0, 0, 0)$ exist only if *and only if* $r > \mu, s < \alpha$. Let

$$R_0 = \frac{\beta N \alpha K\Big(1 - \frac{\mu}{r}\Big)}{\xi\Big(\alpha - \frac{\mu}{r}s\Big)}$$

Further, R_0 is L.A.S when $\beta < \frac{r\xi}{NK(1-\frac{\mu}{r})}$

R_0, the basic reproductive number, represents the average number of newly infected cancer cells produced from one viral cell during the treatment period (Brauer *et al.* (2001)).

The condition for stability of E_2 depends on σ staying below a given threshold. Biologically, this could represents the suppression, inactivity or delayed immune response to the viral infection. The first conditions found are where anti-viral CTL response is established. The condition of this response varies depending if the virus has obtained 100% prevalence or not.

3.3 Model Fitting

Experimental design

The majority of clinical trials performing OV have been administered via intratumoral injection. Few studies have examined regional or intravenous delivery (Prestwich *et al.* (2008)). The data used for this work is from (Huang *et al.* (2010)). The goal of the experiment was to use gene-based cytokine treatment as a means of therapy. There were 8-9 mice in each group, where each subject with B16-F10 subcutaneous murine melanoma were intratumorally injected with various treatments. First, PBS, which is a saline, resents the control group with no treatment. The second treatment was Ad-ΔB7, which is a modified adenovirus. The third treatment was Ad-ΔB7/IL-12 , the modified adenovirus with the interleukin, IL-12 attached. The fourth was the adenovirus expressing IL-12 and a cytokine molecule, 41BBL,Ad-ΔB7/4-1BBL. The fifth treatment was adenovirus expressing both Il-12 and 41BBl, Ad-ΔB7/IL-12/4-1BBL. Mice injected with phosphate-buffered saline (PBS) rapidly formed large tumors, over 3,000 mm^3. On day 12, the tumors were large enough that the mice were killed. The mice with oncolytic Ad treatment were associated with growth inhibition. Twelve days post treatment, the mean tumor volume for tumors treated with Ad-ΔB7, Ad-ΔB7/IL-12 , Ad-ΔB7/4-1BBL or Ad-ΔB7/IL-12/4-1BBL were $1,265 \pm 155, 383 \pm 71$, and 136 ± 22 mm^3, respectively showing 60, 88, 89 and 96% tumor growth inhibition compared to the PBS group.

Parameter Fitting

The model was fit to experimental data from (Huang *et al.* (2010)) and (Kim *et al.* (2015a)) under particular assumptions. The fitting was done in MATLAB using the nonlinear least squares solver, *lsqnonlin*. Parameters N, ξ, α, K and ϕ were estimated

from prior sources. The oncolytic adenovirus burst size of virions, $N = 3500$, was used from an experiment of a prostate specific adenovirus variant (Chen *et al.* (2001),Kim *et al.* (2015a)). The viral decay rate, $\xi = 2.3$ is used from (Kim *et al.* (2015a)), estimated from (Li *et al.* (2008),Wang *et al.* (2006)). The lysing rate $\alpha = 1$, represents the time for infected cells to undergo lysis on average of once per day, as 90 percent of viruses exit the tumor site in one day (Worgall *et al.* (1997)). The carrying capacity, $K = 4000 \times 10^6$, is estimated as the data is rounded up to the nearest thousandth, i.e the ceiling of the size of death for mice. CTL death rate, $\phi = 0.35$ was shown in (De Boer *et al.* (2001)).

Parameters r, μ, β, s, σ and ρ were fit to experimental data that measured the overall tumor growth (X+Y) over time during treatment of oncolytic adenovirus. The data was fit to the following three conditions: i) Phosphate buffered saline (PBS), or the control group, ii) Ad-ΔB7, and iii)Ad-ΔB7/IL-12 [Fig 2a, (Huang *et al.* (2010))]. Two additional experiments were done for the combination of Ad-ΔB7/4-1BBL and Ad-ΔB7/IL-12/4-1BBL, but were not fit to (3.1), as its co-stimulatory properties expressed on antigen presenting cells are not a variable in this model. The initial conditions for the three data sets were used from the experiment as: $(73.7, 0, 0, 0), (59.2, 0, 0, 10^{10})$ and $(74.6, 0, 0, 5 * 10^9)$. Note, the experiment for Ad-ΔB7/IL-12 will display immune stimulatory effects from IL-12, thus, where T cells are not initially present, their production is further stimulated.

Parameter	Description	PBS	Ad-ΔB7	Ad-ΔB7/IL-12
r	Uninfected tumor cell growth rate	0.43	0.33	0.17
μ	uninfected tumor cell death rate	0.0008	0.0008	0.0008
β	Viral infectious rate	-	$1 * 10^{-13}$	$1 * 10^{-12}$
s	Infected tumor cell growth rate	-	$[1, 1 * 10^{3}]$	$[1, 1 * 10^{2}]$
σ	CTL response rate	-	-	$[0.1, 4]$
ρ	death from CTL cells	-	-	$[0.01, 1]$
K	Carrying capacity	$4000 * 10^{6}$	$4000 * 10^{6}$	$4000 * 10^{6}$
N	Burst size of virions	-	3500	3500
ξ	viral decay rate	-	2.3	2.3
α	lyse rate	-	1	1
ϕ	CTL death rate	-	-	0.35

Table 3.3: Parameter estimates for model (3.1). The top 6 parameters were fit to data. The bottom 5 were fixed from previous sources.

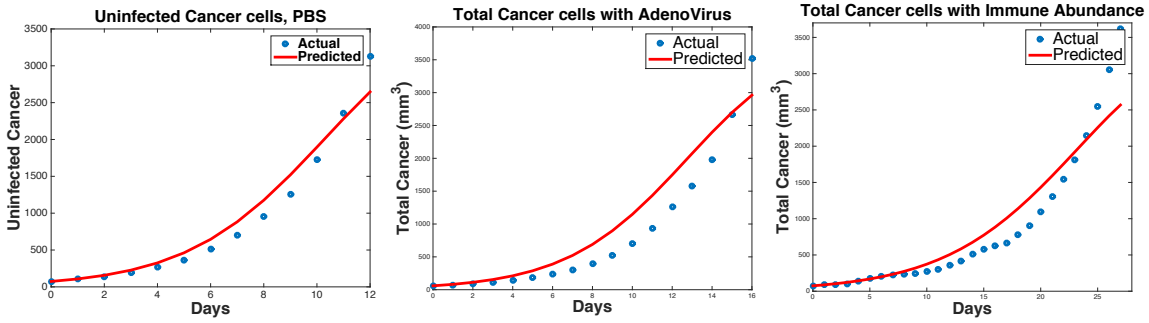

(a) (b) (c)

Figure 3.1: Parameter fit to a)PBS data, for $r = 0.43, \mu = 0.0008$. b)Parameter fit to adenovirus data, $r = 0.33, \beta = 1 * 10^{-13}, s = 1$. c) Parameter fit for adenovirus with immune response; $r = 0.17, \beta = 1 * 10^{-12}, \sigma = 3.7, \rho = 0.82$

Figure (3.1) represents the parameter fits from experimental data using oncolytic virotherapy (Huang *et al.* (2010)). First, the model fit for parameters r and μ compared from the control group. Those values, were then used as the base to estimate the values to fit for treatment, r, μ, β, s. The estimates for the treatment fit were used as the base to estimate the parameters used for treatment in the presence of immune response, fitting for r, μ, β, s, σ, and ρ. There are three key insensitive parameters: s, σ and ρ that carry similar numerical dynamics for a range of values. The values listed in Figure (3.1) were true to the values used in the figure, however, the same results exist for Fig. (3.1 b) for $s = [1, 10^3]$ and Fig. (3.1 c) for $s = [1, 10^2], \sigma = [0.1, 4]$ and $\rho = [0.01, 1]$.

Simulations

Substituting parameter values fit to data for initial conditions $(74.6{*}10^6, 0, 0, 5{*}10^9)$. These values are experimental initial conditions (Huang *et al.* (2010)).

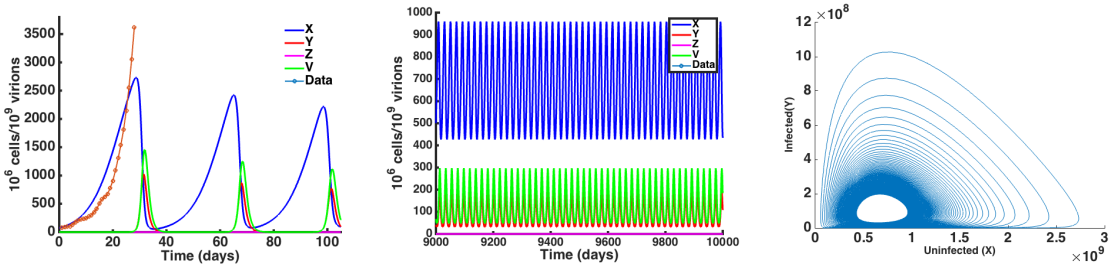

(a) (b) (c)

Figure 3.2: Sustained oscillations for $E_4 : \beta > \beta_c$ a) Plots all population over the data, showing sustained oscillation for uninfected and infected cancer cells, as the viral population oscillates. b) Shows oscillations persist later in time. c) Phase portrait of sustained oscillations

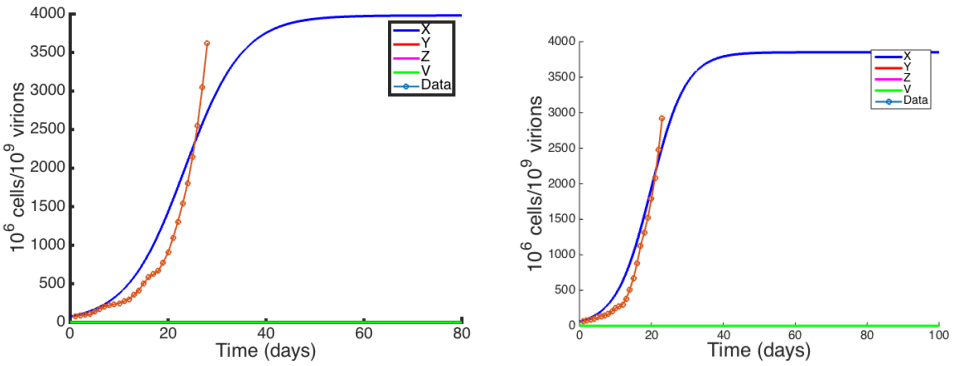

(a) (b)

Figure 3.3: a) Viral free equilibria at $E_1 : \beta < \beta_c$. b) For $Z_0 = 1, E_1$ is reached.

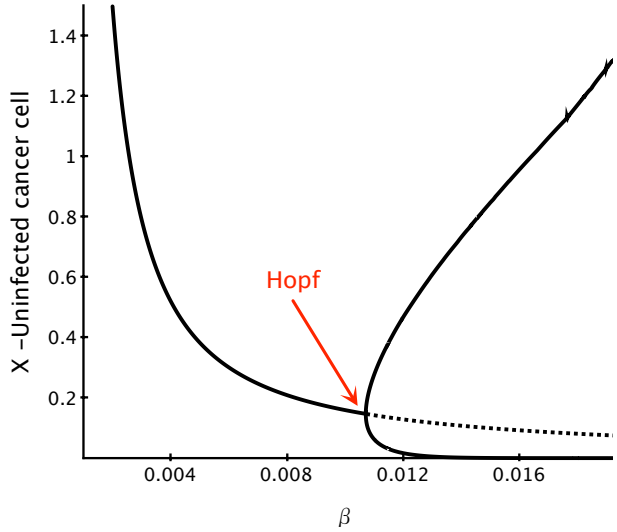

Figure 3.4: Hopf bifurcation diagram of, shown stable to unstable as β increases

We can see in Figure (3.2) that the natural equilibria for these values are $E_4 = X^*, Y^*, 0, V^*$. There are sustained oscillations that appear as β changed threshold values, which numerically verify the Hopf bifurcation. Extending time to 27 years,4 months and 6 days; or 10,000 days, we can see oscillations continue to occur. At this point, $R_0 > 1$ since $\beta > \beta_c$; $R_0 = 6.09, \beta = 1e-12, \beta_c = 1.65e-13$. In Figure(3.3), $\beta < \beta_c, \implies R_0 < 1$. $\beta = 1e-13, \beta_c = 1.65e-13$ and $R_0 = 0.6$. Note: Figure 3.4

represents the qualitative behavior of the Hopf bifurcation, however, the quantitative parameter values were not used here.

Viral reproducibility: Viral reproducibility is the duplication or process of making a copy of viral cells. We can look at the dynamics of viral reproducibly, by changing s. In the absence of immune system, at E_4 and $t = 1000$, we can change s to be on or off, (1,0). The populations to the solutions for the total tumor size (X+Y)=TumorTot, with Xtot, Ytot, Vtot as the total sizes for uninfected, infected and viral populations. The total population sizes from s=(1,0) are TumorTot=(5.42E+08,5.45E+08); Xtot=(4.34E+08,4.35E+08); Ytot=(1.08E+08,1.1E+08) and Vtot=(1.85E+11,1.87E+11); respectively. Based on the values from model (3.1), there is little to no change in the overall populations from including the viral replication. This could suggest that upon viral engineering or viral selecting, under immune suppression, there is little to no effect whether the virus can self replicate or not. This is due to the initial viral load being able to be replicated upon the lysing of infected cells.

3.4 Discussion

This chapter was able to highlight the third goal of this dissertation, to shed light on the dynamics of continuous oncolytic viraltherapy with immune response. There are many improvements model (3.1) can benefit from. A major modification of this model was to incorporate $sY\left(1-\frac{(X+Y)}{K}\right)$ with viral production term $N\alpha y$. It is not practical that infected growth rate s, can fluctuate with little quantitative nor qualitative change in overall tumor population. Thus, the condition representing, $sY\left(1-\frac{(X+Y)}{K}\right)$ must change according to a more detailed understanding of the positive feedback upon infected cancer cells.

Absence of immune response could happen for some period of time for oncolytic viruses that are polymer coated (Cattaneo *et al.* (2008)). Coating viruses with non-antigenic polymers is a method of blocking antibody recognition (Green *et al.* (2004).) The coated viruses deflect the immune system by being coated with polyethylene glycol (PEG), which physically blocks the adhesion of proteins that carry foreign antigens, that are attacked by macrophages. These coats delay the onset of the immune response, but do not prevent it Phys.org (2013). The nonlinear term σyz will not have any immune population whenever infected cells are not present. This is biologically unrealistic; thus, the model needs to include σy to represent immune response term. This model does not capture the immune stimulation by the OV, and ought to include an immune response to the uninfected cancer cells, such as $\rho_T xz$.

Regarding the burst size, N, previous models suggest the birth size is a contributing factor to the reduction of uninfected tumor cells (Bajzer *et al.* (2008), Tian (2011), Nowak and Bangham (1996)). Based off these works, one could propose that an increase in N would decrease the uninfected cells. It is important to find biologically realistic values that support types of replicating viruses with higher burst sizes, and then incorporate into an extended model. It is suggested that immune response may affect the parameters determining viral reproduction. CTL mediated lysis may increase the death rate of infected cells, α. Cytokines released by CD8 or CD4 positive T cells could reduce the infectivity parameter β and/or the viral production rate, in this model is α as well (Nowak and May (2000)).

Death rate of uninfected cells, μ can be eliminated, as its value is least sensitive, small and could be clumped into a maximal growth rate r; r=(growth-death) rate. Lastly, the impulses of the virotherapy must be introduced via a delta function of the type $u(t) = u_0\delta(t) + \delta(t-2) + \delta(t-4)$, for improved parameter fit accuracy. The

model needs to investigate treatment regimes, with regards to frequency and dosage quantity.

Chapter 4

OPTIMIZING COMBINATION ONCOLYTIC VIRAL AND IMMUNO-THERAPY TREATMENT STRATEGIES WITH A PREDICTIVE MODEL

4.1 Introduction

This chapter investigates dosage regimes for oncolytic virotherapy, combined with dendritic cell vaccine, in order to address which is the most beneficial to reduce tumor size, with minimal relapse. After developing these regimes, the most optimal was implementing into an intermittent schedule regimen. The general goal is to investigate how sensitive tumor reduction is to combination intermittent oncolytic viral therapy and immunotherapy. First, this chapter will develop a mathematical model that can represent clinical variations for administering oncolytic viral therapy. Then the model will be parameterized using empirical data. The results then identify optimal treatment strategies for varying dose sizes and treatment schedules, that could be used towards a proposed model for personalized medicine.

Dendritic cell therapy stimulates anti-tumor responses by causing dendritic cells to present tumor antigens, such as Tumor-Specific Antigens(TSA) or Tumor-Associated Antigens (TAA). The immune system is adept at pathogen recognition and provides receptors specific to pathogen-associated molecular patterns, which included toll-like receptors (TLR) (Prestwich *et al.* (2008), Pichlmair and e Sousa (2007)). The innate immune response can provide an important link to the generation of adaptive immune responses. Dendritic cells play a critical role in the early immune response. Dendritic cells are professional antigen presenting cells and are key in innate immune responses, as they transfer information to the T cells, regarding the identity of foreign antigens.

A deterministic mathematical model consisting of of 5 differential equations was developed to predict changes in tumor size in response to virotherapy, immunotherapy and combinations of both. Various types of oncolytic adenoviruses expressing various immunostimulatory molecules represent the virotherapy. Mathematical models using dendritic cell treatments been done by (Kareva *et al.* (2010), Kuang *et al.* (2016), Portz and Kuang (2013)).

To better understand which regimen would be best, a clinical trial table was produced in order to gain clinical insight to use in the model. The type of cancer is foremost in order to find which cancers are being treated with oncolytic viraltherapy on people. The name of the drug and company who owns the name, in order to see which drugs are beings used on cancers with a name specific to a certain virus. The phase of the trial can give information pertaining to the quantity of people involved. The route of administration can have an effect on the viral infectivity rate or maximum uptake rate of drug. The key focus lies in the quantity of drug, schedule and whither there is and immune combination. It is important to see the quantities for its count and order of magnitude of OVs. The schedule of the OV could differ per cancer and/or virus, thus, ideas for intermittent treatment types could be gathered. Since this work considers immunotherapy, an option for whither or not immune combination of any sort was used, is included without bias.

Cancer /Stage	O-Virus	Drug Name	Company	Phase Trial	R.O.A$_V$[1] R.O.A$_I$[2]	Quantity$_V$ (pfu/ml)	Schedule	Immune-Combo	Cite
Melanoma IIIB-IV	HSV-1	T-VEC	AMGen	III	I-LES[3] Sub-C$_I$[4]	10^6 10^8 10^8	D1-WK1; D2-WK4; DN+/2WKS; ≤ 24 wks; ≤ 48 wks(1 yr/ D1) $\leq$ 72wks (18mos from D1)	Option(OR) GM-CSF $125\mu g/m^2$ 14 Days(daily)	Andtbacka *et al.* (2015)
Varied:NSCLC, Col,Mel,Thy, Pan,Ova,Gas, Lei, Mes	Vaccinia Poxvirus	JX-594 (Pexa-Vec)	Jennerex	I	I-VEN	1×10^5,1×10^6, 3×10^6,1×10^7, 1.5×10^7, 3×10^7 *(pfu/kg)	Singe infusion	Express: GM-CSF, β-gal	Breitbach *et al.* (2011)
Ova, Mes	Adenovirus	Ad5-D24-GMCSF		I	I-VEN I-CAV	D1; 8×10^9. Doses escalate to: 1×10^{10}, 3.6×10^{10}, 1×10^{11}, 2×10^{11}, 2.5×10^{11}, 3×10^{11},and 4×10^{11}	Single infusion	GM-CSF	Cerullo *et al.* (2010)
Liver Cancer	Vaccinia Poxvirus	Pexa-Vec	Jennerex	II	I-VEN	Low 10^8; High 10^9	Infused low and high dose on D1, D15 & D29	No. Inserted GM-CSF and β Gal	Heo *et al.* (2013)
Gastrointestinal Carcinoma	Adenovirus	Onyx-015	Onyx Pharmaceuticals	II	HAI	2×10^{12}	D1,D8 . Chemotherapy administered on D22	-	Reid *et al.* (2002)

Table 4.1: Various clinical trials using OVs to seek treatment types

Table 4.1 was created to gain insight on some key components of using OVTs clinically. The main focus of this table is expressed in columns Quantity, Schedule

and Immune-Combo. The clinical variability within these columns could imply there in not enough suggested OV dose quantity pertaining to a particular schedule, with or without a source of immunotherapy. Therefore, there are opportunities to explore the these variations which will be a key motivation within the construction of model in this work.

4.2 Materials and Methods

4.2.1 Experimental Design

The experiment done by (Zhang *et al.* (2011)) varied the anti tumor effect of an IL-12 and GM-CSF co-expressing oncolytic Ad, Ad-Δ B7/IL-12/GMCSF, with dendritic cells. Ad- Δ B7 is an oncolytic adenovirus, with mutations in the retinoblastoma binding sites of E1A and has the E1B binding region deleted, shown in Figure 4.2. The E1A region has a paradoxical functionality such that they act as oncoproteins and tumor suppressor proteins, i.e; both stimulating cancer growth and suppressing it (Frisch and Mymryk (2002)). The creation of Ad-Δ B7/IL-12/GMCSF was generated by inserting shuttle vectors expressing murine IL-12 and GM-CSF genes into the E1 and E3 regions of the Ad- Δ B7 viral vector, respectively. Shuttle vectors are vectors constructed to propagate into two different host species. Thus, DNA inserted into a shuttle vector can be tested or manipulated in two different cell types (Lodish *et al.* (2000)). It has been previously confirmed that Ad-ΔB7/IL-12/GMCSF expresses cancer-specific viral replication and cytotoxicity (Kim *et al.* (2007)).

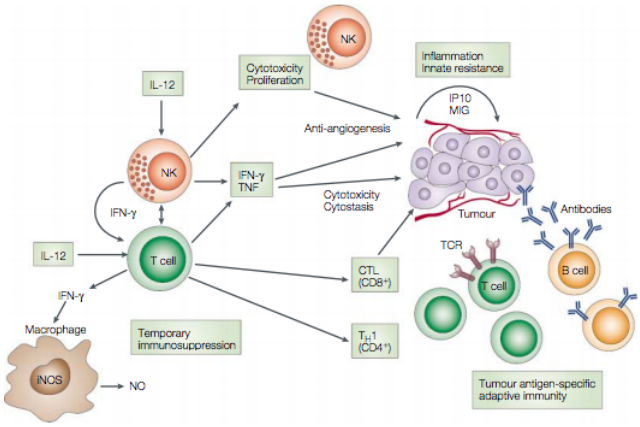

Figure 4.1: The anti tumor activity of IL12 shown. Cytotoxic lymphocytes, $CD8^{+}$T cells, natural killer (NK) and NKT cells, are often involved in the mechanism of action of IL-12 (Trinchieri (2003)).

Dendritic cells were derived from bone marrow cells harvested from cavities of femurs and tibias of C57BL/6 mice (Zhang *et al.* (2011)). The dendritic cells were isolated and grown. Male mice of 6-7 weeks of age, of type C57BL/6, a common inbred strain of laboratory mice, were injected subcutaneously into the right abdomen with 5×10^5 cultured murine melanoma B16-F10 cells.

When the tumor volumes reached around 120-130 mm^3, mice were sorted into groups with similar tumor volumes. The five treatment groups included phosphate-buffered saline (PBS) only, as the control, 5×10^9 viral particles/injection of Ad-ΔB7/IL-12/GMCSF only, 1×10^6 particles/injection of DCs only, combination of 5×10^9 viral particles/injection of Ad-ΔB7/IL-12/GMCSF and 1×10^6 particles/injection of DCs and combination treatment of 5×10^{10} viral particles/injection of Ad-ΔB7/IL-12/GMCSF and 1×10^6 particles/injection of DCs. The last combination was referred as the high dose combination therapy. The mice were injected with three doses of Ad-ΔB7/IL-12/GMCSF on days 0-2. For the combination treatment, the mice were

then injected with three doses of DC's on days 3-5. The minimum number of mice per experiment was seven. Tumor growth was monitored every other day. The tumor volume was calculated with a caliper with the formula volume= 0.523 LW^2. Mice with tumor size $> 3{,}000$ mm^3 were sacrificed for ethical purposes. Empirical data is presented in Figure **??**.

IL-12 and GM-CSF expression were determined using an ELISA in accordance with the manufacturers's instructions. ELISA stands for "enzyme-linked immunosorbent assay", a rapid immunochemical test that involves an antibody or antigen (immunologic molecule). A schematic representation of the genomic stitchers of adenovirus Ad-ΔB7 and Ad-ΔB7/IL-12/GMCSF is displayed in Figure 4.2. The open star represents the mutation at the retinoblastoma protein binding site, lacking E1B 19 and ΔE1B; and ΔE3. Murine IL-12 and GM-CSF were inserted into E1 and E3 regions of the Ad-ΔB7 genome, respectively (Zhang *et al.* (2011)). DCs were labeled with CellTracker Red CMTPX on day 6 of DC culture and harvested on day 8. The tumor-bearing mice were intramurally injected with 1×10^6 DCs alone for 3 days or intratumorally injected with Ad-ΔB7/IL-12/GMCSF at 5×10^9VP/injection or 5×10^{10}VP/injection three time prior to DC injection.

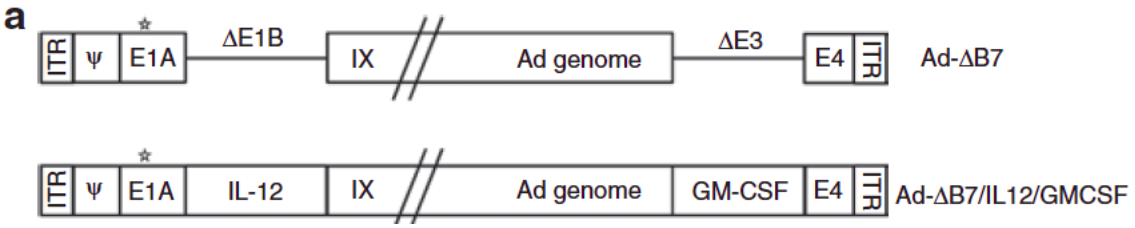

Figure 4.2: Characterization of the oncolytic adenovirus co-expressing interleukin 12 (IL-12) and (GM-CSF)

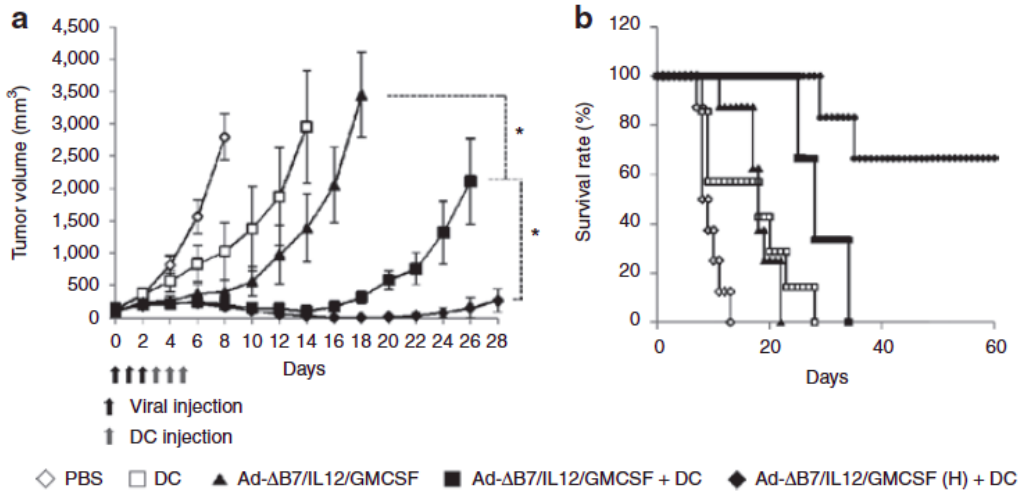

Figure 4.3: Data from Figure 2 Zhang *et al.* (2011) represents the anti tumor effect of Ad-Δ B7/IL-12/GMCSF in combination with dendritic cells (DCs)

4.2.2 Model Development

With the base model constructed in Chapter 3 and the pre-clinical approaches used for combination oncolytic and immunotherapy, Model 4.1 is constructed to find tumor volume changes over different doses, schedules and immune combination.

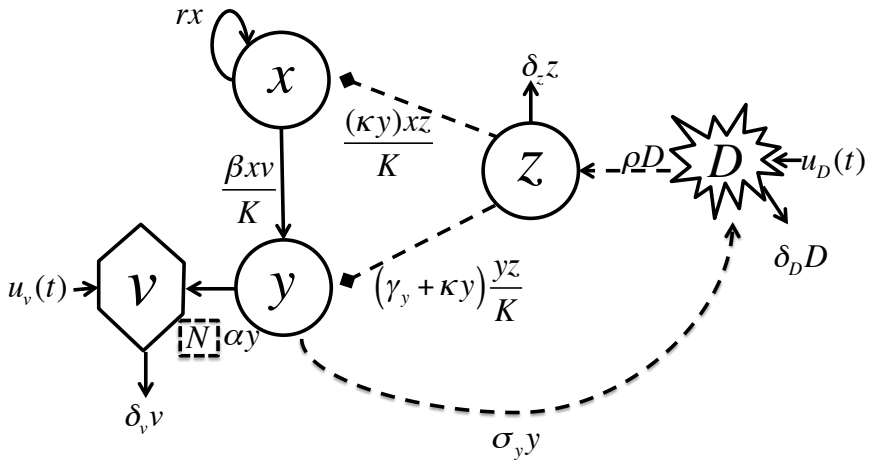

Figure 4.4: Model schematic. Solid lines depict model flow between compartments. Dashed lines depict interactions between compartments.

Uninfected cells grow exponentially at intrinsic growth r, and are destroyed by T killer (CTL) cells at rate κ. The term κy is dependent on infected cells, as oncolytic viruses facilitate immune response, here via the T killer cells towards the tumor. Uninfected cancer cells are infected at rate β, as standard incidence, where carrying capacity $K = x + y + z + D$. Free viral particles are grown from lysing rate α with burst size N, and decays at rate δ_v. Viruses have several ways of shedding. The model assumes viral shedding is done through apoptosis. The mechanisms by which this happens in the model is via an abundance of viral particles that cause the cell to explode, releasing viral progeny at rate $N\alpha y$ and by stimulating the immune to attack by OV facilitation rates: $\kappa y\frac{yz}{K}$ and $\kappa x\frac{yz}{K}$. T killer cells are activated by dendritic cells at rate ρ and are deactivated at rate δ_z. Furthermore, ρ is representing the enhanced activation/maturation of the dendritic cells via cytokine and interleukin attachments: GM-CSF and IL-12. Since the model assumes the immune system functions only in the presence of oncolytic virus, the dendritic population,D, depends on σ_y, the infected population. The infected population only exists when there is an oncolytic virus. Thus, the assumption is the immune response depends on the oncolytic virus. This is due to the understanding that a tumor microenvironment inhibits the cancer cells from interacting with immune activation and response signals. The oncolytic viral immunogenicity trait further enhances the immune response to infected cells, at rate γ_y. In Appendix 2, a model constructed in this dissertation included an immune response term for uninfected cancer cells, γ_x, which resulted to be insensitive in the model based off the parameter fit results. Therefore, only γ_y is included in this simplified, full model. Dendritic cells decay at rate δ_D. Therapies are introduced as delta functions for $u_v(t)$ and $u_d(t)$ for virotherapy and immunotherapy. The model has fit to experiment time injections via the delta functions: $u_v(t) = u_0\delta(0) + \delta(2) + \delta(4)$, and $u_d(t) = u_0\delta(1)+\delta(3)+\delta(5)$. This work will alter $u_i(t) = u_0\delta(t-a_i)+\delta(t-b_i)+\delta(t-c_i), i \in \{v, d\}$,

corresponding to the schedule of oncolytic viral and dendritic therapy, to investigate the sensitivity changes on the dynamics.

The equations are as follows:

$$\frac{dx}{dt} = rx - \beta\frac{xv}{K} - (\kappa y)\frac{xz}{K} \tag{4.1a}$$

$$\frac{dy}{dt} = \beta\frac{xv}{K} - \alpha y - (\gamma_y + \kappa y)\frac{yz}{K} \tag{4.1b}$$

$$\frac{dv}{dt} = N\alpha y - \delta_v v + u_v(t) \tag{4.1c}$$

$$\frac{dD}{dt} = \sigma_y y - \delta_d D + u_d(t) \tag{4.1d}$$

$$\frac{dz}{dt} = \rho D - \delta_z z \tag{4.1e}$$

This models variables include x, y, v, z and D representing uninfected cancer cells, infected cancer cells, virus free particles, T killer cells, and dendritic cells, respectively. This model was reduced from (Kim *et al.* (2015a) and Wares *et al.* (2015)). Model 4.1 has fewer variables and parameters, with intensions to gain pre-clinical and clinical insights from a simpler approach. The model in Wares *et al.* (2015) includes an additional variable, with an equation to represent the antigen buffer between infection and dendritic cell. The CTL cells from Wares *et al.* (2015) grow based off antigen presenting cells, dendritic cells and infected cells. Model 4.1 includes only the dendritic cell population for the vaccine count, and CTL cells for the immune attack onto uninfected and infected cancer cells. Further, Model 4.1 keeps CTL population only dependent on dendritic cells, which depends on the infected cell population. Additionally, Model 4.1 accounts for additional immune attack on the infected cell populations due to the nature of the oncolytic virus enhanced immune stimulation trait, $-\gamma_y y$. The delta functions used here in Model 4.1, $u_v(t)$ and $u_d(t)$, are not limited to 6 days, as in Wares *et al.* (2015). Also,Wares *et al.* (2015) used only 3 quantities of each treatment, but Model 4.1 accommodates for extended time functions, depending upon dose limiting conditions.

4.2.3 Parameterization

Model (4.1) was fit to experimental data from Zhang *et al.* (2011). The fitting was done in MATLAB 2014b using the Levenberg-Marquardt algorithm with nonlinear least squares solver, *lsqnonlin*. The solver was ode23.

Parameter	Description	PBS	Ad-ΔB7/ IL12/ GMCSF	Ad-ΔB7/IL12/ GMCSF +DC	Ad-ΔB7/IL12/ GMCSF_H +DC
r	Uninfected tumor cell growth rate	0.385	0.385	0.385	0.385
γ_y	T cell contact rate via IL-12, infected	-	0.5	1	1
σ_y	innate dendritic activation response from infected cells	-	1.2	1.5	0.9
β	Viral infectious rate	-	2.588×10^{-4}	7.5703×10^{-4}	3.12×10^{-5}
κ	T cell killing rate facilitated by OV	-	5×10^{-5}	7×10^{-5}	1.5×10^{-3}
ρ	adaptive T cell activation rate by dendritic cells via GM-CSF	-	10	0.8	1
δ_z	T cell decay rate	-	0.35	0.35	0.35
δ_D	Dendritic cell death rate	-	0.35	0.35	0.35
u_{0V}	Adenovirus concentration	-	5×10^9	5×10^9	5×10^{10}
u_{0D}	Dendritic concentration	-	-	1×10^6	1×10^6
N	adenovirus burst size	-	-	3500	3500
α	Infected lysis	-	-	1	1
δ_V	Viral decay rate	-	-	2.3	2.3

Table 4.2: Parameter estimates for Model (4.1). Values obtained using nonlinear least squares, lsqnonlin, to fit the model to empirical data from Zhang *et al.* (2011).

Parameter estimates were obtained for six parameters, as seven were estimated from previous literature, described from (4.1). The exception is ρ, as we allow ρ to be fit here. ρ represents the T cell activation rate by dendritic cells; therefore, it will represent the effect of GMCSF and IL-12. The experiment done in Zhang *et al.* (2011) varied the anti tumor effect of an IL-12 and GM-CSF co-expressing oncolytic Ad, Ad-Δ B7/IL-12/GMCSF, with dendritic cells.

One is required to sacrifice a mouse with tumor size greater than 3,000 mm^3. The data points represent the mean $\pm$ standard error for the combined tumor sizes of the mice shown in Figure**??**. The control group of PBS only allowed for aggressive growth of melanoma, rapidly forming large tumors by the 8th day of treatment, reaching over 2,500 mm^3. Mice treated with DC's or Ad-Δ B7/IL-12/GMCSF alone, showed substantial inhibition of tumor growth. More specifically, the treatment optional that demonstrated the maximum tumor reduction was the combination of dendritic cell vaccine with high concentration oncolytic virotherapy.

As the model assumes the immune system reacts to the presence of the oncolytic virus, all data sets were used to parameter fit except the data for Dendritic cells (ii), as there is no viral therapy involved nor parameter to fit. The top six parameters estimated in Table 4.2 were fit to the data sets. To start, the growth term r, was fit to the PBS data set, setting all other parameter values to 0. Since there was virus and immune response in the remaining sets, all of the parameters were fit to the data. The values fit for data Ad-Δ B7/IL-12/GMCSF were used as a base to estimate the subsequent experimental data in a hierarchical fashion.

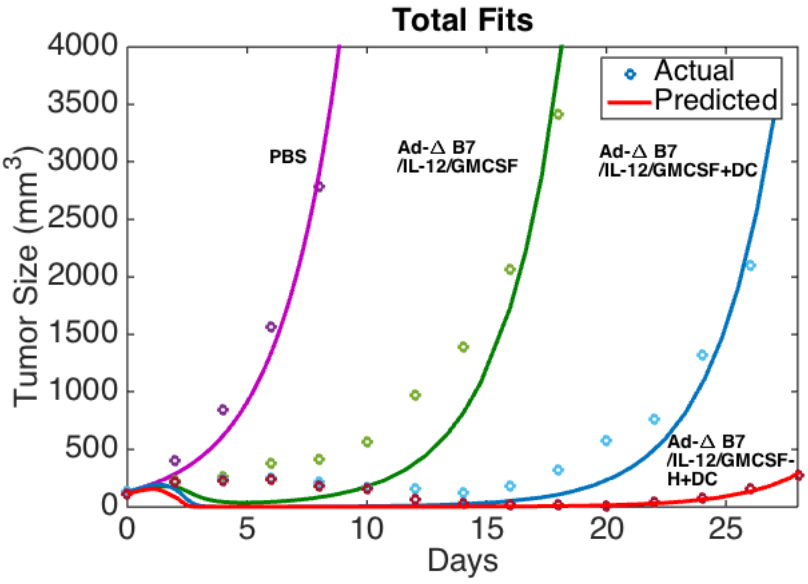

Figure 4.5: Model (4.1) fits to data sets of Zhang *et al.* (2011)

4.3 Results

The Levenberg-Marquardt algorithm was used since the problem is undetermined, since the model was constructed with fewer equations than dimensions. The limitations of the Levenberg-Marquardt algorithm is that is does not handle bound constraints. These strength of this algorithm is it is the algorithm that suits the number and equations and dimensions of the model, due to the complexity. The weakness of not having bound limits on the parameters values is that the range base selection is based off literature, or previous fits from simpler models.

Using the parameter fits from Section 4.2, relevant modeling questions are now considered. 1) Are there better treatment regimens that reduce overall tumor size by day 30? Since the fits include up to day 30, end tumor volume at day 30 can be compared for a variety of regimens. 2) Can metronomic treatment further reduce overall tumor size? Once regimens are considered over the initial 6 days, the model can extend the time to compare end tumor volume. 3) How do the effects of intermittent

combination oncolytic viraltherapy and immunotherapy reduce overall tumor size? Once optimal regimens are found for short and longer treatments, these treatments can be considered one sequence, administered intermittently over extended period of time.

When administering combination treatment, order does matter; therefore, this section will cover a variety of permutations for combining oncolytic virotherapy and dendritic therapy. Included are data generated from permutations of possible treatment regimens under varying administration conditions to show the overall tumor size. All data and figures were generated in Matlab2014.

4.3.1 Dose Regimen

A dosage regimen is the schedule of doses of a therapeutic agent over time. This includes the time between doses, the time when the doses are to be administered, and the quantity of treatment to be given at each specific time.

It will be assumed that any treatment is a permutation of OV, DC and/or days off. Note: For Sections 4.3.1-4.3.2, all permutation calculations were simulated over 30 days; the Tumor Volume presented is on day 30. This was to match the overall treatment done experimentally. Section 4.3.3 allows for further time and will be discussed then.

Regimen	End Tumor Volume mm^3
DVVVDD	49
DDDVVV	50.3
DDVDVV	53.1
DDVVVD	55.9
DDVVDV	56.7
DVDDVV	58.4
DVDVDV	62.3
DVDVVD	62.7
DVVDDV	64.6
DVVDVD	65.9
VDDDVV	77.4
VDDVDV	86.7
VDDVVD	94.2
VDVVDD	98.6
VDVDDV	101.2
VDVDVD	113.6
VVDDDV	146.3
VVDDVD	181.9
VVDVDD	209.3
VVVDDD	630.7

Table 4.3: Exactly 3 oncolytic viruses and 3 dendritic cell vaccines as treatment strategy. The above table represents all 20 permutations that predict the tumor size at day 30. Each injection included V=5×10^{10}, D=1×10^{6}.

This work will assumes the maximum viral and dendritic dosage is parallel to the

optimal experimental dosages used in Zhang *et al.* (2011), for the experiment regimen. Since there are three doses for each treatment of V at 5×10^{10} and D at 1×10^{6}, the maximum dose per treatment is $V_{max} = 1.5 \times 10^{11}$ and $D_{max} = 3 \times 10^{6}$. In Sections (4.3.1-4.3.4), maximum dosage will vary and will be represented by V_{Tot} and D_{Tot}.

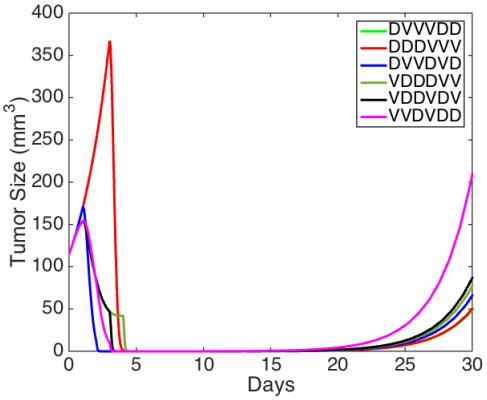

Figure 4.6: Represents the top 3 in each group starting with Dendritic Vaccination and Oncolytic Virotherapy corresponding to Table 4.3

Figure(4.6) shows the top best treatment's for altering the administration of OV and DC treatments, maintaining a maximum of 3 and 3 for each treatment type.

Permutations of V and D with Flexible Frequency

Permutation Rank	Day 1	2	3	4	5	6	End Tumor Volume (mm^3)	Oncolytic Virus dose number	Dendritic Cells dose number
1	V	V	V	V	V	V	4.3	6	0
2	D	V	V	V	V	V	6.4	5	1
3	V	D	V	V	V	V	13.6	5	1
4	V	V	V	V	V	D	14	5	1
5	D	V	V	V	V	D	17.9	4	2
6	D	D	V	V	V	V	22	4	2
7	V	V	D	V	V	V	22.1	5	1
8	V	V	V	V	D	V	22.8	5	1
9	D	V	V	V	D	V	24	4	2
10	D	V	D	V	V	V	25.2	4	2
11	D	V	V	D	V	V	27.3	4	2
12	V	V	V	D	V	V	29.2	5	1
13	V	D	V	V	V	D	35	4	2
14	V	D	D	V	V	V	35.7	4	2
15	V	D	V	V	D	V	40	4	2
16	V	D	V	D	V	V	40.9	4	2
17	D	V	V	V	D	D	49	3	3
18	V	V	V	V	D	D	49.6	4	2
19	D	D	D	V	V	V	50.3	3	3
20	D	D	V	D	V	V	53.1	3	3

Table 4.4: Permutation table representing flexible count for oncolytic viruses and dendritic cell vaccines, over 6 days. 20 permutations of the 64 are displayed, that predict the tumor size at day 30. Each injection included V=5×10^{10}, D=1×10^{6}.

Table (4.4) represents all possible 64 permutations of six treatments for the first six days of therapy. The data is sorted from treatment permutations predicting the lowest tumor size through highest tumor size over 30 days. Since each dose of V is 5×10^{10} (VP) and D is 1×10^{6} (DC), these permutations allow for $[0 \leq V \leq 3 \times 10^{11}]$ and $[0 \leq D \leq 6 \times 10^{10}]$. The regimen leading to the lowest tumor volume over the

experimental time frame predicts to administer oncolytic virotherapy for six days in a row at 5×10^{10} (VP), i.e $V_{max} = 3 \times 10^{11}$, with a total tumor volume of 4.3 mm^3. The worst scenario was administering dendritic vaccine daily for six days, predicting tumor size of 1.1861×10^7 mm^3. Based on these permutations from the model, a large tumor, such as results from D-D-D-D-D-D-D, is not optimal, but the scenario of V-V-V-V-V-V-V with a drastic tumor reduction may also have unfeasible implications. Although this could represent tumor remission, we take into account that this may also include high cytotoxicity of VPs in the subject.

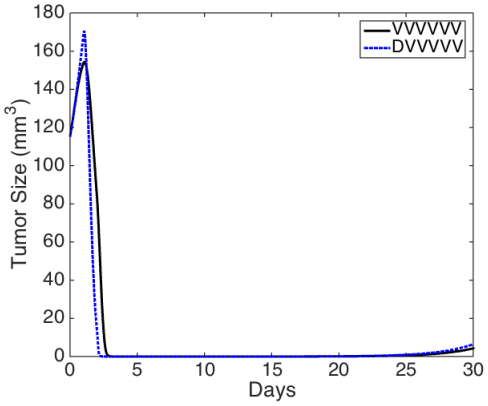

Figure 4.7: Represents the top 2 regimens of non-restricted therapy for Dendritic Vaccination and Oncolytic Virotherapy corresponding to Table 4.4

Assuming the initial maximum dose administered for the experiment done in Zhang *et al.* (2011), we can look into the permutations of altering dendritic cell injections at 1×10^6 and oncolytic virotherapy at 5×10^{10} as will be shown in Section 4.3.2

4.3.2 Maximum Tolerated Dose

The goal of the maximum tolerated dose (MTD) applied to cancer is to generate the highest level of cancer cell mortality without causing unacceptable side effects.

Assuming there is a maximum tolerated dose for the patient, it is important to search for an altered schedule that keeps the total dose bounded, but allows frequency and order to vary.

Permutation Rank	Day 1	2	3	4	5	6	End Tumor Volume (mm^3)	Oncolytic Virus dose number	Dendritic Cells dose number
1	D	V	V	V	V	D	42.9	4	2
2	V	V	V	V	V	V	44.1	6	0
3	D	V	V	V	D	D	49	3	3
4	D	D	D	V	V	V	50.3	3	3
5	D	D	V	V	V	V	50.3	4	2
6	D	V	V	V	V	V	51.9	5	1
7	D	D	V	D	V	V	53.1	3	3
8	D	V	V	V	D	V	54.2	4	2
9	D	D	V	V	V	D	55.9	3	3
10	D	D	D	D	V	V	56.2	2	4
11	D	V	D	V	V	V	56.5	4	2
12	D	D	V	V	D	V	56.7	3	3
13	D	D	D	V	D	V	57.6	2	4
14	D	V	D	D	V	V	58.4	3	3
15	D	V	V	D	V	V	59.7	4	2
16	D	D	V	D	D	V	61	2	4
17	D	V	D	V	D	V	62.3	3	3
18	D	V	D	V	V	D	62.7	3	3
19	D	V	V	D	D	V	64.6	3	3
20	D	V	V	D	V	D	65.9	3	3

Table 4.5: Permutation table of limited maximum doses for oncolytic viruses and dendritic cell vaccines. 20 permutations of the 64 are displayed, that predict the tumor size at day 30. $V_{max} = 1.5 \times 10^{11}$, $D_{max} = 3 \times 10^6$, where the dosages were fractioned over 6 days.

Table (4.5) shows the options for administering combination treatment without limitations on frequency per treatment; however the maximum dosage concentration is limited to the amount used in the experiment from (Zhang *et al.* (2011)). This

modeling approach allows for a varied number of base values for a given order of magnitude. The theory behind optimal control, however, would suggest a specific optimal value for a dose and frequency, which could be infeasible. It could be useful in future work for a very specific dose or frequency condition, without as many constraints on the model.

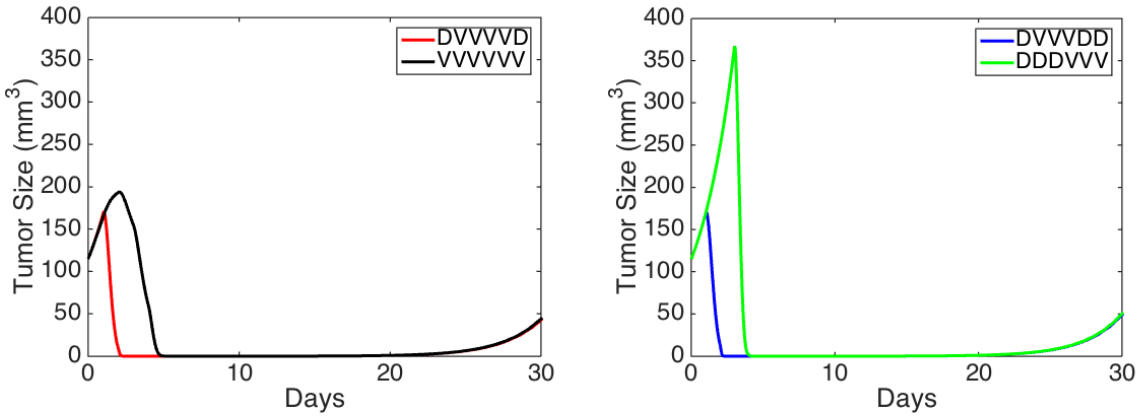

(a) (b)

Figure 4.8: 6 days of altered treatment, limited to maximum OV and DC dose corresponding to Table 4.5

In Figure(4.8), the top 4 are plotted from the 64 permutations listed in Table (4.5) in an ascending order in the legend. Figure(4.8a) compares the most optimal of all 6 limited doses at DVVVVD and VVVVVVV. Although the total tumor size is 42.9 mm^3 and 44.1 mm^3, respectively, we can see slight peak differences early on. It seems that having some dendritic build up before oncolytic treatment, can prime the immune system. Furthermore, the presence of the oncolytic virus redirects the immune response to the tumor site and/or through the potentially restricted tumor microenvironment. This could justify why the peak is lower for simulations of initial administration of dendritic vaccine followed by oncolytic virotherapy. Fig4.8b

compares the third and fourth optimal regimen of the 64 permutations, from top to bottom. Continuing the idea of optimal treatment of dendritic vaccination followed by oncolytic virus, DVVVVDD has a lower peak and slightly smaller tumor size than DDDVVV.

Rest Days

Having rest days during treatment is commonly done to allow the body to recover. This also may entail increased doses of treatment on one particular day, rather than what would be administered on a more dense dosing scheduled. This section investigates the inclusion of rest days during treatment.

Permutation Rank	Day 1	2	3	4	5	6	Tumor Volume (mm^3)	Oncolytic Virus dose number	Dendritic Cells dose number	Rest Day count
1	V	-	V	-	-	V	26.6	3	0	3
2	V	V	-	V	-	V	27.7	4	0	2
3	V	V	V	-	-	V	29.7	4	0	2
4	V	V	V	-	V	V	33.8	5	0	1
5	V	V	-	-	-	V	34.1	3	0	3
6	V	V	V	V	-	V	37	5	0	1
7	V	-	V	V	-	V	37.8	4	0	2
8	D	V	-	V	V	D	37.9	3	2	1
9	D	-	V	-	V	V	39.5	3	1	2
10	D	-	-	V	-	V	39.6	2	1	3
11	D	V	-	-	V	V	39.9	3	1	2
12	D	-	V	-	-	V	40.1	2	1	3
13	D	-	-	V	V	V	40.3	3	1	2
14	V	V	-	-	V	V	40.5	4	0	2
15	D	-	V	V	V	D	40.9	3	2	1
16	D	V	-	-	-	V	41.3	2	1	3
17	D	-	V	-	V	D	41.5	2	2	2
18	V	V	-	V	V	V	41.5	5	0	1
19	D	-	-	-	V	V	41.8	2	1	3
20	D	V	-	-	V	D	41.8	2	2	2

Table 4.6: Permutation table representing flexible count for oncolytic viruses and dendritic cell vaccines, allowing for rest days. 20 permutations of the 729 are displayed, that predict the tumor size at day 30. Injection quantities: $V_{max} = 1.5 \times 10^{11}$, $D_{max} = 3 \times 10^6$, where the dosages were fractioned over 6 days

Table(4.6) represents keeping the schedule of six days fixed, but allowing for off days of treatments. The maximum dosage for OV and DC are the same over 6 days as used in Zhang *et al.* (2011), but divided out accordingly. This also could suggest that some days may have higher doses per day than the initial dose per original treatment quantity, but would be administered less frequently of the treatment time frame.

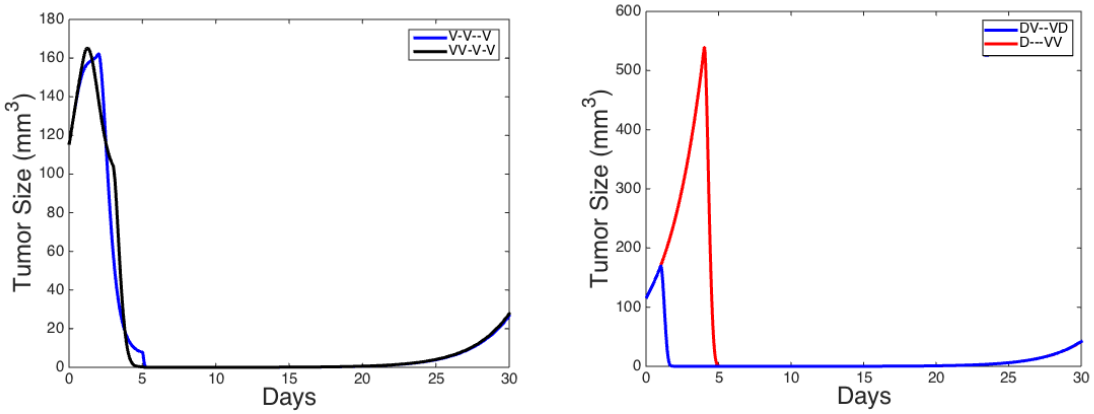

Figure 4.9: Top simulations from Table 4.6

These results have caused some question in the use of combination treatment. It appears that the optimal outcome of including treatment over rest days shown in Table 4.6 is V-V- -V at tumor volume at 26.6 mm^3. Interestingly enough, the 39th permutation rank from Table 4.5 is VDVDDV at tumor volume at 101.2 mm^3. It seems that the same sequence of V at dose 5×10^{10} with rest days did better than that of substituting dendritic treatment within those rest days.

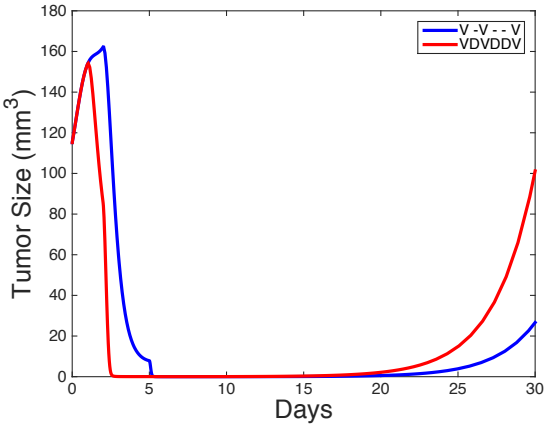

Figure 4.10: V rest vs V D

Table, Rank	Permutation Rank	Day 1	2	3	4	5	6	Tumor Volume (mm^3)	Oncolytic Virus dose number	Dendritic Cells dose number	Total OV dose
[4.6], 1	1	V	-	V	-	-	V	26.6	3	0	1.5×10^{11}
[4.5], 39	2	V	D	V	D	D	V	101.2	3	3	1.5×10^{11}

Table 4.7: OV in the same sequence as off days as of dendritic vaccination does better alone. Tumor volume predicted at day 30. $V_{max} = 1.5 \times 10^{11}$, $D_{max} = 3 \times 10^6$

We can see here that oncolytic monotherapy performs better than combination of viral and immunotherapy. In fact, the top 7 of the top 20 of the 64 permutations of V and D with rest days at limited maximum dose listed in Table (4.6), only include oncolytic virus. As mentioned earlier, the model makes the assumption that the cancer is in an aggressive stage where the tumor microenvironment does not allow for the immune system to naturally attack the uninflected cancer cells. Only infected cancer cells are subject to immune attack due to the oncolytic viral immunogenic traits induced in the cancer cells. Thus, under excessive dendritic vaccination, the immune system annihilates the infected cancer cells quickly. A majority of the infected cancer cells undergo cell lyses, releasing virions which can reinfect cancer cells and re-stimulate the immune system to attack both uninfected and infected cancer populations at rate κy. If the infected cells,y, are removed too quickly, the immune system cannot kill the uninfected cancer cells and thus, the cancer will continue to grow. Due to the inhibition of the infected cells from the dendritic cells, Table (4.7) includes the regimen in rank 2, represent the dendritic vaccination attack and kill infected cells rapidly; the effect from the oncolytic virus will be reduced since its progeny cells are not present, allowing for cancer to grow further. In Section (4.3.2), we look into optimal regimens lowering the total dendritic concentration from 3×10^6 to 3×10^5.

Maximum Tolerated Dose with Rest Days with limited DC

"Less is more", as the saying goes, applies to the models results, as excessive dendritic vaccination in several regimens is not only less effective, but can increase tumor growth. In Section 4.3.1, we've assumed the optimal dose for oncolytic virotherapy is 5×10^{10}(VP)/dose and 3×10^{6} (DC)/dose based off the concentration values used in the experimental work of Zhang *et al.* (2011) for Ad-ΔB7/IL12/ GMCSF$_H$ +DC in Table [4.2]. The dose ranges have been $[0 \leq V \leq 1.5\times10^{11}]$ and $[0 \leq D \leq 3\times10^{6}]$. Suppose $\mathrm{D}_{max_L} < D_{max}$. We can conjecture that there will be enough dendritic vaccination to boost the immune response to kill uninfected and infected cancer cells, but not so excessive that it will kill off the infected cells. Table [4.8] represents therapy with $V_{max} = 1.5\times10^{11}$ and $D_{max_L} = 3\times10^{5}$.

Permutation Rank	Day 1	2	3	4	5	6	End Tumor Volume (mm^3)	Oncolytic Virus dose number	Dendritic Cells dose number	Rest Day count
1	D	V	-	-	-	V	12.9	2	1	3
2	D	V	-	V	-	V	14.5	3	1	2
3	D	V	V	-	V	V	14.6	4	1	1
4	D	V	V	-	-	V	15.1	3	1	2
5	D	V	-	-	V	V	15.4	3	1	2
6	D	V	V	V	V	V	18	5	1	0
7	D	V	-	V	V	V	18.2	4	1	1
8	D	V	V	V	-	V	19.3	4	1	1
9	V	D	V	-	V	V	20	4	1	1
10	V	D	V	-	-	V	20.6	3	1	2
11	V	D	-	V	-	V	21	3	1	2
12	D	V	-	-	V	-	23	2	1	3
13	D	V	D	V	-	V	23.2	3	2	1
14	V	D	D	V	-	V	24	3	2	1
15	V	D	V	V	V	V	24.1	5	1	0
16	D	V	-	V	V	-	24.8	3	1	2
17	V	D	V	V	-	V	25.3	4	1	1
18	V	D	V	D	-	V	25.6	3	2	1
19	V	D	V	-	D	V	26.1	3	2	1
20	D	V	V	-	V	-	26.5	3	1	2

Table 4.8: Permutation table representing flexible count, limited dose, lower dose dendritic cell vaccines, while allowing for rest days. 20 permutations of the 729 are displayed, that predict the tumor size at day 30. Injection quantities: $V_{max} = 1.5 \times 10^{11}$, $D_{max} = 3 \times 10^5$, where the dosages were fractioned over 6 days.

Table [4.8] includes 729 permutations of OV and DC with maximum total dosage of $V_{max} = 1.5 \times 10^{11}$ and $D_{max_L} = 3 \times 10^5$, including rest days. Evidently, lowering D_{max_L} in combination with OV actually reduces overall tumor size. In contrast with Table [4.6], the top 8 out of the top 20 of the 729 permutations start with DC and end with OV. These results could suggest that starting with dendritic vaccination keeps

these cells at bay, and await for the signal from the OV to deploy. At one order of magnitude lower than used in the experimental work by Zhang *et al.* (2011), dendritic cells allow the immune population to attack, but not wipe out all infected cells needed for viral reproduction. We can also see that as the order of magnitude decreased by 1, it also seems optimal to use the entire D_{max_L} all in one go, as opposed to dispersing fractioned out dendritic treatments.

In Table [4.8], D_{max} has at least one rest day. This could allow the system to replenish the overall health of the subject via time for cell growth from cytotoxicity. The $(\text{OV Count})_{total} > (\text{DC Count})_{total}$. Consistent with the limited maximum dose function in Table [4.6], the OV seems to be carrying the weight of the combination treatment, where the top 7 of 20 were only OV. With lower dosed dendritic treatment, the OV combines with at least one DC for the top 12 of 20 in Table [4.8].

As we approach smaller tumor size, Table 4.7 compared regimens that made the top 20 in Table [4.6] and Table [4.8].

Table 4.6, 4.8	Day 1	2	3	4	5	6	Tumor Volume (mm^3)	Oncolytic Virus dose number	Dendritic Cells dose number	Rest Days
Permutation Rank							D_{max}, D_{max_L}			
11,5	D	V	-	-	V	V	39.9, 15.4	3,3	1,1	2,2

Table 4.9: Same sequence; D_{max} compared to D_{max_L}. Total tumor size at day 30

Table 4.9 compared the same 6 day sequence with bounded maximum dose, rest days allowed. Reducing the order of magnitude by one, during this sequence, subsequently reduced the tumor size from 39.9 mm^3 to 15.4 mm^3, shown in Figure 4.11.

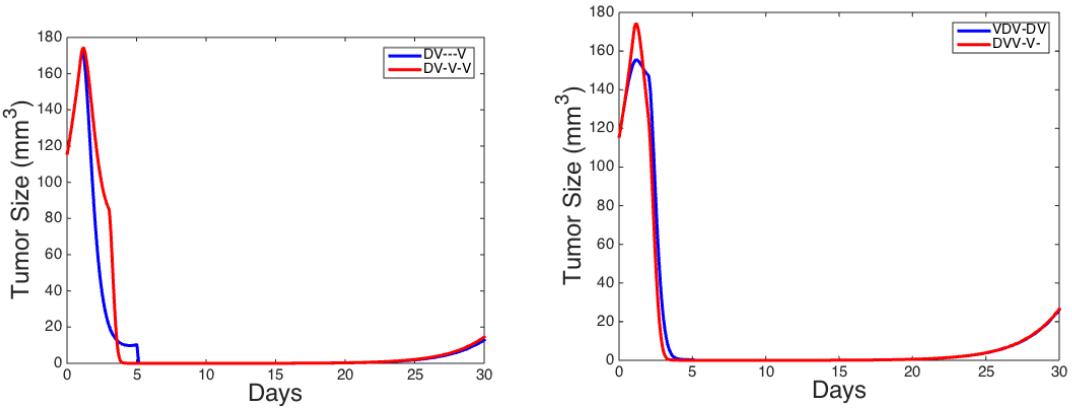

Figure 4.11: Top results from Table 4.8

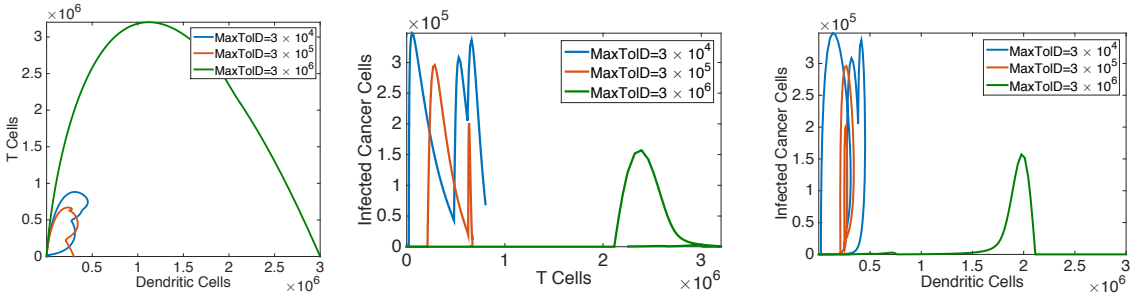

(a) (b) (c)

Figure 4.12: Effects from changes of dendritic cell concentration on infected cancer cells, directly and indirectly, over a 30 period. $D_{max} = [3 \times 10^4, 3 \times 10^5, 3 \times 10^6]$. a) Adaptive immune response from dendritic cells to T cells for varying maximum tolerated dose. b) T cell population change on Infected cells. c) Dendritic cell population change on Infected cells.

According to regimen D V- - V V, Figure 4.12 represents phase plane diagrams showing the effects from changes the dendritic cell concentration makes on infected cell populations. DCs have no direct lytic activity on infected caner cells, since dendritic cells have to activate T cells, which then respond to infected cells. Figure4.12a shows the adaptive immune response from dendritic cells to T cells for varying maximum

tolerated dose values overall 30 period. Figure 4.12b shows the effect of T cells on the infected cancer population at varying maximum tolerated dose values, which occur at a 30 day simulation. The end time in this figure is 6 days, in order to clearly show the trajectories without overlapping lines. We can then see that for high populations of dendritic cells, most of the infected cancer cells have a small population, in green, a peak population at approximately 1.5×10^5 infected cancer cells. The reduced dendritic vaccine count, shows higher infected cancer populations. Figure4.12c shows a similar correlation, only from dendritic to infected cancer cells.

Higher peaks of infected cells occurred from lowering the dendritic vaccine dose, seen in Figures 4.12b. More infected cells, could become viral which then reinfects uninfected cancer cells. Therefore, it is best to monitor the intensity of the dendritic vaccine dose. Similarly, this can be shown through the variation of the dendritic activation rate, ρ, in Figure 4.13.

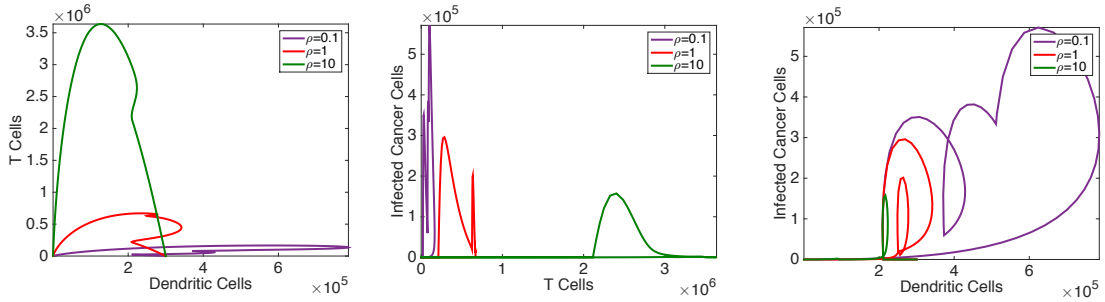

(a) (b) (c)

Figure 4.13: Changes in ρ: Effects from changes of dendritic cell concentration on infected cancer cells from altering adaptive immune response rate, $\rho = [0.1, 1, 10]$. a) Adaptive immune response from dendritic cells to T cells for varying ρ values. b) T cell population change on Infected cells. c) Dendritic cell population change on Infected cells.

4.3.3 *Metronomic Therapy*

The model assumes that cancer cells do not develop a resistance to OV, such that all cells are sensitive to treatment. It could be the case that maintaining a certain quantity of cancer cells may keep the tumor from reaching a noticeable low threshold, which could produce more cancer cells quickly. Or depending on age, high toxic dose may not be the best option. Hahnfeldt *et al.* (2003) found that treatment administered over long term at lower low doses, could be optimal to maintain tumor growth in the long term, instead of eradicating nearly all cells in the short term. This strategy is defined as metronomic treatment,as the administration of lower dose treatment over extended period of time (Hahnfeldt *et al.* (2003) , Kuang *et al.* (2016)).

Permutation	Day												End Tumor Volume	Oncolytic Virus	Dendritic Cells
Rank	1	2	3	4	5	6	7	8	9	10	11	12	(mm^3)	dose number	dose number
1	D	V	V	V	V	V	V	V	V	V	V	D	1.9	10	2
2	D	V	V	V	V	V	V	V	V	V	V	V	2.2	11	1
3	D	V	V	V	V	V	V	V	V	V	D	D	2.2	9	3
4	D	D	V	V	V	V	V	V	V	V	V	V	2.3	10	2
5	D	D	D	V	V	V	V	V	V	V	V	V	2.6	9	3
6	D	V	D	V	V	V	V	V	V	V	V	V	2.8	10	2
7	D	D	V	D	V	V	V	V	V	V	V	V	2.9	9	3
8	D	D	D	D	V	V	V	V	V	V	V	V	2.9	8	4
9	D	D	V	V	V	V	V	V	V	V	V	D	2.9	9	3
10	D	D	D	V	D	V	V	V	V	V	V	V	3.1	8	4
11	V	D	V	V	V	V	V	V	V	V	V	D	3.1	10	2
12	V	D	V	V	V	V	V	V	V	V	V	V	3.2	11	1
13	D	V	D	D	V	V	V	V	V	V	V	V	3.2	9	3
14	D	D	V	D	D	V	V	V	V	V	V	V	3.2	8	4
15	D	V	V	V	V	V	V	V	V	D	D	D	3.3	8	4
16	D	V	V	V	V	V	V	V	V	V	D	V	3.3	10	2
17	D	D	V	V	D	V	V	V	V	V	V	V	3.3	9	3
18	D	D	D	V	V	D	V	V	V	V	V	V	3.4	8	4
19	V	D	D	V	V	V	V	V	V	V	V	V	3.4	10	2
20	D	D	D	V	D	D	V	V	V	V	V	V	3.4	7	5

Table 4.10: Permutation table representing for flexible dosing. 20 permutations of the 4096 are displayed, that predict the tumor size at day 30. Injection quantities: $V_{max} = 1.5 \times 10^{11}$, $D_{max} = 3 \times 10^{6}$, where the dosages were fractioned over 12 days

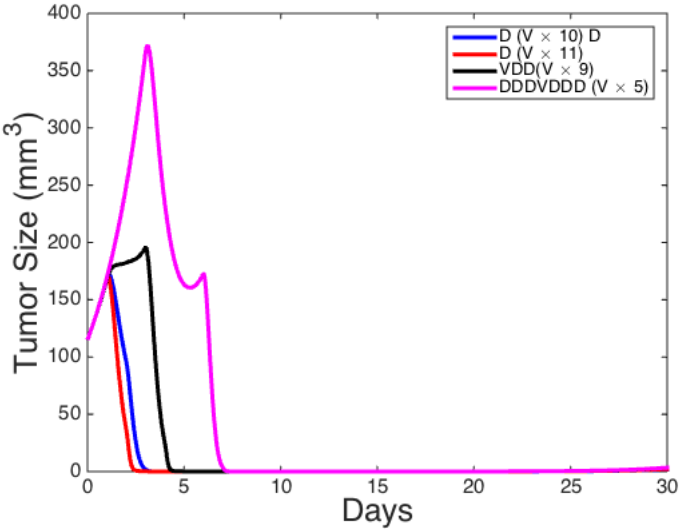

Figure 4.14: Top results from Table 4.10. Tumor Volume size is listed at day 30.

Permutation Rank	Day 1	2	3	4	5	6	7	8	9	10	11	12	Tumor Volume (mm^3)	Oncolytic Virus dose number	Dendritic Cells dose number
1	V	V	D	V	D	D	D	D	D	D	D	V	1.59	4	8
2	V	V	D	D	V	D	D	D	D	D	D	V	1.61	4	8
3	V	D	V	D	V	D	D	D	D	D	D	V	1.64	4	8
4	V	D	V	D	D	V	D	D	D	D	D	V	1.74	4	8
5	V	D	V	V	D	D	D	D	D	D	D	V	1.8	4	8
6	V	V	D	D	D	V	D	D	D	D	D	V	1.97	4	8
7	D	V	V	V	V	V	V	V	V	V	V	V	2.06	11	1
8	V	V	D	V	D	D	V	D	D	D	D	V	2.17	5	7
9	V	V	V	D	D	D	D	D	D	D	D	V	2.2	4	8
10	V	V	V	D	D	V	D	D	D	D	D	V	2.19	5	7
11	V	D	V	D	D	D	D	D	D	D	D	V	2.2	3	9
12	V	V	D	V	D	V	D	D	D	D	D	V	2.2	5	7
13	V	V	V	D	V	D	D	D	D	D	D	V	2.21	5	7
14	V	V	D	V	D	D	D	V	D	D	D	V	2.23	5	7
15	V	V	V	D	D	D	V	D	D	D	D	V	2.27	5	7
16	V	V	D	V	V	D	D	D	D	D	D	V	2.3	5	7
17	V	V	V	V	D	D	D	D	D	D	D	V	2.4	5	7
18	V	D	V	V	D	V	D	D	D	D	D	V	2.41	5	7
19	V	D	V	V	D	D	V	D	D	D	D	V	2.44	5	7
20	V	D	V	D	D	D	V	D	D	D	D	V	2.45	4	8

Table 4.11: Permutation table representing flexible dosing and low DC vaccine dose. 20 permutations of the 4096 are displayed, that predict the tumor size at day 30. Injection quantities: $V_{max} = 1.5 \times 10^{11}$, $D_{max} = 3 \times 10^5$, where the dosages were fractioned over 12 days

According to Table 4.15, all low dose treatments should end with virotherapy on the last day. In 19 of the 20 of the 4096 permutations, treatments started with V and ended with a sequence of at least 3 DDDV.This could suggest building a dendritic army that will be activated once the oncolytic virotherapy is administered last.

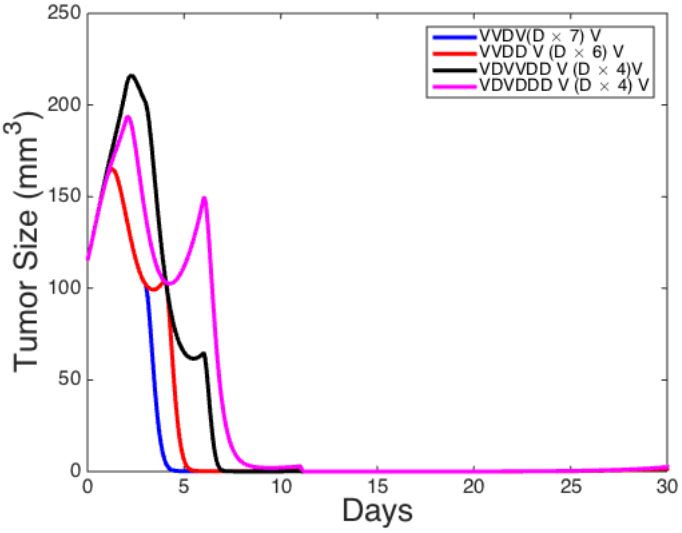

Figure 4.15: Top results from Table 4.15

The most optimal treatment within a 30 day time frame would be V V D V D D D D D D D V at $V_{max} = 1.5 \times 10^{11}$ and $D_{max} = 3 \times 10^5$. Each viral treatment would administer 3.75 $\times 10^{10}$(VP)/dose and dendritic treatment would administer 3.75 $\times 10^4$(VP)/dose .

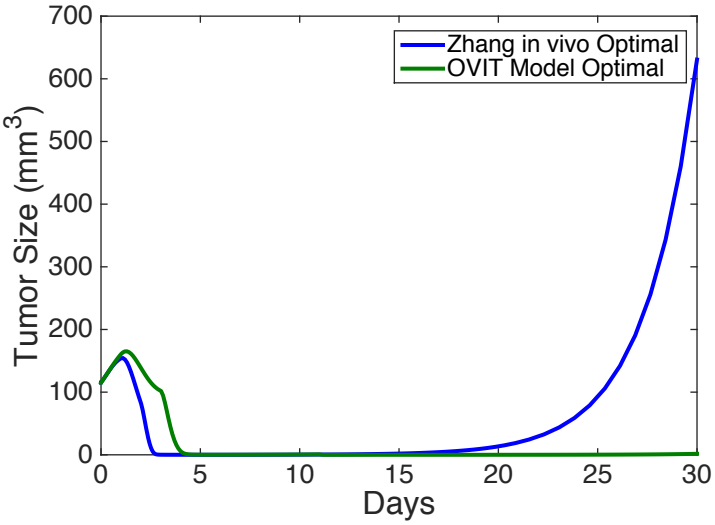

Figure 4.16: Optimal dose used in Zhang *et al.* (2011) compared to OVIT model (4.1)

Figure 4.16 compared the optimal dose and frequency used experimentally in Zhang *et al.* (2011) against the optimal result of the OVIT model. We can conclude that administering a fraction of the treatment over double the amount of time, leaves the tumor burden low and size smaller.

4.3.4 Intermittent Therapy

Intermittent therapy consists of altering periods of on- and off- treatments, in order to keep tumor size below a given threshold. As this therapy was implementing in the metronomic case, once per day over twelve days, this section will look at each regimen; 6 days or 12 a single treatment, intermittently distributed over months. While monitoring the growth of a tumor, a period of on-treatment can be initiated once the tumor reaches a defined size ($T_{\max}$). On-treatment periods correspond with a six to twelve day treatment regime. A period of off-treatment follows a given treatment regime, during which cancer growth is monitored. Once a tumor reaches $T_{\max}$, the patient is put back on-treatment and receives another full treatment regime (Figure 4.17).

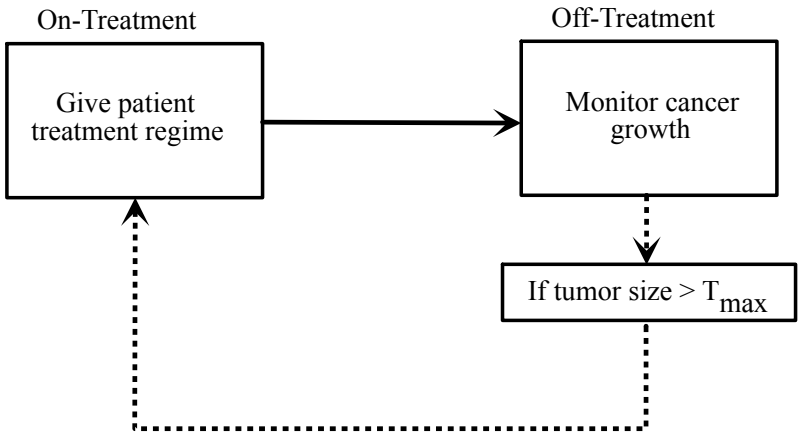

Figure 4.17: Proposed Optimal Intermittent Therapy strategy

Here, model (4.1) is applied to a scenario of intermittent therapy over a six month period with $T_{\max} = 700\text{mm}^3$. Figure 4.18 and Table 4.12 shows results of sample treatment regimes under intermittent therapy. The optimal treatment regimen is used for a six day treatment allowing days off: (D V - - - V) with D dose size of 3×10^5 on the first day of the on-treatment period and V dose size of 7.5×10^{10} on the second and sixth days of the on-treatment period (Figure 4.18 a). This regime was found to be optimal in Table 4.8. These results were compared to the optimal metronomics strategy found in Table 4.15, a twelve day treatment of: (V V D V D D D D D D V) with D dose size of 7.5×10^3 and V dose size of 1.875×10^{10} on the respective days of the on-treatment period (Figure 4.18 b). These two intermittent strategies are summarized in Table 4.12.

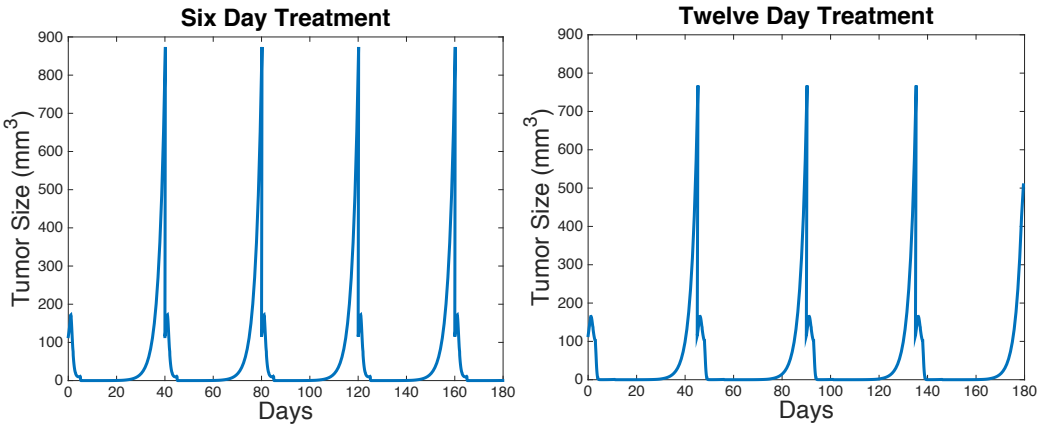

(a) (b)

Figure 4.18: Intermittent therapy over six month period: Model (4.1) predictions with $T_{\max} = 700$ mm^3 for treatment regimes a.) Six day treatment regime of (D V - - - V)with D dose size of 3×10^5 and V dose size of 7.5×10^{10} and b.) Twelve day metronomics treatment regime of (V V D V D D D D D D V) with D dose size of 7.5×10^3 and V dose size of 1.875×10^{10}.

Regimen for on-treatment	off-treatment period (days)	# of on-treat-ment periods	Total V over 6 months	Total D over 6 months	Tumor min size	Tumor max size
6 day treatment regimen (D V - - - V)	40	5	$7.5 * 10^{11}$	$6 * 10^{6}$	0.0023 mm^3	874 mm^3
12 day metronomic treatment regimen (V V D V D D D D D D V)	45	4	$6 * 10^{11}$	$1.2 * 10^{6}$	0.0027 mm^3	768 mm^3

Table 4.12: Intermittent therapy over six month period, model (4.1) predictions with $T_{\max} = 700$ mm^3

Using a metronomics treatment strategy for intermittent therapy has some clear advantages over traditional approaches. The total number of on-treatment periods of the metronomic 12 day-low dose regime is lower than the number of on-treatment periods of the traditional 6 day-high dose regime. Therefore the total amount of viral and dendritic injections over a six month period is reduced using a metronomic strategy (see Table 4.12).

4.4 Discussion

Oncolytic viruses enhance the production of antigens that signal immune responses. There is also the understanding that OVs disrupt the microenvironment, which can allow opportunities for the immune system to penetrate the cancer cell barrier. More specifically, it is becoming fashionable to compliment dendritic cell vaccines with oncolytic viruses.

For a variety of cancer types, oncologists have repertoires of treatment options. However, for nearly all cancers, the optimal dose quantity, frequency and synergy with potentially combining treatments, seems to invariably be of concern. Recent pre-clinical and clinical studies suggest using oncolytic virotherapy as a means of cancer treatment. Oncolytic virotherapy alone are not as effective as a monotherapy,

as there is much focus on the safety components as there is to the cytotoxic traits. Recent work showed combination therapy of OV and dendrites cell vaccines is better than one or more alone (Zhang *et al.* (2011)). The work in this dissertation also has shown the outcomes with smallest tumor volume are due to combination oncolytic viral and immunotherapy. Summary table 4.13 includes a chart showing all the treatment strategies for scheduling, dosing and timing against the end tumor volume for 30 days.

Table	Regimen Strategy Summary	permu - tations	rest days	limits MTD	low D dose	Metro - nomic	Optimal Regime	Tumor vol. day 30
4.3	6 FIXED sized injections over 6 days; 3 V (5×10^{10}) & 3 D (1×10^{6}) injections	20		✓			DVVVDD	49 mm^3
4.4	6 FIXED sized injections over 6 days; composed of any # (0-6) of V (5×10^{10}) & any # of D (1×10^{6}) injections	64					VVVVVV	4.3 mm^3
4.5	6 VARIED sized injections over 6 days; composed of any # (0-6) of V & any # of D injections. Total V injected: 1.5×10^{11}. Total D injected: 3×10^{6}	64		✓			DVVVVD	42.9 mm^3
4.6	6 VARIED sized injections over 6 days; any # (0-6) of V & any # of D injections & REST days.Total V injected: 1.5×10^{11}. Total D injected: 3×10^{6}	729	✓	✓			V - V - - V	26.6 mm^3
4.8	6 VARIED sized injections over 6 days; any # (0-6) of V & any # of D injections & REST days.Total V injected: 1.5×10^{11}. Total D injected: 3×10^{5}	729	✓	✓	✓		D V - - - V	12.9mm^3
4.10	12 VARIED sized injections over 12 days; composed of any # (0-12) of V & any # of D injections. Total V injected: 1.5×10^{11}. Total D injected: 3×10^{6}	4096		✓		✓	DVVVVVVVVVVD	1.9 mm^3
4.11	12 VARIED sized injections over 12 days; composed of any # (0-12) of V & any # of D injections. Total V injected: 1.5×10^{11}. Total D injected: 3×10^{5}	4096		✓	✓	✓	VVDVDDDDDDDV	1.56 mm^3

Table 4.13: Summary of all optimal treatment strategies

4.4.1 Results Summary

Section 4.3.1 Altered experiments optimal with maintaining 3 doses of each, as was done in previous experimental work for combination OV and DCs (Huang *et al.* (2010), Zhang *et al.* (2011)).

Assuming that combination treatment using exactly half DCs and OVs, results show from permutations of 20 results, altering treatments starting with dendritic cells did the best Note, the optimal treatment used in experimental work of Zhang *et al.* (2011), (VVVDDD), ranked 20 out of 20.

Section 4.3.1 allowed 6 treatments, with flexible frequency on the quantity of each treatment, with a maximum of one treatment type per day. The treatment regimen that reduced the tumor size over 30 days 6 full days of OV. This option, however, may not be optimal since its total dose was doubled of that used in experimental work over this time frame. Potential cytotoxic effects are a concern. Note, the optimal treatment used in experimental work of Zhang *et al.* (2011), (VVVDDD), ranked 55 of 64.

Section 4.3.1 used exactly 3 and 3 of each type of therapy, which innately limited the maximum permitted dose, given each OV dose was 5×10^{10} and DC 1×10^{6}. Section 4.3.1 allowed for a flexible count of each therapy over 6 days, which leads to altered total dose ranges per treatment. Although the best was 6 days of OV, this result could be a disservice to an individual who has a toxic reaction over a short amount of time. Introducing the maximum tolerated dose (MTD) can provide an upper cytotoxic bound.

Section 4.3.2 allows for flexibility in the timing and count per treatment, but

assume a limitation for the maximum tolerated dose. Results show combination therapy is best, specifically when starting with DC. Nineteen of the top 20 of the 64 permutations started with DCs. The best treatment was DVVVVD. Note, the optimal treatment used in experimental work of Zhang *et al.* (2011), (VVVDDD), ranked 61 of 64.

Many cancer treatments allow for rest days for the body to recover. The incorporation of rest days, in Section 4.3.2, showed the top 7 of the top 20 of the 729 permutations included only virus. There was a minimum of 3 treatments of V for these top 7. Comparing the best treatment of V-V- - V with rest days to V D V D D V without rest days, the observation was made that the treatment regimen without DC did better than with. After various hypotheses, the conclusion came that DC were too high. If the DC is too high, they will kill off the infected population, needed to lyse into OV to kill uninfected cancer. The next hypothesis was lowering DC would improve the reduction of tumor volume.

Section 4.3.2 explored rest days with D_{max_L}. Permutations of DC from $(3 \times 10^0 - 3 \times 10^6)$ were made to find the most optimal DC count, fixing $V_{max} = 1.5 \times 10^{11}$. We found 1×10^5 was the optimal order of magnitude for DCs. Similar to the results for 6 days with rest days, in Table 4.8, OV count was greater than every DC count per treatment. This observation is similar but not exact because 4.6 included OV greater than or equal to the DC count. Simulations show that for one order of magnitude of reduced DC treatment, there is enough infected cancer cells not attacked from the immune system, via T cells, to re-infect more cancer cells. Following the same immune trajectory, altered values were checked for the dendritic activation T cell rate, ρ, shown in Figure 4.13. For ρ high, D_{max_L}, there are more T cells, which allow more

infected cancer cells to be annihilated. With less infected cancer cells, there are less virions to infect uninfected cancer cells, which leads to an increase in overall tumor volume.

Section 4.3.2 allowed for a flexible schedule and maximum tolerated dose. Under conditions where less dose per day is favorable to a patient, for purposes such as species, age, health conditions, etc, the metronomic treatment idea was implemented in Section 4.3.3 as part of the regimen schedule for model (4.1), to use less dose per day over a longer period of time. Table 4.10 showed the top 20 of the 4096 permutations calculated for tumor size at day 30. The range for the top 20 was [1.9-3.4] mm^3; $\bar{x} = 2.93$ mm^3,thus, it seems they all produce significantly smaller tumors than of the previous treatment experimented throughout Sections (4.3.1-4.3.2). 85% of the top 20 regimens in Table 4.10 started with DCs followed mostly by OVs, where the ratio of DCs:OVs is 1:3.21. These regimens, however, allowed for $D_{max} = 3 \times 10^6$. As learned from Section 4.3.2 tumor size was smaller when the dendritic maximum tolerated dose decreased, therefore this idea was also applied into lower dose over a longer time frame for treatment, with metronomic. Table 4.11 shows the top 20 of the 4096 permutations for lower dose DCs. The range for tumor size over 30 days was [1.6-2.45];$\bar{x} = 2.1$ mm^3. This range is the most optimal from all of this works findings. The difference is there are more DCs on average than of OVs, contrary to metronomic with $D_{max} = 3 \times 10^6$, with a ratio of OVs:DCs is 1:1.5, where 95% of the regimens start with OV and 20 out of 20 end with OV, as well. The model is built such that infected population declines quickly due to the high magnitude of $\kappa y\frac{yz}{K}$. There is an interface competitive effect, allowing for $\kappa x\frac{yz}{K}$ to represent a stronger benefit from the immune system to the uninfected cancer population. The metronomic treatment allows for at least a constant population of infected cells, y, which reduces both uninfected and infected cancer cells. The non-metronomic case,

under higher dosages in short amount of time, allowed for the reduction of infected cells, without having the ability to be regrown. Thus, this interference competition can allow the higher portion of uninfected cancer cells to take advantage of the CTL cells more than the infected cancer cells. Moreso, the infected cancer cells are not being depleted by the facilitation rate as much as the uninfected population, allowing for further regeneration of free viral particles to reinfects the unfitted cancer cells

These results could support sigmoidal growth models that suggest treatments administered closer in time results in higher cell kill, which deprives the regrowth of cancer cells between treatment (Kuang *et al.* (2016)). More specifically, keeping compact treatment schedules over a longer period of time, as in the case of using metronomic treatment strategies used in Section 4.3.3.

4.4.2 Overall impact

To summarize, the initial research questions and results for this chapter were: 1)Are there better treatment regimens that reduce overall tumor size by day 30? Yes, with MTD with Rest days and limited DC. 2)Can metronomic treatment further reduce overall tumor size by day 30? Yes, with Metronomic therapy with limited DC. 3)How do the effects of intermittent combination oncolytic viraltherapy and immunotherapy reduce overall tumor size over time? Options for six day treatment or twelve day treatment can be used as one single treatment option, intermittently over time. Depending on the personal scenario, either could be used accordingly to reduce overall tumor size, depending on a maximum tolerated tumor volume and cytotoxicity.

This model has expressed that timing, order and dose is sensitive to overall tumor volume, over 30 days and up to 6 months. The timing at which either immunotherapy or viraltherapy could be of clinical relevance. The time at which dendritic cells are

injected seems to have relevance to the effectiveness of the combination, once OVT is administered. It seems that DC prior to OV allows the DC's to prime the area of infection and can attack once OVT is administered. If DC are inject for the first few days of treatment, they have no where to go, as their population is building up and waits for the OV. During this time, the tumor can grow exponentially. This could be an issue under circumstances where the tumor must be depressed within the initial stages. Otherwise, it could be beneficial as a synergistic approach to prime the OV effectiveness. Furthermore, reducing the order of magnitude for the DCs allowed for improved effectiveness of OV, as 3×10^6, was ultimately killing off the infected cancer cells too quickly, inhibiting the re-infectivity of the OV genome. This result can suggest that under combination treatment, it is important to monitor the quantity of immunotherapy, such that too much can interfere the the benefits of the viraltherapy if these infected cells are destroy by the immune system too quickly. According to the model, maximum infectivity of oncolytic virotherapy is needed in order for OVT treatment to be successful, which can be obtain with a light boost of DC's prior or in between treatments. The results of this work to find optimal treatment schedule, supports that of Metronomic Therapy (Hahnfeldt *et al.* (2003)). The key reason the metronomic treatment is ch the best in this work, is due to the constant influx of OV to the infected cell population. In shorter days, such as the cases of 6 day treatment, the infected cell populations would die off rather quickly, which dampens the potential for further growth of the OV, independent of external injection. Including less dose over a longer time frame, even at a lower dose, allows for a constant population of infected cells to maintain the free viral population, which can persist to infect more cancer cells. Model (4.1) under metronomic treatment, will be considered the "Metronomic Oncolytic Viral-Immunotherapy", or "MOVIT" model.

Chapter 5

CONCLUSION

The research goals for this work were: 1) Develop a mathematical model that can represent clinical variations for administering oncolytic viral therapy. 2) Parameterize models using empirical data 3) Shed light on the complex dynamics of combined oncolytic viral and immunotherapy and 4) Identify optimal treatment strategies (dose sizes, treatment schedules) for a proposed personalized medicine model.

Modeling biology through in silico experimentation can provide great insight on deep dynamical, relevant concerns. Chapter 3 presented a framework model of dynamical interactions between oncolytic viruses, cancer and the immune response. The mathematical analysis provided insight on understanding which type of biological conditions are necessary for drastic changes to occur in the system. It is important to have mathematical analysis, but it may be difficult to plausibly apply the details biologically. An important condition found for the threshold of oncolytic infection on cancer, was the sensitivity of viral replication rate, β, shown with the occurrence of a Hopf bifurcation. Biologically, changes in the viral replication value could depend on the route of administration or efficacy of the drug. Most OVs are administered intratumorally to enhance viral efficacy, and decrease chance of viral spread outside the target region. In other cases, many OVs are coated with temporal protection against the immune response in order to allow for viral replication. Mathematically, the viral replication value could change depending on mass action or standard incidence, both used in this work. In general, the mathematical analysis provides great insight on conditions that occur clinically, and on which parameters play key roles on improving questions of biological dynamics.

The idea of curing cancer seems optimistic, yet perhaps, slightly unrealistic. Treating cancer to maintain a lower, tolerable level may be a more practical goal for clinicians and could ameliorate effects and responses for patient viability. Chapter 4 explored optimal regimens that reduce tumor size, while attempting to account for qualify of life conditions for a patient. Numerical analysis was a great tool enriching the application of the model in various clinical dimensions. My foremost goal was to fit the model to pre-clinical data. Although it is hoped that this work will be applied clinically, the advantage of pre-clinical, non-human, data is its abundance. A table of clinical trial regimens, Table 4.1 using oncolytic virotherapy, was constructed to maintain a clinical-like direction for the model using pre-clinical data. Various treatment strategies were then adapted into Model (4.1), accounting for dose quantity, frequency and order of combination treatment administration. The key approach for cancer treatment used in Chapter 4, was to reduce tumor growth and alleviate the cancer burden of the patient, rather than indirectly kill them from drug toxicity. For this, various permutations for schedule regimens of strategic concern were investigated.

Under assumptions made for Model (4.1), key results showed that keeping two treatments at high concentrations while combined together, may not allow for their maximal, synergistic benefits to reduce tumor size. Moreover, administering treatments at fractionated doses over a longer time period, showed maximal reduction in overall tumor size for a given time-span. Stronger doses in shorter time frames did reduce tumor size quickly, but soon relapsed. Thus, metronomic oncolytic viral-immunotherapy (MOVIT) could have clinical significance, whether in one treatment as a sequence of doses, or intermittently as sequences of doses administered multiple times. Overall, this work was able to show that timing and order of combination

treatment is important for reducing overall tumor size, evaluate the synergistic effects of combining treatments and develop a proposed scheme for personalize treatment using intermittent therapy.

The following models are altered forms of Model (4.1).

Dynamics of Free Virus and Immune Response

We have seen in previous models (3.1)- (4.1) interactions between free viral populations lysed from oncolytic virus, infect cancer cells. The antigens presented from the infection induce dendritic cells, that ultimately activated T killer cells that attack uninfected and infected cells, respectively. As mention in the development of Model (4.1), the tumor-microenvironment inhibits the immune system to attack cancer cells. A trait of OVs is the ability to disrupt the tumor-microenvironment, which allows access for the immune system to function near the tumor site. However,as the OV is within the tumor during this time, and it is foreign, the immune system will unbiasedly attack those free virions. With an decrease in OV population resulting from attacks from the immune response , there will be a decline in free virions that can disrupt the tumor micro-environment. This will subsequently close the time gap for the immune system to attack the cancer cells, leading to an increase in tumor volume. Thus, it is crucial to explore the dynamics between the interactions of OV and immune cells. The below model is altered from (4.1).

$$\frac{dx}{dt} = rx - \beta\frac{xv}{K} - f(y)\frac{xz}{K} \tag{5.1a}$$
$$\frac{dy}{dt} = \beta\frac{xv}{K} - \alpha y - f(y)\frac{yz}{K} \tag{5.1b}$$
$$\frac{dv}{dt} = N\alpha y - \delta_v v + u_v(t) - g(x, v, z) \tag{5.1c}$$
$$\frac{dD}{dt} = \sigma_y y - \delta_d D + u_d(t) \tag{5.1d}$$
$$\frac{dz}{dt} = \rho D - \delta_z z \tag{5.1e}$$

where term $g(x, v, z)$ represents the immune attack on OVs free virions near the site of the tumor microenvironment disruption. Also, $f(y)$ denotes a function to represent the mechanism of T killer cell facilitation depending on infected cancer cells.

OVIT model with Cancer-Immune Response

Model (4.1) assumed the tumor microenvironment was inhibiting the immune system from attacking cancer cells. In the event the tumor microenvironent is disrupted by the virus, or another factor, it would be useful to compare previous regimens from Chapter 4 with allowing for a small, ϵ, immune response term. Thus, the uninflected caner cell loss term -$\kappa y\frac{xz}{K} - \epsilon\frac{xz}{K}$, would not be completely dependent on the presence of the infected cell, once initiated by the virus.

$$\frac{dx}{dt} = rx - \beta\frac{xv}{K} - (f(y) - \epsilon)\frac{xz}{K} \tag{5.2a}$$
$$\frac{dy}{dt} = \beta\frac{xv}{K} - \alpha y - f(y)\frac{yz}{K} \tag{5.2b}$$
$$\frac{dv}{dt} = N\alpha y - \delta_v v + u_v(t) \tag{5.2c}$$
$$\frac{dD}{dt} = \sigma_y y - \delta_d D + u_d(t) \tag{5.2d}$$
$$\frac{dz}{dt} = \rho D - \delta_z z \tag{5.2e}$$

OVIT model with Delayed Dendritic Cell Response

Dendritic cells function rather slowly in the immune system. Model (4.1) allows for an immediate response from dendritic activation to T cells. Since the dendritic cell vaccine was combined with oncolytic virotherapy, it would be of biological interest to compare the regimens found in Chapter 4 with a delayed dendritic response. Allowing a delay in this response time could permit the virus to persist and conquer some cancer cells, reducing the uninfected cancer cell population. If the delay is too long, it could be possible the response is out of clinical time for sufficient therapeutic conditions.

$$\frac{dx}{dt} = rx - \beta\frac{xv}{K} - f(y)\frac{xz}{K} \tag{5.3a}$$
$$\frac{dy}{dt} = \beta\frac{xv}{K} - \alpha y - f(y)\frac{yz}{K} \tag{5.3b}$$
$$\frac{dv}{dt} = N\alpha y - \delta_v v + u_v(t) \tag{5.3c}$$
$$\frac{dD}{dt} = \sigma_y y - \delta_d D + u_d(t) \tag{5.3d}$$
$$\frac{dz}{dt} = \rho D(t-\tau) - \delta_z z \tag{5.3e}$$

$\rho D(t-\tau)$ incorporated to represent the slow response from dendritic cells to T killer cells where, the delay τ can be considered a discrete delay.

Future Direction

It is vital to understand how cancer interacts with non-conventional treatments, in order to minimize tumor growth and maximize life. I feel in silico mathematical model experimentation will play a crucial role in the clinical setting and can help gain insight into clinical trials to pursue.

The era of using oncolytic viruses as a means of cancer treatment has just begun its

horizon, clinically. Hopefully, an increase in pre-clinical and clinical experimentation using oncolytic virotherapy will linearly produce abundant data sets. Certainly, the data is irrelevant without good questions. Luckily, there are so many opportunities of investigation within the unconventional usage of oncolytic viruses to treat cancer, and unbounded permutations to unite the tools of mathematical modeling towards improving cancer burden.

Albrecht T, B. I. e. a., Fons M, *Medical Microbiology*, no. Chapter 44. in Effects on Cells (University of Texas Medical Branch at Galveston, 1996), 4 edn.

Anderson, R. M., R. M. May *et al.*, "Infectious diseases and population cycles of forest insects", Science **210**, 4470, 658–661 (1980).

Andtbacka, R. H., H. L. Kaufman, F. Collichio, T. Amatruda, N. Senzer, J. Chesney, K. A. Delman, L. E. Spitler, I. Puzanov, S. S. Agarwala *et al.*, "Talimogene laherparepvec improves durable response rate in patients with advanced melanoma", Journal of Clinical Oncology pp. JCO–2014 (2015).

Bajzer, Ž., T. Carr, K. Josić, S. J. Russell and D. Dingli, "Modeling of cancer virotherapy with recombinant measles viruses", Journal of theoretical Biology **252**, 1, 109–122 (2008).

Bajzer, Z., M. Marušić and S. Vuk-Pavlović, "Conceptual frameworks for mathematical modeling of tumor growth dynamics", Mathematical and computer modelling **23**, 6, 31–46 (1996).

Bell, G. I., "Mathematical model of clonal selection and antibody production", Journal of theoretical biology **29**, 2, 191–232 (1970).

Bell, J. and G. McFadden, "Viruses for tumor therapy", Cell host & microbe **15**, 3, 260–265 (2014).

Brauer, F., C. Castillo-Chavez and C. Castillo-Chavez, *Mathematical models in population biology and epidemiology*, vol. 1 (Springer, 2001).

Breitbach, C. J., J. Burke, D. Jonker, J. Stephenson, A. R. Haas, L. Q. Chow, J. Nieva, T.-H. Hwang, A. Moon, R. Patt *et al.*, "Intravenous delivery of a multi-mechanistic cancer-targeted oncolytic poxvirus in humans", Nature **477**, 7362, 99–102 (2011).

Byrne, H. M., "Modelling avascular tumour growth", Cancer modelling and simulation **3** (2003).

Cattaneo, R., T. Miest, E. V. Shashkova and M. A. Barry, "Reprogrammed viruses as cancer therapeutics: targeted, armed and shielded", Nat Rev Microbiol **6**, 7, 529–40 (2008).

Cerullo, V., S. Pesonen, I. Diaconu, S. Escutenaire, P. T. Arstila, M. Ugolini, P. Nokisalmi, M. Raki, L. Laasonen, M. Särkioja *et al.*, "Oncolytic adenovirus coding for granulocyte macrophage colony-stimulating factor induces antitumoral immunity in cancer patients", Cancer research **70**, 11, 4297–4309 (2010).

Chen, Y., T. DeWeese, J. Dilley, Y. Zhang, Y. Li, N. Ramesh, J. Lee, R. Pennathur-Das, J. Radzyminski, J. Wypych *et al.*, "Cv706, a prostate cancer-specific adenovirus variant, in combination with radiotherapy produces synergistic antitumor efficacy without increasing toxicity", Cancer research **61**, 14, 5453–5460 (2001).

Chiocca, E. A., K. M. Abbed, S. Tatter, D. N. Louis, F. H. Hochberg, F. Barker, J. Kracher, S. A. Grossman, J. D. Fisher, K. Carson *et al.*, "A phase i open-label, dose-escalation, multi-institutional trial of injection with an e1b-attenuated adenovirus, onyx-015, into the peritumoral region of recurrent malignant gliomas, in the adjuvant setting", Molecular Therapy **10**, 5, 958–966 (2004).

De Boer, R., I. Kevrekidis and A. Perelson, "A simple idiotypic network model with complex dynamics", Chemical Engineering Science **45**, 8, 2375–2382 (1990).

De Boer, R. J., M. Oprea, R. Antia, K. Murali-Krishna, R. Ahmed and A. S. Perelson, "Recruitment times, proliferation, and apoptosis rates during the cd8+ t-cell response to lymphocytic choriomeningitis virus", Journal of virology **75**, 22, 10663–10669 (2001).

de Pillis, L. G., W. Gu and A. E. Radunskaya, "Mixed immunotherapy and chemotherapy of tumors: modeling, applications and biological interpretations", Journal of theoretical biology **238**, 4, 841–862 (2006).

de Pillis, L. G., A. E. Radunskaya and C. L. Wiseman, "A validated mathematical model of cell-mediated immune response to tumor growth", Cancer research **65**, 17, 7950–7958 (2005).

Dibrov, B., M. Livshits and M. Volkenstein, "Mathematical model of immune processes", Journal of theoretical biology **65**, 4, 609–631 (1977).

Dingli, D., M. D. Cascino, K. Josić, S. J. Russell and Ž. Bajzer, "Mathematical modeling of cancer radiovirotherapy", Mathematical Biosciences **199**, 1, 55–78 (2006).

Dingli, D., C. Offord, R. Myers, K. Peng, T. Carr, K. Josic, S. Russell and Z. Bajzer, "Dynamics of multiple myeloma tumor therapy with a recombinant measles virus", Cancer gene therapy **16**, 12, 873–882 (2009).

Dingli, D., K.-W. Peng, M. E. Harvey, P. R. Greipp, M. K. O'Connor, R. Cattaneo, J. C. Morris and S. J. Russell, "Image-guided radiovirotherapy for multiple myeloma using a recombinant measles virus expressing the thyroidal sodium iodide symporter", Blood **103**, 5, 1641–1646 (2004).

Donnelly, O., K. Harrington, A. Melcher and H. Pandha, "Live viruses to treat cancer", Journal of the Royal Society of Medicine **106**, 8, 310–314 (2013).

Farmer, J. D., N. H. Packard and A. S. Perelson, "The immune system, adaptation, and machine learning", Physica D: Nonlinear Phenomena **22**, 1, 187–204 (1986).

Forterre, P., "Defining life: the virus viewpoint", Origins of Life and Evolution of Biospheres **40**, 2, 151–160 (2010).

Frisch, S. M. and J. S. Mymryk, "Adenovirus-5 e1a: paradox and paradigm", Nature reviews Molecular cell biology **3**, 6, 441–452 (2002).

Gatenby, R. A. and T. L. Vincent, "Application of quantitative models from population biology and evolutionary game theory to tumor therapeutic strategies", Molecular cancer therapeutics **2**, 9, 919–927 (2003).

Gey, G., W. Coffman and M. T. Kubicek, "Tissue culture studies of the proliferative capacity of cervical carcinoma and normal epithelium", in "Cancer research", vol. 12, pp. 264–265 (AMER ASSOC CANCER RESEARCH PO BOX 11806, BIRMINGHAM, AL 35202, 1952).

Green, N., C. W. Herbert, S. Hale, A. Hale, V. Mautner, R. Harkins, T. Hermiston, K. Ulbrich, K. Fisher and L. Seymour, "Extended plasma circulation time and decreased toxicity of polymer-coated adenovirus", Gene therapy **11**, 16, 1256–1263 (2004).

Hahnfeldt, P., J. Folkman and L. Hlatky, "Minimizing long-term tumor burden: the logic for metronomic chemotherapeutic dosing and its antiangiogenic basis", Journal of theoretical biology **220**, 4, 545–554 (2003).

Hanahan, D. and R. A. Weinberg, "Hallmarks of cancer: the next generation", cell **144**, 5, 646–674 (2011).

Harrow, S., V. Papanastassiou, J. Harland, R. Mabbs, R. Petty, M. Fraser, D. Hadley, J. Patterson, S. Brown and R. Rampling, "Hsv1716 injection into the brain adjacent to tumour following surgical resection of high-grade glioma: safety data and long-term survival", Gene therapy **11**, 22, 1648–1658 (2004).

Heo, J., T. Reid, L. Ruo, C. J. Breitbach, S. Rose, M. Bloomston, M. Cho, H. Y. Lim, H. C. Chung, C. W. Kim *et al.*, "Randomized dose-finding clinical trial of oncolytic immunotherapeutic vaccinia jx-594 in liver cancer", Nature medicine **19**, 3, 329–336 (2013).

Hethcote, H. W., "Qualitative analyses of communicable disease models", Mathematical Biosciences **28**, 3, 335–356 (1976).

Hsu, F. J., C. Benike, F. Fagnoni, T. M. Liles, D. Czerwinski, B. Taidi, E. G. Engleman and R. Levy, "Vaccination of patients with b–cell lymphoma using autologous antigen–pulsed dendritic cells", Nature medicine **2**, 1, 52–58 (1996).

Huang, J.-H., S.-N. Zhang, K.-J. Choi, I.-K. Choi, J.-H. Kim, M. Lee, H. Kim and C.-O. Yun, "Therapeutic and tumor-specific immunity induced by combination of dendritic cells and oncolytic adenovirus expressing il-12 and 4-1bbl", Molecular Therapy **18**, 2, 264–274 (2010).

Kareva, I., F. Berezovskaya and C. Castillo-Chavez, "Myeloid cells in tumour–immune interactions", Journal of biological dynamics **4**, 4, 315–327 (2010).

Kareva, I., F. Berezovskaya and C. Castillo-Chavez, "Transitional regimes as early warning signals in resource dependent competition models", Mathematical biosciences **240**, 2, 114–123 (2012).

Kareva, I. and P. Hahnfeldt, "The emerging hallmarks of metabolic reprogramming and immune evasion: distinct or linked?", Cancer research **73**, 9, 2737–2742 (2013).

Kaufman, H. L., G. DeRaffele, J. Mitcham, D. Moroziewicz, S. M. Cohen, K. S. Hurst-Wicker, K. Cheung, D. S. Lee, J. Divito, M. Voulo *et al.*, "Targeting the local tumor microenvironment with vaccinia virus expressing b7. 1 for the treatment of melanoma", The Journal of clinical investigation **115**, 7, 1903–1912 (2005).

Kelly, E. and S. J. Russell, "History of oncolytic viruses: genesis to genetic engineering", Molecular Therapy **15**, 4, 651–659 (2007).

Kermack, W. O. and A. G. McKendrick, "A contribution to the mathematical theory of epidemics", in "Proceedings of the Royal Society of London A: mathematical, physical and engineering sciences", vol. 115, pp. 700–721 (The Royal Society, 1927).

Kim, J., J.-H. Kim, K.-J. Choi, P.-H. Kim and C.-O. Yun, "E1a-and e1b-double mutant replicating adenovirus elicits enhanced oncolytic and antitumor effects", Human gene therapy **18**, 9, 773–786 (2007).

Kim, P. S., J. J. Crivelli, I.-K. Choi, C.-O. Yun and J. R. Wares, "Quantitative impact of immunomodulation versus oncolysis with cytokine-expressing virus therapeutics.", Mathematical biosciences and engineering: MBE **12**, 4, 841–858 (2015a).

Kim, Y., D. R. Clements, A. M. Sterea, H. W. Jang, S. A. Gujar and P. W. Lee, "Dendritic cells in oncolytic virus-based anti-cancer therapy", Viruses **7**, 12, 6506–6525 (2015b).

Kirschner, D. and J. C. Panetta, "Modeling immunotherapy of the tumor–immune interaction", Journal of mathematical biology **37**, 3, 235–252 (1998).

Komarova, N. and D. Wodarz, "Targeted cancer treatment in silico", in "Modeling and simulation in science, engineering and technology", (Springer, 2014).

Kuang, Y., J. D. Nagy and S. E. Eikenberry, *Introduction to Mathematical Oncology*, vol. 59 (CRC Press, 2016).

Ledford, H., "Cancer-fighting viruses win approval", Nature **526**, 7575, 1 (2015).

Li, H., S. Li, J. Shao, X. Lin, Y. Cao, W. Jiang, R. Liu, P. Zhao, X. Zhu, M. Zeng *et al.*, "Pharmacokinetic and pharmacodynamic study of intratumoral injection of an adenovirus encoding endostatin in patients with advanced tumors", Gene therapy **15**, 4, 247–256 (2008).

Lodish, H., A. Berk and S. Zipursky, "Molecular cell biology 4th edition", (2000).

Lotka, A. J., "Contribution to the theory of periodic reactions", The Journal of Physical Chemistry **14**, 3, 271–274 (1910).

Lotka, A. J. *et al.*, "Elements of physical biology", (1925).

Marušic, M., Ž. Bajzer, S. Vuk-Pavlovic and J. P. Freyer, "Tumor growthin vivo and as multicellular spheroids compared by mathematical models", Bulletin of mathematical biology **56**, 4, 617–631 (1994).

May, R. M. *et al.*, "Simple mathematical models with very complicated dynamics", Nature **261**, 5560, 459–467 (1976).

Michelson, S., B. Miller, A. Glicksman and J. Leith, "Tumor micro-ecology and competitive interactions", Journal of theoretical biology **128**, 2, 233–246 (1987).

Miller, E., "Population dynamics of infectious diseases: Theory and applications", Immunology **50**, 4, 677 (1983).

Mullen, J. T. and K. K. Tanabe, "Viral oncolysis", The oncologist **7**, 2, 106–119 (2002).

Nagy, J. D., "The ecology and evolutionary biology of cancer: a review of mathematical models of necrosis and tumor cell diversity.", Mathematical biosciences and engineering: MBE **2**, 2, 381–418 (2005).

Nemunaitis, J., F. Khuri, I. Ganly, J. Arseneau, M. Posner, E. Vokes, J. Kuhn, T. McCarty, S. Landers, A. Blackburn *et al.*, "Phase ii trial of intratumoral administration of onyx-015, a replication-selective adenovirus, in patients with refractory head and neck cancer", Journal of Clinical Oncology **19**, 2, 289–298 (2001).

Nesrua, F. O., S. Atuaolcl, M. GILLIE, Y. SUNZ and S.-Z. Gimasr, "Vaccination of melanoma patients with peptide-or tumor lysate-pulsed dendritic cells", peptides **1**, A2 (1998).

Nowak, M. and R. M. May, *Virus dynamics: mathematical principles of Immunology and virology: mathematical principles of Immunology and virology* (Oxford university press, 2000).

Nowak, M. A. and C. R. Bangham, "Population dynamics of immune responses to persistent viruses", Science **272**, 5258, 74–79 (1996).

Okamoto, K. W., P. Amarasekare and I. T. Petty, "Modeling oncolytic virotherapy: Is complete tumor-tropism too much of a good thing?", Journal of theoretical biology **358**, 166–178 (2014).

Oster, G. F. and A. S. PERELSON, "The physics of cell motility", Journal of Cell Science **1987**, Supplement 8, 35–54 (1987).

Patel, M. R. and R. A. Kratzke, "Oncolytic virus therapy for cancer: the first wave of translational clinical trials", Translational Research **161**, 4, 355–364 (2013).

Perelson, A. S., "Immune network theory", Immunological reviews **110**, 1, 5–36 (1989).

Perelson, A. S., M. Mirmirani and G. F. Oster, "Optimal strategies in immunology", Journal of mathematical biology **3**, 3-4, 325–367 (1976).

Perelson, A. S. and G. F. Oster, "Theoretical studies of clonal selection: minimal antibody repertoire size and reliability of self-non-self discrimination", Journal of theoretical biology **81**, 4, 645–670 (1979).

Phys.org, "Nanoparticles with protein 'passports' evade immune system, deliver more medication to tumors", (2013).

Pichlmair, A. and C. R. e Sousa, "Innate recognition of viruses", Immunity **27**, 3, 370–383 (2007).

Pol, J. G., J. Rességuier and B. Lichty, "Oncolytic viruses: a step into cancer immunotherapy", Virus Adapt Treat **4**, 1–21 (2012).

Portz, T. and Y. Kuang, "A mathematical model for the immunotherapy of advanced prostate cancer", in "BIOMAT 2012", pp. 70–85 (World Scientific, 2013).

Power, A. T., J. Wang, T. J. Falls, J. M. Paterson, K. A. Parato, B. D. Lichty, D. F. Stojdl, P. A. J. Forsyth, H. Atkins and J. C. Bell, "Carrier cell-based delivery of an oncolytic virus circumvents antiviral immunity", Mol Ther **15**, 1, 123–30 (2007).

Prestwich, R. J., K. J. Harrington, H. S. Pandha, R. G. Vile, A. A. Melcher and F. Errington, "Oncolytic viruses: a novel form of immunotherapy", (2008).

Rabinovich, G. A., D. Gabrilovich and E. M. Sotomayor, "Immunosuppressive strategies that are mediated by tumor cells", Annual review of immunology **25**, 267 (2007).

Reid, T., E. Galanis, J. Abbruzzese, D. Sze, L. M. Wein, J. Andrews, B. Randlev, C. Heise, M. Uprichard, M. Hatfield *et al.*, "Hepatic arterial infusion of a replication-selective oncolytic adenovirus (dl1520) phase ii viral, immunologic, and clinical endpoints", Cancer research **62**, 21, 6070–6079 (2002).

Relph, K., H. Pandha, G. Simpson, A. Melcher and K. Harrington, "Cancer immunotherapy via combining oncolytic virotherapy with chemotherapy: recent advances", Oncolytic Virotherapy **2016**, 5, 1–13 (2016).

Russell, S. J., K.-W. Peng and J. C. Bell, "Oncolytic virotherapy", Nature biotechnology **30**, 7, 658–670 (2012).

Shah, A. C., D. Benos, G. Y. Gillespie and J. M. Markert, "Oncolytic viruses: clinical applications as vectors for the treatment of malignant gliomas", Journal of neuro-oncology **65**, 3, 203–226 (2003).

Shors, T., *Understanding viruses* (Jones & Bartlett Publishers, 2011).

Srinivasan, P. *et al.*, "Adenoviruses in gene therapy-a review", Bioengineering and Bioscience **3**, 1, 1–5 (2015).

Strogatz, S. H., *Nonlinear dynamics and chaos: with applications to physics, biology, chemistry, and engineering* (Westview press, 2014).

Tian, J. P., "The replicability of oncolytic virus: defining conditions in tumor virotherapy", Math Biosci Eng **8**, 3, 841–60 (2011).

Tjoa, B., S. Erickson, V. Bowes, H. Ragde, G. Kenny, O. Cobb, R. Ireton, M. Troychak, A. Boynton and G. Murphy, "Follow-up evaluation of prostate cancer patients infused with autologous dendritic cells pulsed with psma peptides", The Prostate **32**, 4, 272–278 (1997).

Toth, K. and W. S. Wold, "Increasing the efficacy of oncolytic adenovirus vectors", Viruses **2**, 9, 1844–1866 (2010).

Trinchieri, G., "Interleukin-12 and the regulation of innate resistance and adaptive immunity", Nature Reviews Immunology **3**, 2, 133–146 (2003).

Vähä-Koskela, M. and A. Hinkkanen, "Tumor restrictions to oncolytic virus", Biomedicines **2**, 2, 163–194 (2014).

Varghese, S. and S. D. Rabkin, "Oncolytic herpes simplex virus vectors for cancer virotherapy", Cancer Gene Ther **9**, 12, 967–78 (2002).

Veal, E., M. Eisenstein, Z. H. Tseng and G. Gill, "A cellular repressor of e1a-stimulated genes that inhibits activation by e2f", Molecular and cellular biology **18**, 9, 5032–5041 (1998).

Verhulst, P.-F., "Notice sur la loi que la population suit dans son accroissement. correspondance mathématique et physique publiée par a", Quetelet **10**, 113–121 (1838).

Walsh, M. P., J. Seto, E. B. Liu, S. Dehghan, N. R. Hudson, A. N. Lukashev, O. Ivanova, J. Chodosh, D. W. Dyer, M. S. Jones *et al.*, "Computational analysis of two species c human adenoviruses provides evidence of a novel virus", Journal of clinical microbiology **49**, 10, 3482–3490 (2011).

Wang, K., W. Wang, H. Pang and X. Liu, "Complex dynamic behavior in a viral model with delayed immune response", Physica D: Nonlinear Phenomena **226**, 2, 197–208 (2007).

Wang, Y., H. Wang, C.-Y. Li and F. Yuan, "Effects of rate, volume, and dose of intratumoral infusion on virus dissemination in local gene delivery", Molecular cancer therapeutics **5**, 2, 362–366 (2006).

Wares, J. R., J. J. Crivelli, C.-O. Yun, I.-K. Choi, J. L. Gevertz and P. S. Kim, "Treatment strategies for combining immunostimulatory oncolytic virus therapeutics with dendritic cell injections", Mathematical biosciences and engineering: MBE **12**, 6, 1237–1256 (2015).

Wierecky, J., M. R. Müller, S. Wirths, E. Halder-Oehler, D. Dörfel, S. M. Schmidt, M. Häntschel, W. Brugger, S. Schröder, M. S. Horger *et al.*, "Immunologic and clinical responses after vaccinations with peptide-pulsed dendritic cells in metastatic renal cancer patients", Cancer Research **66**, 11, 5910–5918 (2006).

Wodarz, D., "Viruses as antitumor weapons defining conditions for tumor remission", Cancer research **61**, 8, 3501–3507 (2001).

Wodarz, D., "Gene therapy for killing p53-negative cancer cells: use of replicating versus nonreplicating agents", Human gene therapy **14**, 2, 153–159 (2003).

Wodarz, D., P. Klenerman and M. A. Nowak, "Dynamics of cytotoxic t–lymphocyte exhaustion", Proceedings of the Royal Society of London B: Biological Sciences **265**, 1392, 191–203 (1998).

Wodarz, D. and N. Komarova, "Lecture notes and mathematical modeling", (2005).

Worgall, S., G. Wolff, E. Falck-Pedersen and R. G. Crystal, "Innate immune mechanisms dominate elimination of adenoviral vectors following in vivo administration", Human gene therapy **8**, 1, 37–44 (1997).

Wu, J. T., H. M. Byrne, D. H. Kirn and L. M. Wein, "Modeling and analysis of a virus that replicates selectively in tumor cells", Bull Math Biol **63**, 4, 731–68 (2001).

Zhang, S.-N., I.-K. Choi, J.-H. Huang, J.-Y. Yoo, K.-J. Choi and C.-O. Yun, "Optimizing dc vaccination by combination with oncolytic adenovirus coexpressing il-12 and gm-csf", Molecular Therapy **19**, 8, 1558–1568 (2011).

APPENDIX A

PROOFS

Positive Invariance proof from 3.2.1

Proof. Suppose $x+y=K \rightarrow \frac{d(x+y)}{dt} = rx\left(1-\frac{x+y}{K}\right)-\mu x-\beta\, xv+\beta\, xv+sy\left(1-\frac{x+y}{K}\right)-\alpha y-\rho yz < 0$. Logistic growth terms $rx\left(1-\frac{x+y}{K}\right) \rightarrow 0$ and $sy\left(1-\frac{x+y}{K}\right) \rightarrow 0$, $\beta\, xv-\beta xv=0$,
$\implies \frac{d(x+y)}{dt} = -\mu x-\alpha y-\rho yz < 0$. It is trivial to show that $\frac{dx}{dt}, \frac{dy}{dt}, \frac{dz}{dt} \& \frac{dv}{dt} \geq 0$.
$\therefore$ the system is positively invariant. □

Proof for Theorem 1

The Generalized Jacobian matrix is:

$$J(E^*) = \begin{bmatrix} r\left(1-\frac{x^*+y^*}{K}\right)-\frac{rx^*}{K}-\mu-\beta\, v^* & -\frac{rx^*}{K} & 0 & -\beta\, x^* \\ \beta\, v^*-\frac{sy^*}{K} & s\left(1-\frac{x^*+y^*}{K}\right)-\frac{sy^*}{K}-\alpha-\rho z^* & -\rho y^* & \beta\, x^* \\ 0 & z^*\sigma & 0 & 0 \\ 0 & N\alpha & 0 & -\xi \end{bmatrix}$$

Proof. To prove that E_0 is stable, it is sufficient to show that the system linearized at this equilibrium has eigenvalues with real parts negative. This is represented in the following Jacobian :

We look at the Jacobian to assess the stability of E_0, represented as:

$$J(E_0) = \begin{bmatrix} r-\mu & 0 & 0 & 0 \\ 0 & s-\alpha & 0 & 0 \\ 0 & 0 & -\phi & 0 \\ 0 & N\alpha & 0 & -\xi \end{bmatrix}$$

From the diagonal matrix, the eigenvalues $\lambda_1 = -\xi, \lambda_2 = -(\mu-r), \lambda_3 = -\phi$ and $\lambda_4 = -(\alpha-s)$ are deduced. Whenever, $\lambda_1, \lambda_2, \lambda_3, \lambda_4 < 0$, the equilibria is locally asymptotically stable. Thus, whenever $r < \mu$, and $s < \alpha$, E_0 is L.A.S. Otherwise E_0 is unstable.

□

Proof for Theorem 2

Proof. The Jacobian to asses the stability of E_1, represented as:

$$J(E_1) = \begin{bmatrix} -(r-\mu) & -(r-\mu) & 0 & -\frac{\beta K(r-\mu)}{r} \\ 0 & -\frac{\alpha r-\mu s}{r} & 0 & \frac{\beta K(r-\mu)}{r} \\ 0 & 0 & -\phi & 0 \\ 0 & N\alpha & 0 & -\xi \end{bmatrix}$$

From the matrix, the eigenvalues $\lambda_1 = -(r-\mu), \lambda_2 = -\phi$, and the other eigenvalues can be funded by the solution of the next quadratic form

$$\lambda^2 + a_1\lambda + a_0$$

with $a_1 = [\xi + \frac{\alpha r - \mu s}{r}]$ and $a_0 = [\xi\frac{\alpha r - \mu s}{r} - \frac{\beta N \alpha K(r-\mu)}{r}] = \xi\frac{\alpha r - \mu s}{r}(1 - R_0)$, for all $r > \mu$.

In case of $\alpha r - \mu s > 0$ the roots of the quadratic equation are negative if and only if $R_0 < 1$ and also it is easy to see that if $R_0 \geq 1$ E_1 is unstable.

In case of in case of $\alpha r - \mu s < 0$ it is clear to see that $a_0 < 0$; then E_1 is unstable. Moreover, it is easy to prove that $a_1^2 - 4a_0 > 0$ in both cases. Thus E_1, is locally-asymptotically stable if and only if $R_0 < 1$ and $\alpha > s$ for all $r > \mu$.

□

Note that $R_0 < 1$ if and only if $\mu < r < \dfrac{N\beta K\alpha - s\xi}{N\beta K\alpha - \alpha\xi}\mu$

Proof for Theorem 3

Proof. The Jacobian to assess the stability of E_1, represented as:

$$J(E_2) = \begin{bmatrix} r\frac{\alpha}{s} - \mu - (s-\alpha)\frac{\beta N\alpha K}{s\xi} & 0 & 0 & 0 \\ \beta\frac{NK\alpha(s-\alpha)}{s\xi} - (s-\alpha) & -(s-\alpha) & -p\frac{K(s-\alpha)}{s} & 0 \\ 0 & 0 & \sigma\frac{K(s-\alpha)}{s} - \phi & 0 \\ 0 & N\alpha & 0 & -\xi \end{bmatrix}$$

From the matrix, the eigenvalues $\lambda_1 = -(s-\alpha), \lambda_2 = -\xi$, $\lambda_3 = -(\frac{\phi s}{K(s-\alpha)} - \sigma)$ and $\lambda_4 = r\frac{\alpha}{s} - \mu - (s-\alpha)\frac{\beta N\alpha}{s\xi}$. Thus, $\lambda_3 < 0$ if and only if $\sigma < \frac{\phi s}{K(s-\alpha)}$ also $\lambda_4 < 0$ if and only if $r < \mu$.

□

Proof for Theorem 4

Proof. The Jacobian to asses the stability of E_3, represented as:

$$J(E_3) = \begin{bmatrix} r(1-\frac{y}{K}) - \mu - \beta\, v & 0 & 0 & 0 \\ \beta\, v - \frac{sy}{K} & s\left(1-\frac{y}{K}\right) - \frac{sy}{K} - \alpha - pz & -py & 0 \\ 0 & z\sigma & 0 & 0 \\ 0 & N\alpha & 0 & -\xi \end{bmatrix}$$

From the matrix, the eigenvalues are $\lambda_1 = -\{\frac{K}{K-\frac{\phi}{\sigma}}(\mu + \frac{\beta N\alpha\phi}{\sigma\xi}) - r\}, \lambda_2 = -\xi$, and the other eigenvalues can be funded by the solutions of the next quadratic form

$$\lambda^2 + b_1\lambda + b_0$$

with $b_1 = \frac{s\phi}{\sigma K}$ and $b_0 = \phi(s\frac{K-\frac{\phi}{\sigma}}{K} - \alpha)$. Since $b_1 > 0$ and $b_0 > 0$ for all $\sigma > \frac{\phi s}{K(s-\alpha)}$ Thus, E_3 is stable if and only if $\sigma > \frac{\phi s}{K(s-\alpha)}$ and $\sigma > \frac{\beta NK\alpha b + rb\xi}{K\xi(r-\mu)}$, otherwise E_3 is unstable.

□

APPENDIX B

PRE-OVIT MODEL

Experimental Design

Mice with B16-F10 subcutaneous tumors were intratumorally infected with PBS, $Ad-\Delta B7$, $Ad-\Delta B7/IL-12$, $Ad-\Delta B7/4-1BBL$ and $Ad-\Delta B7/IL-12/4-1BBL$. Each experiment contained n=8-9 mice.

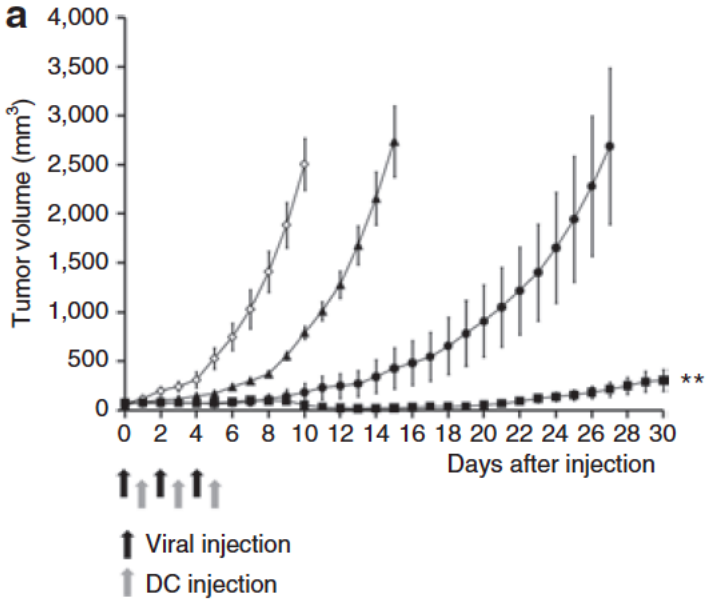

This data set developed the following model that can capture the dual oncolytic and immunotherapy aspects.

Model Formulation

$$\frac{dx}{dt} = rx - \beta\frac{xv}{K} - (\gamma_x + \kappa y)\frac{xt}{K} \tag{B.1a}$$

$$\frac{dy}{dt} = \beta\frac{xv}{K} - \alpha_y y - (\gamma_y + \kappa y)\frac{yz}{K} \tag{B.1b}$$

$$\frac{dv}{dt} = u_v(t) + N\alpha y - \delta_v v \tag{B.1c}$$

$$\frac{dz}{dt} = \rho D - \delta_z z \tag{B.1d}$$

$$\frac{dD}{dt} = \sigma_x x + \sigma_y y - \delta_d D + u_d(t) \tag{B.1e}$$

The model consists of x, y, v, z and D representing uninfected cancer cells, infected cancer cells, virus free particles, T killer cells, and dendritic cells, respectively. This model is an extension from Wares *et al.* (2015). Uninfected cells grow exponentially at growth r, and are killed off by T killer cells at facilitation rate κy . The term κy is dependent on infected cells, therefore, the assumption is that oncolytic viruses

facilitate an immune response via the T killer cells towards the tumor. Uninfected cancer cells are infected at rate β, as standard incidence, where $K = x + y + z + D$. Infected cells die at lysing rate α, T killer cells have an enhanced immune response at rate γ_x and γ_y, for uninfected and infected cancer cells, respectively. This is due to the OV immunogenicity trait. Viruses are grown from lysing rate α with burst size N, and decay at δ_v. T killer cells are activated by dendritic cells at rate ρ and have a half life at rate δ_z. Dendritic cells are recruited from the presence of tumor and infected tumor populations at rates, σ_x and σ_y, respectively and decay at rate δ_D. Therapies are introduced as delta functions for $u_v(t)$ and $u_d(t)$ for virotherapy and immunotherapy. The model has fit to $u_v(t) = u_0\delta(0) + \delta(2) + \delta(4)$, and $u_d(t) = u_0\delta(1) + \delta(3) + \delta(5)$.

Parameter Fitting

Model (B.1) was fit to experimental data from Huang *et al.* (2010)

Parameter	Description	PBS	DC	Ad-ΔB7 /4-1BBL	Ad-ΔB7 /4-1BBL +DC
r	Uninfected tumor cell growth rate	0.34484	0.34484	0.34484	0.34484
γ_x	T cell contact rate, uninfected	-	0.17206	0.17206	0.17206
γ_y	T cell contact rate, infected	-	0.17206	0.17206	0.17206
σ_x	dendrite activation from uninfected cells	-	0.15113	0.15113	0.15113
σ_y	dendrite activation from infected cells	-	-	$\sigma_x * 1.1$	$\sigma_x * 1.1$
β	Viral infectious rate	-	-	0.0053884	0.0058385
κ	T cell killing rate	-	-	8.5×10^{-7}	8.5×10^{-7}
δ_z	T cell decay rate	-	0.35	0.35	0.35
δ_D	Dendritic cell death rate	-	0.35	0.35	0.35
ρ	T cell activation rate by dendritic cells	-	1	1	1
u_{0D}	Dendritic concentration	-	10^6	-	10^6
u_{0V}	Adenovirus concentration	-	-	2.5 x 10^9	2.5 x 10^9
N	adenovirus burst size	-	-	3500	3500
α	Infected lysis	-	-	1	1
δ_V	Viral decay rate	-	-	2.3	2.3

Table B.1: Parameter estimates for model (B.1)

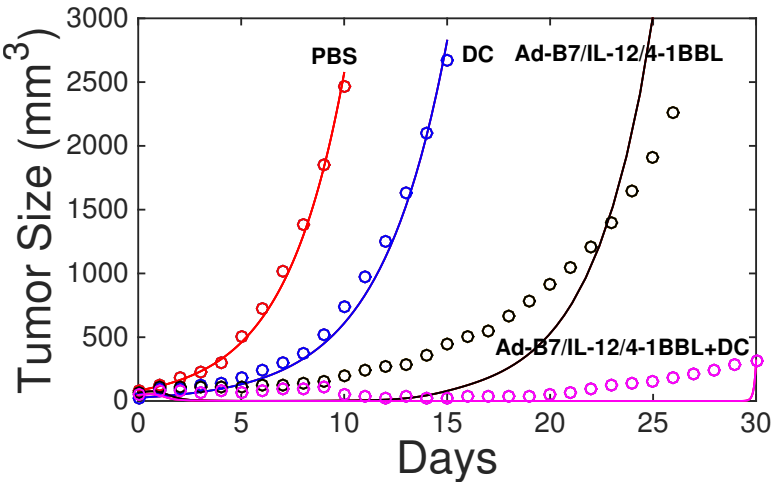

From the fits, one could confer that since there is no difference between γ_x and γ_y, the model may not convey the T cell immune response independently. Furthermore, it is suggested that OV activate immune response near the infected cells, such that $\gamma_x << \gamma_y$, which does not seem to be captured in these fittings.
Additionally, σ_x is removed as the dendritic cell activation from the uninfected cells is considered relatively small compared to infected cells, under common immune suppressed conditions. Therefore, $\sigma_y = \sigma_x * 1.1$ to attempt to account for a more abundant immune response from the infected cell.

The model may could be improved to capture suggested dynamics of the immune response by further simplifying it, by removing parameters that carry less weight within the biology. Parameters γ_x and σ_x are removed in the model in Chapter 4, as they seem to be considered biologically not as significant as the interactions from the infected populations to the immune components.

APPENDIX C

PERMUTATION TABLES

All tables presented in Chapter 4 included up to 20 permutations. This appendix includes more data. However, data sets that include 729 - 4096 permutations were capped at 60 permutations in this appendix.

Tables C.1-C.2 shows all 64 permutations for altering regimes, with flexible frequencies.

Table (C.1) represents all possible 64 permutations of six treatments for the first six days of therapy.

Permutation Rank	Day 1	2	3	4	5	6	Tumor Volume (mm^3)	Oncolytic Virus dose number	Dendritic Cells dose number
1	V	V	V	V	V	V	4.3	6	0
2	D	V	V	V	V	V	6.4	5	1
3	V	D	V	V	V	V	13.6	5	1
4	V	V	V	V	V	D	14	5	1
5	D	V	V	V	V	D	17.9	4	2
6	D	D	V	V	V	V	22	4	2
7	V	V	D	V	V	V	22.1	5	1
8	V	V	V	V	D	V	22.8	5	1
9	D	V	V	V	D	V	24	4	2
10	D	V	D	V	V	V	25.2	4	2
11	D	V	V	D	V	V	27.3	4	2
12	V	V	V	D	V	V	29.2	5	1
13	V	D	V	V	V	D	35	4	2
14	V	D	D	V	V	V	35.7	4	2
15	V	D	V	V	D	V	40	4	2
16	V	D	V	D	V	V	40.9	4	2
17	D	V	V	V	D	D	49	3	3
18	V	V	V	V	D	D	49.6	4	2
19	D	D	D	V	V	V	50.3	3	3
20	D	D	V	D	V	V	53.1	3	3
21	V	V	D	D	V	V	55.5	4	2
22	D	D	V	V	V	D	55.9	3	3
23	D	D	V	V	D	V	56.7	3	3
24	D	V	D	D	V	V	58.4	3	3
25	V	V	D	V	V	D	58.5	4	2
26	V	V	D	V	D	V	61.3	4	2
27	D	V	D	V	D	V	62.3	3	3
28	D	V	D	V	V	D	62.7	3	3
29	D	V	V	D	D	V	64.6	3	3
30	D	V	V	D	V	D	65.9	3	3
31	V	D	D	D	V	V	77.4	3	3
32	V	V	V	D	D	V	86.1	4	2
33	V	D	D	V	D	V	86.7	3	3
34	V	V	V	D	V	D	87	4	2
35	V	D	D	V	V	D	94.2	3	3
36	V	D	V	V	D	D	98.6	3	3
37	V	D	V	D	D	V	101.2	3	3
38	V	D	V	D	V	D	113.6	3	3
39	D	D	D	V	D	V	123.6	2	4
40	D	D	D	D	V	V	124	2	4
41	D	D	V	D	D	V	130.5	2	4
42	D	V	D	D	D	V	143.7	2	4
43	V	V	D	D	D	V	146.3	3	3
44	D	D	D	V	V	D	153	2	4
45	D	D	V	D	V	D	159.5	2	4
46	D	D	V	V	D	D	167.7	2	4
47	D	V	D	D	V	D	179.1	2	4
48	V	V	D	D	V	D	181.9	3	3
49	D	V	V	D	D	D	188.8	2	4
50	D	V	D	V	D	D	189	2	4
51	V	V	D	V	D	D	209.3	3	3
52	V	D	D	D	D	V	224.1	2	4
53	V	D	D	D	V	D	301.1	2	4
54	V	D	D	V	D	D	385.9	2	4
55	V	V	V	D	D	D	630.7	3	3
56	V	D	V	D	D	D	640	2	4
57	D	D	D	D	D	V	1594.3	1	5
58	D	D	D	D	V	D	1639.7	1	5
59	D	D	D	V	D	D	1755.6	1	5
60	D	D	V	D	D	D	2203.7	1	5
61	D	V	D	D	D	D	5171.3	1	5
62	V	V	D	D	D	D	29485	2	4
63	V	D	D	D	D	D	715180	1	5
64	D	D	D	D	D	D	11861000	0	6

Table C.1: Permutation table representing flexible count for oncolytic viruses and dendritic cell vaccines, over 6 days. All 64 are displayed, predicting the tumor size at day 30. Each injection included V=5×10^{10}, D=1×10^{6}.

Table (4.5) shows the 64 permutations for administering combination treatment without limitations on frequency per treatment, however the max dosage concentration is limited to the amount used in the experiment from Zhang *et al.* (2011).

Permutation Rank	Day 1	2	3	4	5	6	Tumor Volume (mm^3)	Oncolytic Virus dose number	Dendritic Cells dose number
1	D	V	V	V	V	D	42.9	4	2
2	V	V	V	V	V	V	44.1	6	0
3	D	V	V	V	D	D	49	3	3
4	D	D	D	V	V	V	50.3	3	3
5	D	D	V	V	V	V	50.3	4	2
6	D	V	V	V	V	V	51.9	5	1
7	D	D	V	D	V	V	53.1	3	3
8	D	V	V	V	D	V	54.2	4	2
9	D	D	V	V	V	D	55.9	3	3
10	D	D	D	D	V	V	56.2	2	4
11	D	V	D	V	V	V	56.5	4	2
12	D	D	V	V	D	V	56.7	3	3
13	D	D	D	V	D	V	57.6	2	4
14	D	V	D	D	V	V	58.4	3	3
15	D	V	V	D	V	V	59.7	4	2
16	D	D	V	D	D	V	61	2	4
17	D	V	D	V	D	V	62.3	3	3
18	D	V	D	V	V	D	62.7	3	3
19	D	V	V	D	D	V	64.6	3	3
20	D	V	V	D	V	D	65.9	3	3
21	D	V	D	D	D	V	67.9	2	4
22	D	D	D	V	V	D	68.8	2	4
23	V	D	V	V	V	D	70.7	4	2
24	V	D	V	V	V	V	73	5	1
25	D	D	V	V	D	D	73.3	2	4
26	D	D	V	D	V	D	73.3	2	4
27	V	D	D	V	V	V	73.4	4	2
28	D	V	V	D	D	D	75.2	2	4
29	V	D	D	D	V	V	77.4	3	3
30	V	D	V	V	D	V	81.3	4	2
31	V	D	V	D	V	V	83.5	4	2
32	D	V	D	D	V	D	83.8	2	4
33	D	V	D	V	D	D	86.5	2	4
34	V	D	D	V	D	V	86.7	3	3
35	V	D	D	D	D	V	92.3	2	4
36	V	D	D	V	V	D	94.2	3	3
37	V	V	V	V	V	D	97.9	5	1
38	V	D	V	V	D	D	98.6	3	3
39	V	D	V	D	D	V	101.2	3	3
40	V	V	D	V	V	V	106.6	5	1
41	V	D	V	D	V	D	113.6	3	3
42	V	V	D	D	V	V	114.7	4	2
43	D	D	D	D	D	V	121.9	1	5
44	V	D	D	D	V	D	123	2	4
45	V	V	D	V	V	D	123.8	4	2
46	V	V	D	V	D	V	132.2	4	2
47	V	V	D	D	D	V	146.3	3	3
48	D	D	D	D	V	D	148.5	1	5
49	V	D	D	V	D	D	151.8	2	4
50	V	V	V	D	V	V	156.3	5	1
51	D	D	D	V	D	D	168.1	1	5
52	V	V	D	D	V	D	181.9	3	3
53	D	D	V	D	D	D	196.5	1	5
54	V	V	V	D	D	V	201	4	2
55	V	V	V	D	V	D	208.4	4	2
56	V	V	D	V	D	D	209.3	3	3
57	V	D	V	D	D	D	212.3	2	4
58	V	V	V	V	D	D	216	4	2
59	V	V	V	V	D	V	245.5	5	1
60	D	V	D	D	D	D	315.5	1	5
61	V	V	V	D	D	D	630.7	3	3
62	V	V	D	D	D	D	2063.2	2	4
63	V	D	D	D	D	D	4154.4	1	5
64	D	D	D	D	D	D	11900000	0	6

Table C.2: Permutation table of limited maximum doses for oncolytic viruses and dendritic cell vaccines. All permutations of the 64 are displayed, that predict the tumor size at day 30. $V_{max} = 1.5 \times 10^{11}$, $D_{max} = 3 \times 10^6$, where the dosages were fractioned over 6 days.

Tables C.3-C.4 show 60 of the 729 permutations for altering regimes with flexible frequencies, rest days included.

Permutation Rank	Day 1	2	3	4	5	6	Tumor Volume (mm^3)	Oncolytic Virus dose number	Dendritic Cells dose number	Rest Day count
1	V	-	V	-	-	V	26.6	3	0	3
2	V	V	-	V	-	V	27.7	4	0	2
3	V	V	V	-	-	V	29.7	4	0	2
4	V	V	V	-	V	V	33.8	5	0	1
5	V	V	-	-	-	V	34.1	3	0	3
6	V	V	V	V	-	V	37	5	0	1
7	V	-	V	V	-	V	37.8	4	0	2
8	D	V	-	V	V	D	37.9	3	2	1
9	D	-	V	-	V	V	39.5	3	1	2
10	D	-	-	V	-	V	39.6	2	1	3
11	D	V	-	-	V	V	39.9	3	1	2
12	D	-	V	-	-	V	40.1	2	1	3
13	D	-	-	V	V	V	40.3	3	1	2
14	V	V	-	-	V	V	40.5	4	0	2
15	D	-	V	V	V	D	40.9	3	2	1
16	D	V	-	-	-	V	41.3	2	1	3
17	D	-	V	-	V	D	41.5	2	2	2
18	V	V	-	V	V	V	41.5	5	0	1
19	D	-	-	-	V	V	41.8	2	1	3
20	D	V	-	-	V	D	41.8	2	2	2
21	D	V	V	V	V	D	42.9	4	2	0
22	V	V	V	V	V	V	44.1	6	0	0
23	D	D	-	V	-	V	44.4	2	2	2
24	D	D	V	-	V	V	44.5	3	2	1
25	V	-	-	V	-	V	44.6	3	0	3
26	D	V	-	V	V	V	44.8	4	1	1
27	D	-	V	V	V	V	44.9	4	1	1
28	D	D	-	V	V	V	45.1	3	2	1
29	D	D	V	-	-	V	45.4	2	2	2
30	D	D	-	-	V	V	45.9	2	2	2
31	D	V	V	-	V	D	46.7	3	2	1
32	D	-	V	V	-	V	47.6	3	1	2
33	D	V	-	V	-	V	48.1	3	1	2
34	D	V	-	V	D	D	48.7	2	3	1
35	D	V	V	-	V	V	48.8	4	1	1
36	D	V	V	V	D	D	49	3	3	0
37	-	D	-	V	-	V	49.2	2	1	3
38	V	-	V	-	V	V	49.4	4	0	2
39	-	D	V	-	V	V	49.7	3	1	2
40	D	D	D	V	-	V	49.8	2	3	1
41	-	D	-	V	V	V	49.8	3	1	2
42	D	-	D	V	-	V	50	2	2	2
43	-	D	-	-	V	V	50.1	2	1	3
44	D	D	D	V	V	V	50.3	3	3	0
45	D	D	V	V	V	V	50.3	4	2	0
46	D	V	-	V	D	V	50.3	3	2	1
47	D	-	D	V	V	V	50.5	3	2	1
48	D	D	D	-	V	V	50.7	2	3	1
49	D	-	-	V	V	D	50.8	2	2	2
50	-	D	V	-	-	V	50.8	2	1	3
51	D	V	D	-	V	V	51	3	2	1
52	D	-	D	-	V	V	51	2	2	2
53	-	D	V	-	V	D	51.9	2	2	2
54	D	V	V	V	V	V	51.9	5	1	0
55	V	-	V	-	V	-	52.4	3	0	3
56	-	D	V	V	V	D	52.5	3	2	1
57	D	V	D	-	-	V	52.6	2	2	2
58	D	D	V	D	V	V	53.1	3	3	0
59	D	D	V	V	-	V	53.3	3	2	1
60	D	V	-	D	V	V	53.9	3	2	1

Table C.3: Limited Dose with Rest days at $D_{max} = 3 \times 10^6$. Top 60 of 729 Permutations. Tumor size predicted at day 30. $V_{max} = 1.5 \times 10^{11}$, $D_{max} = 3 \times 10^6$, where the dosages were fractioned over 6 days.

Permutation Rank	Day 1	2	3	4	5	6	Tumor Volume (mm^3)	Oncolytic Virus dose number	Dendritic Cells dose number	Rest Day count
1	D	V	-	-	-	V	12.9	2	1	3
2	D	V	-	V	-	V	14.5	3	1	2
3	D	V	V	-	V	V	14.6	4	1	1
4	D	V	V	-	-	V	15.1	3	1	2
5	D	V	-	-	V	V	15.4	3	1	2
6	D	V	V	V	V	V	18	5	1	0
7	D	V	-	V	V	V	18.2	4	1	1
8	D	V	V	V	-	V	19.3	4	1	1
9	V	D	V	-	V	V	20	4	1	1
10	V	D	V	-	-	V	20.6	3	1	2
11	V	D	-	V	-	V	21	3	1	2
12	D	V	-	-	V	-	23	2	1	3
13	D	V	D	V	-	V	23.2	3	2	1
14	V	D	D	V	-	V	24	3	2	1
15	V	D	V	V	V	V	24.1	5	1	0
16	D	V	-	V	V	-	24.8	3	1	2
17	V	D	V	V	-	V	25.3	4	1	1
18	V	D	V	D	-	V	25.6	3	2	1
19	V	D	V	-	D	V	26.1	3	2	1
20	D	V	V	-	V	-	26.5	3	1	2
21	V	-	V	-	-	V	26.6	3	0	3
22	V	D	-	V	V	V	27	4	1	1
23	V	V	-	V	-	V	27.7	4	0	2
24	V	-	D	V	-	V	27.9	3	1	2
25	V	D	V	D	D	V	28.4	3	3	0
26	V	D	D	V	D	V	28.5	3	3	0
27	V	D	V	D	V	V	28.8	4	2	0
28	V	D	-	V	D	V	29	3	2	1
29	V	V	V	-	-	V	29.7	4	0	2
30	D	V	V	V	V	-	30.2	4	1	1
31	D	V	D	V	V	V	30.5	4	2	0
32	D	V	V	D	-	V	30.5	3	2	1
33	D	V	V	D	V	V	32	4	2	0
34	V	D	D	V	V	V	32.2	4	2	0
35	D	V	-	V	D	V	32.6	3	2	1
36	D	V	V	-	D	V	32.9	3	2	1
37	V	V	D	-	V	V	33.4	4	1	1
38	V	V	V	-	V	V	33.8	5	0	1
39	V	V	-	-	-	V	34.1	3	0	3
40	V	D	-	-	V	V	34.1	3	1	2
41	D	-	V	V	-	V	34.2	3	1	2
42	V	D	V	V	D	V	34.9	4	2	0
43	V	V	D	V	-	V	35.1	4	1	1
44	D	V	D	-	V	V	35.6	3	2	1
45	V	V	D	V	V	V	35.7	5	1	0
46	D	V	D	-	-	V	35.9	2	2	2
47	D	V	D	V	D	V	35.9	3	3	0
48	V	D	V	-	V	-	36	3	1	2
49	V	D	-	-	-	V	36.1	2	1	3
50	V	-	V	D	-	V	36.4	3	1	2
51	V	-	D	V	D	V	36.8	3	2	1
52	V	V	D	D	V	V	36.9	4	2	0
53	V	V	D	-	-	V	37	3	1	2
54	V	V	V	V	-	V	37	5	0	1
55	D	D	V	V	-	V	37.4	3	2	1
56	V	D	V	-	V	D	37.6	3	2	1
57	V	-	V	V	-	V	37.8	4	0	2
58	D	V	V	V	D	V	38.5	4	2	0
59	V	-	V	D	D	V	38.6	3	2	1
60	V	V	D	V	D	V	39.2	4	2	0

Table C.4: Limited Dose with Rest days at $D_{max} = 3 \times 10^5$. Top 60 of 729 Permutations. Tumor size predicted at day 30. $V_{max} = 1.5 \times 10^{11}$, $D_{max} = 3 \times 10^5$, where the dosages were fractioned over 6 days.

Tables C.5-C.6 show the top 60 of the 4096 permutations for altering regimes, with flexible frequencies under the metronomic treatment strategy.

Permutation Rank	Day 1	2	3	4	5	6	7	8	9	10	11	12	End Tumor Volume (mm^3)	Oncolytic Virus dose number	Dendritic Cells dose number
1	D	V	V	V	V	V	V	V	V	V	V	D	1.9	10	2
2	D	V	V	V	V	V	V	V	V	V	V	V	2.2	11	1
3	D	V	V	V	V	V	V	V	V	V	D	D	2.2	9	3
4	D	D	V	V	V	V	V	V	V	V	V	V	2.3	10	2
5	D	D	D	V	V	V	V	V	V	V	V	V	2.6	9	3
6	D	V	D	V	V	V	V	V	V	V	V	V	2.8	10	2
7	D	D	V	D	V	V	V	V	V	V	V	V	2.9	9	3
8	D	D	D	D	V	V	V	V	V	V	V	V	2.9	8	4
9	D	D	V	V	V	V	V	V	V	V	V	D	2.9	9	3
10	D	D	D	V	D	V	V	V	V	V	V	V	3.1	8	4
11	V	D	V	V	V	V	V	V	V	V	V	D	3.1	10	2
12	V	D	V	V	V	V	V	V	V	V	V	V	3.2	11	1
13	D	V	D	D	V	V	V	V	V	V	V	V	3.2	9	3
14	D	D	V	D	D	V	V	V	V	V	V	V	3.2	8	4
15	D	V	V	V	V	V	V	V	V	D	D	D	3.3	8	4
16	D	V	V	V	V	V	V	V	V	V	D	V	3.3	10	2
17	D	D	V	V	D	V	V	V	V	V	V	V	3.3	9	3
18	D	D	D	V	V	D	V	V	V	V	V	V	3.4	8	4
19	V	D	D	V	V	V	V	V	V	V	V	V	3.4	10	2
20	D	D	D	V	D	D	V	V	V	V	V	V	3.4	7	5
21	D	V	V	D	V	V	V	V	V	V	V	V	3.5	10	2
22	D	D	D	D	V	D	V	V	V	V	V	V	3.5	7	5
23	D	V	D	D	D	V	V	V	V	V	V	V	3.5	8	4
24	D	D	V	D	D	D	V	V	V	V	V	V	3.5	7	5
25	D	V	D	V	V	V	V	V	V	V	V	D	3.5	9	3
26	D	D	V	D	V	D	V	V	V	V	V	V	3.6	8	4
27	D	V	D	V	D	V	V	V	V	V	V	V	3.6	9	3
28	D	D	D	D	D	V	V	V	V	V	V	V	3.7	7	5
29	D	D	D	D	V	V	D	V	V	V	V	V	3.7	7	5
30	D	D	D	V	D	V	D	V	V	V	V	V	3.7	7	5
31	D	D	D	V	V	V	V	V	V	V	V	D	3.7	8	4
32	V	D	D	D	V	V	V	V	V	V	V	V	3.7	9	3
33	D	V	V	V	V	V	V	V	V	D	V	D	3.7	9	3
34	D	D	V	D	D	V	D	V	V	V	V	V	3.8	7	5
35	D	V	D	D	D	D	V	V	V	V	V	V	3.8	7	5
36	D	D	D	V	V	V	D	V	V	V	V	V	3.8	8	4
37	D	V	D	D	V	D	V	V	V	V	V	V	3.8	8	4
38	D	D	V	V	V	V	V	V	V	V	D	D	3.8	8	4
39	D	D	D	V	D	D	D	V	V	V	V	V	3.8	6	6
40	D	D	V	V	V	D	V	V	V	V	V	V	3.8	9	3
41	D	D	V	D	D	D	D	V	V	V	V	V	3.8	6	6
42	V	D	V	V	V	V	V	V	V	V	D	D	3.9	9	3
43	D	D	V	V	D	D	V	V	V	V	V	V	3.9	8	4
44	D	D	D	V	D	D	V	D	V	V	V	V	3.9	6	6
45	D	D	D	V	V	D	D	V	V	V	V	V	3.9	7	5
46	D	V	V	V	V	V	V	V	V	D	D	V	3.9	9	3
47	D	D	V	D	D	D	V	D	V	V	V	V	3.9	6	6
48	D	D	V	D	V	V	D	V	V	V	V	V	4	8	4
49	D	V	D	D	D	V	D	V	V	V	V	V	4	7	5
50	D	D	V	D	V	D	D	V	V	V	V	V	4	7	5
51	D	D	D	D	V	D	V	D	V	V	V	V	4	6	6
52	D	D	D	V	D	V	V	D	V	V	V	V	4	7	5
53	D	D	V	D	V	V	V	V	V	V	V	D	4	8	4
54	D	D	D	D	V	V	V	D	V	V	V	V	4	7	5
55	D	V	V	D	D	V	V	V	V	V	V	V	4	9	3
56	D	D	D	D	V	D	D	V	V	V	V	V	4	6	6
57	V	D	V	D	V	V	V	V	V	V	V	V	4.1	10	2
58	V	D	D	D	D	V	V	V	V	V	V	V	4.1	8	4
59	D	D	D	V	D	V	D	D	V	V	V	V	4.1	6	6
60	V	D	D	V	D	V	V	V	V	V	V	V	4.1	9	3

Table C.5: Permutation table representing for flexible dosing. 60 permutations of the 4096 are displayed, that predict the tumor size at day 30. Injection quantities: $V_{max} = 1.5 \times 10^{11}$, $D_{max} = 3 \times 10^6$, where the dosages were fractioned over 12 days

Permutation Rank	Day 1	2	3	4	5	6	7	8	9	10	11	12	Tumor Volume (mm^3)	Oncolytic Virus dose number	Dendritic Cells dose number
1	V	V	D	V	D	D	D	D	D	D	D	V	1.59	4	8
2	V	V	D	D	V	D	D	D	D	D	D	V	1.61	4	8
3	V	D	V	D	V	D	D	D	D	D	D	V	1.64	4	8
4	V	D	V	D	D	V	D	D	D	D	D	V	1.74	4	8
5	V	D	V	V	D	D	D	D	D	D	D	V	1.8	4	8
6	V	V	D	D	D	V	D	D	D	D	D	V	1.97	4	8
7	D	V	V	V	V	V	V	V	V	V	V	V	2.06	11	1
8	V	V	D	V	D	D	V	D	D	D	D	V	2.17	5	7
9	V	V	V	D	D	D	D	D	D	D	D	V	2.2	4	8
10	V	V	V	D	D	V	D	D	D	D	D	V	2.19	5	7
11	V	D	V	D	D	D	D	D	D	D	D	V	2.2	3	9
12	V	V	D	V	D	V	D	D	D	D	D	V	2.2	5	7
13	V	V	V	D	V	D	D	D	D	D	D	V	2.21	5	7
14	V	V	D	V	D	D	D	V	D	D	D	V	2.23	5	7
15	V	V	V	D	D	D	V	D	D	D	D	V	2.27	5	7
16	V	V	D	V	V	D	D	D	D	D	D	V	2.3	5	7
17	V	V	V	V	D	D	D	D	D	D	D	V	2.4	5	7
18	V	D	V	V	D	V	D	D	D	D	D	V	2.41	5	7
19	V	D	V	V	D	D	V	D	D	D	D	V	2.44	5	7
20	V	D	V	D	D	D	V	D	D	D	D	V	2.5	4	8
21	V	V	D	V	D	D	D	D	V	D	D	V	2.45	5	7
22	V	D	D	V	D	V	D	D	D	D	D	V	2.5	4	8
23	V	V	V	D	V	D	D	D	D	V	D	V	2.5	6	6
24	V	V	V	D	V	D	D	D	D	D	V	V	2.5	6	6
25	V	D	V	V	V	D	D	D	D	D	D	V	2.5	5	7
26	V	V	D	D	V	D	V	D	D	D	D	V	2.56	5	7
27	V	V	V	D	V	D	D	D	V	D	D	V	2.59	6	6
28	V	V	V	D	D	D	D	V	D	D	D	V	2.59	5	7
29	V	D	D	V	D	D	D	D	D	D	D	V	2.61	3	9
30	V	V	D	D	V	V	D	D	D	D	D	V	2.61	5	7
31	V	D	V	D	V	D	V	D	D	D	D	V	2.62	5	7
32	V	V	D	V	D	D	D	D	D	D	V	D	2.62	4	8
33	V	V	V	V	D	V	D	D	D	D	V	V	2.63	7	5
34	V	D	V	V	D	D	D	V	D	D	D	V	2.64	5	7
35	V	V	D	D	V	D	D	D	D	D	V	D	2.69	4	8
36	V	D	V	D	V	V	D	D	D	D	D	V	2.69	5	7
37	V	V	D	D	V	D	D	V	D	D	D	V	2.7	5	7
38	V	D	V	D	V	D	D	V	D	D	D	V	2.73	5	7
39	V	V	V	D	V	D	D	V	D	D	D	V	2.73	6	6
40	V	D	V	D	V	D	D	D	D	D	V	D	2.75	4	8
41	V	V	V	V	D	D	D	V	D	D	D	V	2.79	6	6
42	V	V	V	V	D	D	D	D	V	D	D	V	2.79	6	6
43	V	V	V	V	D	D	V	D	D	D	D	V	2.86	6	6
44	V	V	D	V	V	D	D	D	V	D	D	V	2.88	6	6
45	V	V	V	D	V	D	V	D	D	D	D	V	2.9	6	6
46	V	V	D	V	V	D	D	D	D	V	D	V	2.92	6	6
47	V	D	V	V	D	D	D	D	D	D	V	D	2.94	4	8
48	V	D	V	D	D	V	D	D	D	D	V	D	2.94	4	8
49	V	D	V	D	D	D	D	D	D	D	V	D	2.94	3	9
50	V	D	D	V	V	D	D	D	D	D	D	V	2.94	4	8
51	V	V	D	V	V	D	D	V	D	D	D	V	2.95	6	6
52	V	V	V	V	D	D	D	D	D	V	D	V	2.97	6	6
53	V	V	V	V	D	V	D	D	D	V	D	V	2.98	7	5
54	V	V	V	V	D	V	D	D	D	D	D	V	2.98	6	6
55	V	V	D	V	D	V	D	D	D	V	D	V	2.99	6	6
56	V	V	V	V	V	D	D	D	D	D	V	V	2.99	7	5
57	V	V	D	V	D	V	D	D	V	D	D	V	3.03	6	6
58	V	V	D	V	V	D	V	D	D	D	D	V	3.08	6	6
59	V	V	V	D	V	V	D	D	D	D	D	V	3.09	6	6
60	V	V	V	D	D	V	D	D	V	D	D	V	3.13	6	6

Table C.6: Permutation table representing for flexible dosing. 60 permutations of the 4096 are displayed, that predict the tumor size at day 30. Injection quantities: $V_{max} = 1.5 \times 10^{11}$, $D_{max} = 3 \times 10^6$, where the dosages were fractioned over 12 days